1994-03

Monterey Bay geoid

Boener, Joseph H.

Monterey, California. Naval Postgraduate School

NAVAL POSTGRADUATE SCHOOL
Monterey, California

THESIS

MONTEREY BAY GEOID

by

Joseph H. Boener

March, 1994

Thesis Advisor: J. R. Clynch

Approved for public release; distribution is unlimited.

REPORT DOCUMENTATION PAGE

Form Approved OMB No. 0704

1. AGENCY USE ONLY *(Leave blank)*	2. REPORT DATE	3. REPORT TYPE AND DATES COVERED
	March, 1994	Master's Thesis

4. TITLE AND SUBTITLE MONTEREY BAY GEOID

5. FUNDING NUMBERS

6. AUTHOR(S) Joseph H. Boener

7. PERFORMING ORGANIZATION NAME(S) AND ADDRESS(ES)
Naval Postgraduate School
Monterey CA 93943-5000

8. PERFORMING ORGANIZATION REPORT NUMBER

9. SPONSORING/MONITORING AGENCY NAME(S) AND ADDRESS(ES)

10. SPONSORING/MONITORING AGENCY REPORT NUMBER

11. SUPPLEMENTARY NOTES The views expressed in this thesis are those of the author and do not reflect the official policy or position of the Department of Defense or the U.S. Government.

12a. DISTRIBUTION/AVAILABILITY STATEMENT
Approved for public release; distribution is unlimited.

12b. DISTRIBUTION CODE
A

13.

ABSTRACT *(maximum 200 words)*

A high resolution local geoid was calculated for the Monterey Bay, CA using local gravimetry data, digital elevation data and The Ohio State University OSU91A global geopotential model. The theoretical accuracy of the calculated local geoid is 3.5 cm or better over 5 km.

Local gravity data came from three sources: 1,549 land observations from the Defense Mapping Agency, 179 bottom gravity observations from two Naval Postgraduate School gravity surveys of Monterey Bay and 17,098 National Geodetic Survey land and ship gravity observations from the National Geophysical Data Center's Gravity CD-ROM. Digital terrain elevation data came from the Rocky Mountain Communication Inc. 3 Arc Second Digital Terrain Elevation CD-ROM.

A GPS sea surface topography experiment conducted in October, 1993, had indicated an anomalous sea slope across the bay from Santa Cruz, California to Monterey, California. Comparisons between the calculated local geoid and the regional geoid for The United States, the National Geodetic Survey's GEOID93 indicated a possible explanation for the anomalous sea slope being a local slope in the geoid.

14. SUBJECT TERMS Geoid, Monterey Bay, Sea surface

15. NUMBER OF PAGES 152

16. PRICE CODE

17. SECURITY CLASSIFICATION OF REPORT	18. SECURITY CLASSIFICATION OF THIS PAGE	19. SECURITY CLASSIFICATION OF ABSTRACT	20. LIMITATION OF ABSTRACT
Unclassified	Unclassified	Unclassified	UL

NSN 7540-01-280-5500

Standard Form 298 (Rev. 2-89)
Prescribed by ANSI Std. 239-18

Approved for public release; distribution is unlimited.

Monterey Bay Geoid

by

Joseph H. Boener
Lieutenant, United States Navy
B.S., United States Naval Academy

Submitted in partial fulfillment
of the requirements for the degree of

MASTER OF SCIENCE IN PHYSICAL OCEANOGRAPHY

from the

NAVAL POSTGRADUATE SCHOOL
March 1994

Author:

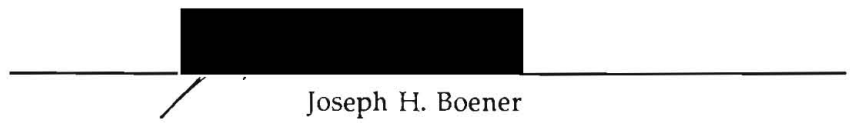

Joseph H. Boener

Approved by:

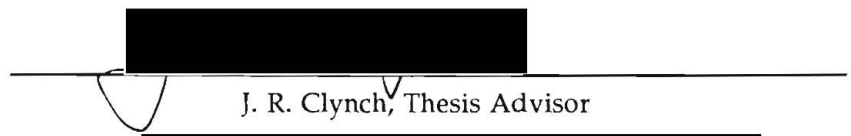

J. R. Clynch, Thesis Advisor

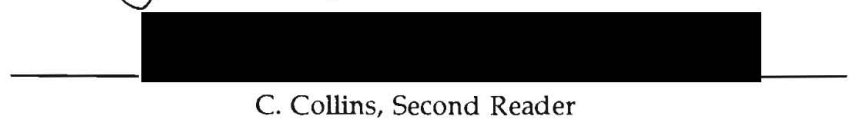

C. Collins, Second Reader

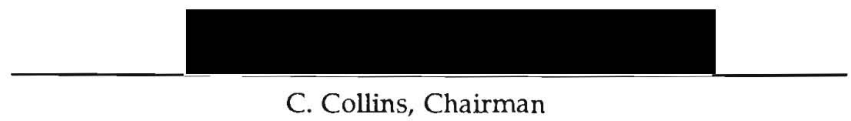

C. Collins, Chairman
Department of Oceanography

ABSTRACT

A high resolution local geoid was calculated for the Monterey Bay, CA using local gravimetry data, digital elevation data and The Ohio State University OSU91A global geopotential model. The theoretical accuracy of the calculated local geoid is 3.5 cm or better over 5 km.

Local gravity data came from three sources: 1,549 land observations from the Defense Mapping Agency, 179 bottom gravity observations from two Naval Postgraduate School gravity surveys of Monterey Bay and 17,098 National Geodetic Survey land and ship gravity observations from the National Geophysical Data Center's Gravity CD-ROM. Digital terrain elevation data came from the Rocky Mountain Communication Inc. 3 Arc Second Digital Terrain Elevation CD-ROM.

A GPS sea surface topography experiment conducted in October, 1993, had indicated an anomalous sea slope across the bay from Santa Cruz, California to Monterey, California. Comparisons between the calculated local geoid and the regional geoid for The United States, the National Geodetic Survey's GEOID93 indicated a possible explanation for the anomalous sea slope being a local slope in the geoid.

TABLE OF CONTENTS

ACKNOWLEDGEMENTS

Many people and organizations have contributed to this study. I feel that it is important that I give all those involved recognition for their contributions.

I would like to extend thanks to Mr. T. Rago of the Naval Postgraduate School, Mr. T. Siems of the Defense Mapping Agency, Ashtech Inc., Mr. J. Norton of Pacific Fisheries Environmental Group and Mr. S. Gill of National Oceanic and Atmospheric Administration for their contributions to the sea surface topography experiment.

Acknowledgement is also due to the Defense Mapping Agency Aerospace Center for supplying the local gravity data for Monterey and Dr. R. Rapp of the Ohio State University who supplied the OSU91A geopotential model and associated software and related literature.

A special thanks is given to Dr. D. Milbert of the National Geodetic Survey for his advice, guidance and the use of his programs. Dr. Milbert's assistance made this study possible.

I would also like to extend heartfelt thanks and deep appreciation to my thesis advisor, Dr. J. R. Clynch whose hard work, guidance and advice during my thesis work and the GPS experiment were invaluable. Dr. Collins, my second reader, was instrumental to my work through his advice on the oceanographic aspects of this thesis and the GPS experiment.

Finally, I would like to thank my wife, Mary, for all the long hours of work which she put into the thesis in addition to taking care of the rest of our lives and our daughter, Kathy.

I. INTRODUCTION

A. GENERAL

German mathematician, Karl Friedrick Gauss, recognized some two hundred years ago that the mean sea surface of the oceans formed a level surface caused by earth's gravity. A level or equipotential surface is a surface over which the potential of gravity is constant and the direction of gravity is normal. (Vanicek 1993) Later this surface came to be known as the geoid. The term, geoid, means "something like the earth" (DMS 1977) in the same fashion as spheroid means "something like a sphere" (ibid.).

Gravity is composed of the gravitation acceleration due to by the mass of the earth and the centrifugal acceleration which is a result of the earth's rotation. The gravity field of the earth exerts a force on all objects on its surface. Local variations in the density of the earth will cause localized variations in the gravity field. When these perturbations in the gravity field exist in the ocean, they distort the surface of the oceans.

In oceanography, the need for an accurate geoid occurs in the study of sea surface topography, tidal heights, absolute geostrophic currents and time-mean ocean circulation. These processes are the result of forces such as horizontal pressure

gradients, wind, atmospheric pressure, lunar and solar gravitational attraction, acting on the water. The forces result in deviations of the mean sea level surface from that of the geoid. (Ashkenazi et al. 1990; Fu et al. 1988) To study tidal records, "...on any geographic scale other than local, the various tide gauge bench marks have to be related to a common geodetic datum" (Ashkenazi et al. 1990). Simply stated, the heights of the tide gauges must be known relative to the geoid. The determination of absolute geostrophic currents and the time-mean ocean circulation, require a geoid accurate to a few centimeters over 100 km (Fu et al. 1988).

To separate the oceanographic affects distorting the surface of the water from the geoid, the geoid must be determined to a comparable or better accuracy and resolution than the oceanographic affects. The Ohio State University, OSU91A global geoid model (Rapp et al. 1991) is representative of a best fit model for the geoid over the entire earth with a standard error of 57 cm and a resolution of 50 km (Rapp 1992). This geoid is used for synoptic and mesoscale studies but because it is a global best fit, local features are not represented in the model's surface. Figures 1 and 2 show the surface and contours of the OSU91A geoid model in the vicinity of Monterey. The OSU model is very smooth due to its long wavelength, global nature. The continental slope, a large topographic feature, can be clearly seen in Figure 1. The

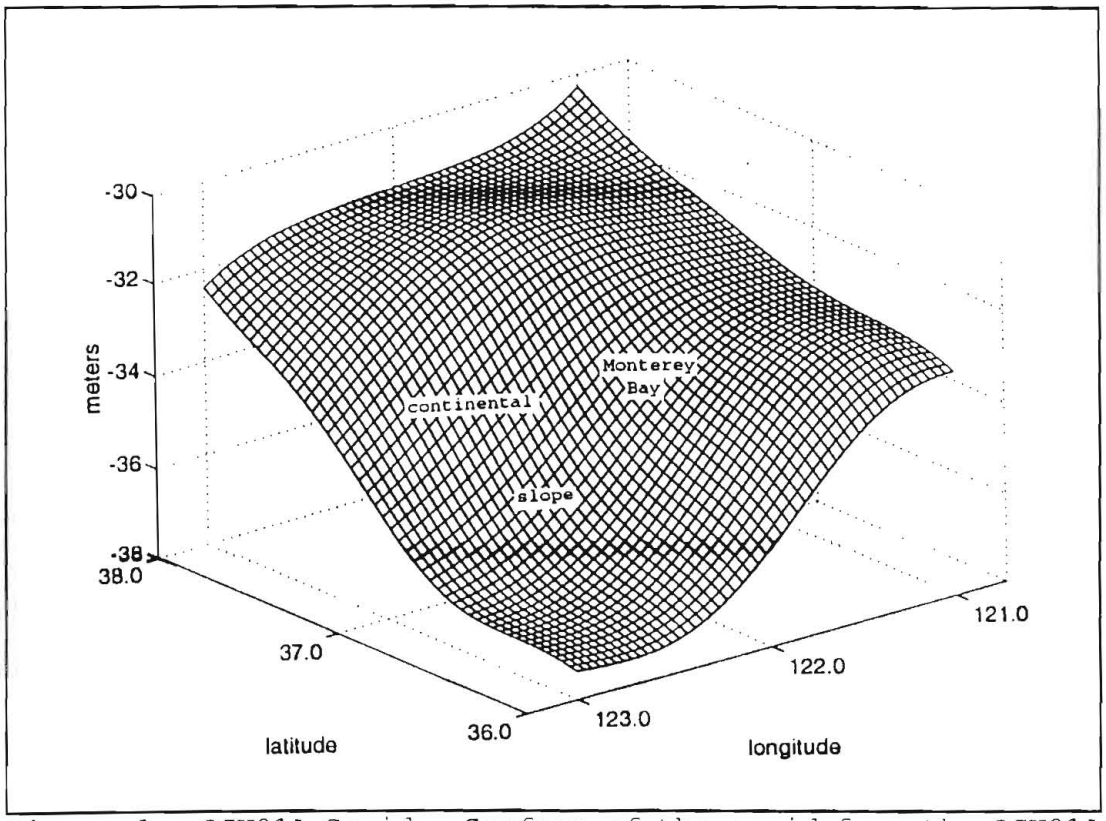

Figure 1. OSU91A Geoid: Surface of the geoid from the OSU91A geopotential model.

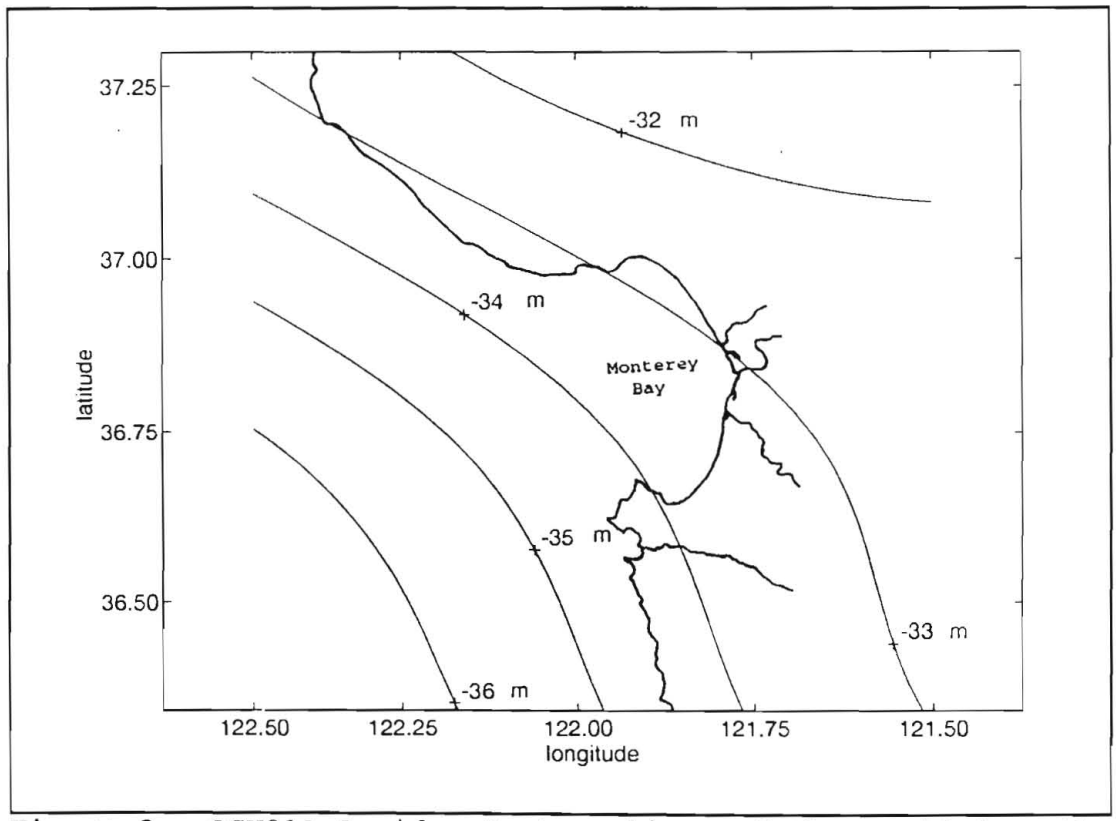

Figure 2. OSU91A Geoid: Contour lines of the geoid from the OSU91A geopotential model in meters.

regional geoid for North America, The National Geodetic Survey (NGS), GEOID93, (Milbert 1993) has a 10 cm accuracy one sigma, over 100 km and has shown 1 cm accuracy over base lines of 10 km. Local variations in this accuracy level may exist up to one to two parts per million. These variations are primarily caused by long wavelength errors in the underlying geopotential model. GEOID93 contains short wavelength features which are not in OSU91A. Figures 3 and 4 are the GEOID93 surface and contours which match the areas in Figures 1 and 2. GEOID93 displays much more short wavelength information about the geoid. The effects of the local mountains can be seen as well as the Monterey Submarine Canyon in the continental slope see Figure 3.

B. THESIS OBJECTIVE AND DESCRIPTION OF METHODS

The objective of this thesis is to develop a high resolution, high accuracy, local geoid for the Monterey Bay. This geoid can be thought of as a local correction to an existing global geoid model, such as OSU91A or WGS84, and a test of how well GEOID93 models the local geoid. The accuracy of the local geoid should approach 3 cm with a resolution of about 5 km. These accuracy and resolution requirements are chosen because they represent the current accuracy limits in the determination of sea surface topography and the resolution should be able to resolve any geodetic effects of the Monterey Submarine Canyon within the Bay.

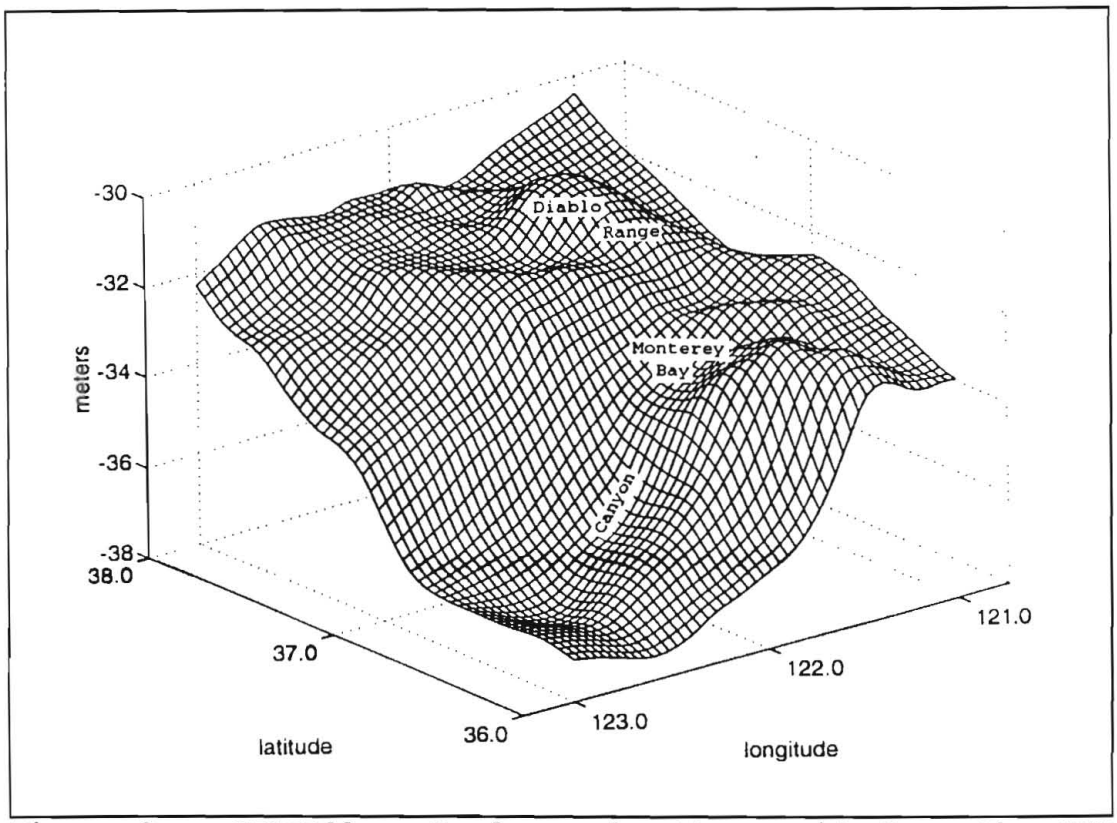

Figure 3. GEOID93: Surface of the geoid from the NGS GEOID93 regional geoid model.

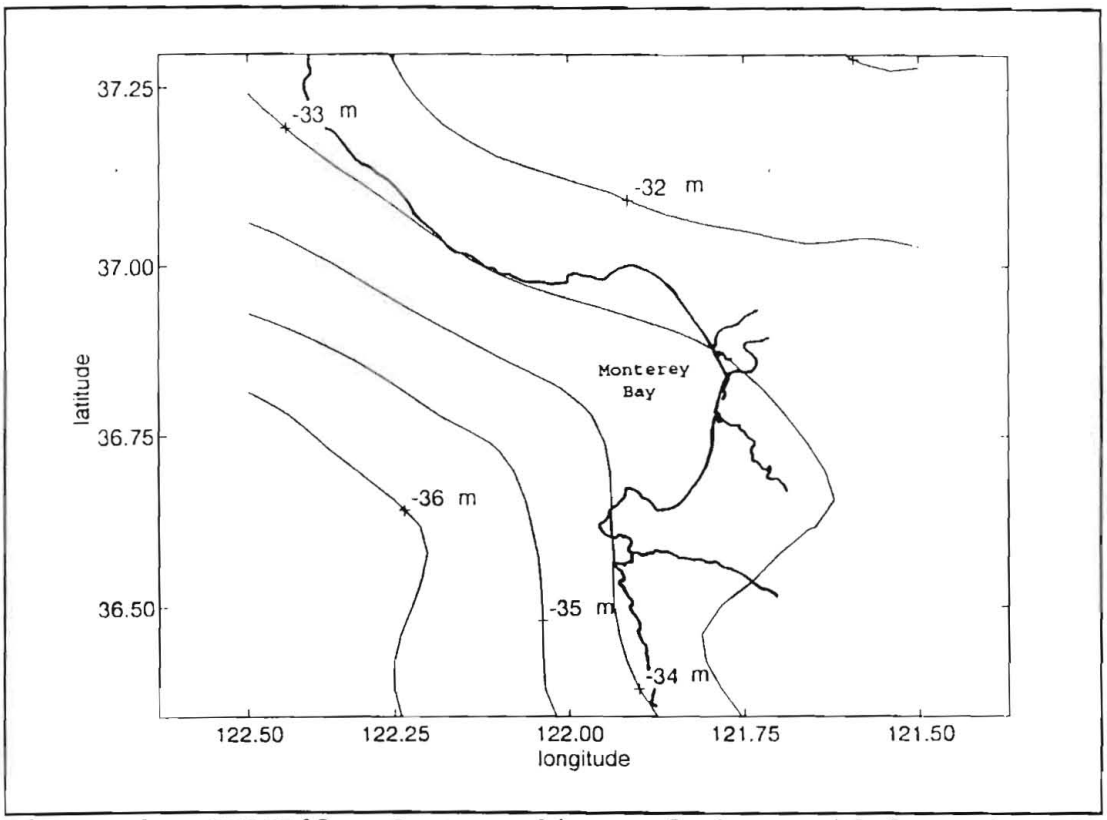

Figure 4. GEOID93: Contour lines of the geoid from the NGS GEOID93 regional geoid model in meters.

The primary data used to calculate the local geoid is gravity measurements on the surface of the earth. The geoid is related to gravity by the Stokes formula which was derived by Sir George G. Stokes in 1849 (Stokes 1849). Stokes' formula uses gravity measurements as a boundary condition for the calculation of the geoid. This method of geoid calculation is called the gravimetric method. Other methods, such as the astrogeodetic and the astro-gravimetric, use observations of the relative direction of gravity, deflections of the vertical, or a combination of gravimetry and deflections of the vertical to calculate the geoid (Bomford 1980). The availability of local gravity data made the gravimetric method the preferred choice for calculation of the Monterey geoid.

C. DESCRIPTION OF THE MONTEREY BAY

The Monterey Bay is located on the central coast of California. It is oriented north-south with its western boundary open to the Pacific Ocean, see Figure 5. The city of Santa Cruz is on the northern shore and the Monterey Peninsula forms the southern shore. Across the mouth of the Bay, Santa Cruz to the Monterey Peninsula, the Bay measures approximately 40 km. East from an imaginary line between Monterey and Santa Cruz, the Bay extends approximately 20 km inland. The village of Moss Landing is centered at the north-south midpoint of the Bay on the eastern shore.

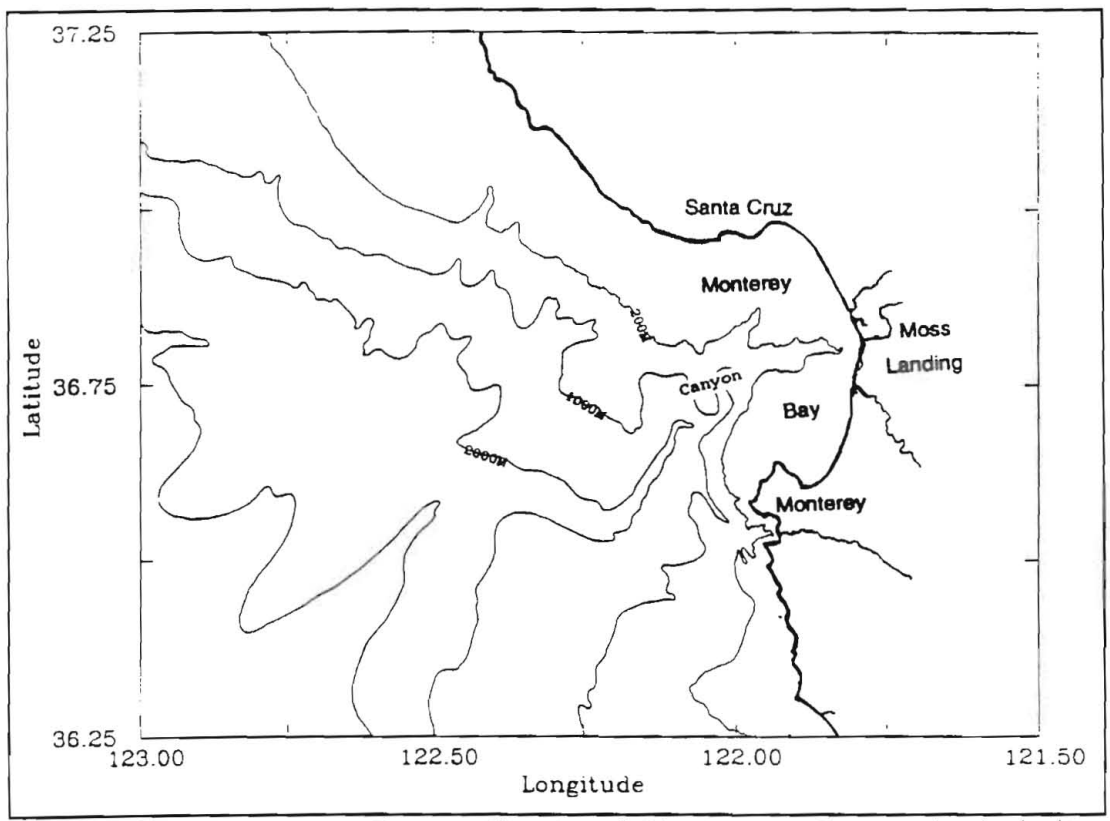

Figure 5. Monterey Bay: Chart of Monterey Bay and vicinity showing bathymetry contours in meters.

The bathymetry of the Bay is one of its most remarkable features, see Figure 5. The Monterey Submarine Canyon extends seaward to the Pacific Ocean from its head which lies near Moss Landing. From there, the Canyon runs east-west through the Bay, deepening and widening. At the open ocean, the canyon is over 10 km wide and 1500 - 2000 m deep. Past this point, the Canyon meanders south and continues to deepen and widen until it opens onto the ocean floor. The Canyon, which is nearly equal in topographic relief to the Grand Canyon, effectively separates the Bay into two shallow sections, north and south, whose depths are generally less the 150 m.

The geoid's shape is the result of density variations in the earth's crust. In a very basic sense, topography represents local density variations. This means that the geoid will mimic topography and bathymetry. The proximity of the continental slope, Figure 5, and its shape along with the mountains in the local area make the geoid in the Monterey area particularly interesting. The continental slope results in a long wavelength tilt in the geoid at Monterey which is visible in Figure 1. The continental slope makes a near 90° turn at Monterey and the geoid makes a similar turn. There are several mountain ranges in the vicinity of Monterey Bay which are of significance in the local geoid. Figure 6 shows the local terrain as a three-dimensional plot for the 1° block surrounding Monterey Bay. The Santa Cruz Mountains are to the north and the Santa Lucia Range is to the south. In the

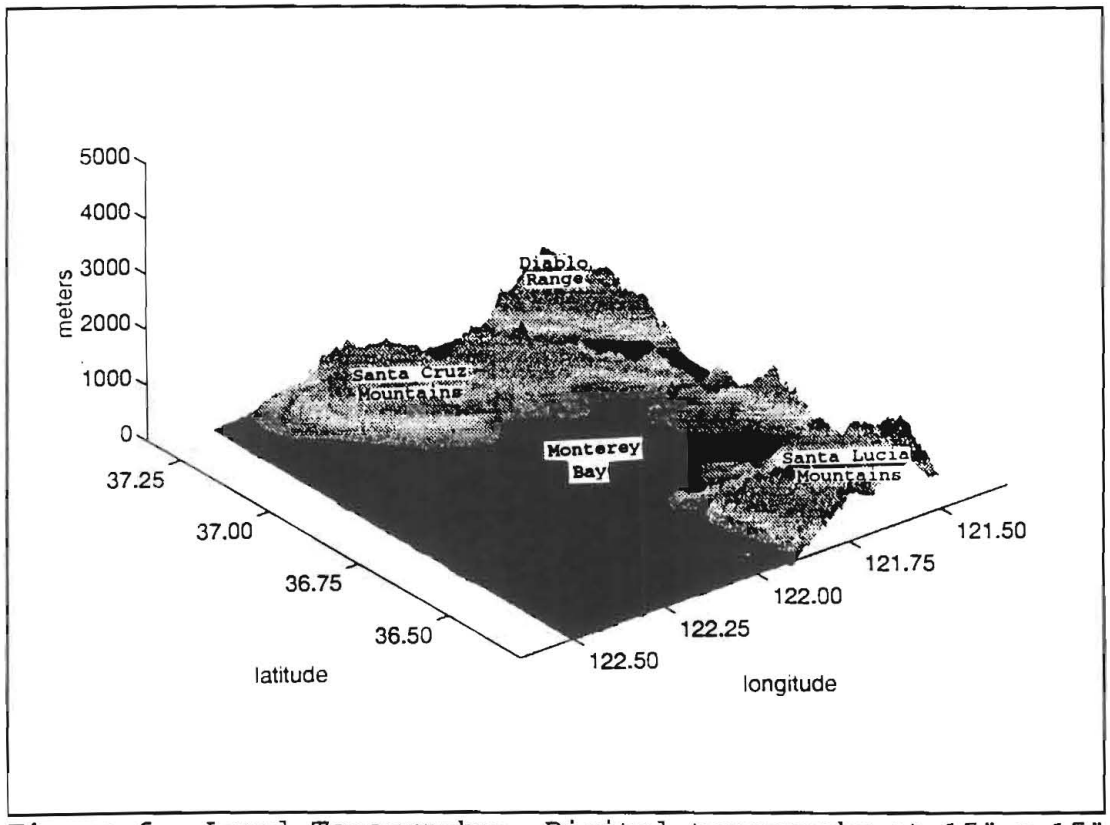

Figure 6. Local Topography: Digital topography at 15" x 15" resolution for Monterey locale.

northeast corner of Figure 6 is a portion of the Diablo Range. These ranges cause short wavelength undulations which can be seen in the GEOID93 surface, Figure 3, but not in the OSU91A surface, Figure 1.

D. THE GEOID AND OCEANOGRAPHY

On large scales the oceans are in nearly hydrostatic and geostrophic balance (Pond and Pickard 1983). Hydrostatic balance occurs when the pressure gradient is balanced by gravity. Geostrophic balance occurs when horizontal pressure gradients are balanced by Coriolis effects. If the relative orientation of these body forces can be determined throughout the oceans, the time-mean circulation of the oceans can, theoretically, be determined. (Wunsch and Gaposhkin 1988)

Oceanographers use equipotential and isobaric surfaces to describe the orientation of gravity and pressure gradients. The definition of an isobaric surface is very similar to the definition of an equipotential surface except an isobaric surface has constant pressure over its entire surface. At deep depths, 1000-4000 m, oceanographers equate equipotential and isobaric surfaces. This approximation is done by choosing a level of no or little motion. Dynamic sea surface heights can then be determined relative to this level by steric leveling. Steric leveling is the process of determining dynamic heights from the horizontal density distribution of the ocean above an isobaric reference surface. Dynamic

heights are used to describe horizontal pressure gradients and determine geostrophic currents. (Pond and Pickard 1983) These geostrophic currents are relative to the currents of the chosen isobaric reference surface. To determine an absolute geostrophic current, the dynamic height must be determined relative to the geoid.

The primary means of monitoring sea level is through the tidal records recorded at tide gauges on the ocean coasts. Tide gauges are surveyed and referenced to a datum which allow their records to be compared with any other tide gauge. The tide gauge datum on the west coast of the United States is the mean sea level at the tide gauge in Neah Bay, Washington (Fischer 1977). The orthometric elevations of all the tide gauges on the west coast are connected to this datum by periodic geodetic leveling. The level of accuracy of this connection is a function of how well the geoid has been determined between the tide gauges.

E. THESIS SUMMARY

This first chapter introduced the surface known as the geoid and its relationship to oceanography. Some of the current geoid models were discussed as well as the general features of the geoid in the Monterey area.

Chapter II goes over some of the terms, concepts and definitions which are used in physical geodesy. A brief

history of the study of the earth's shape and gravity is also discussed in Chapter II.

Chapter III covers the mathematical background of geodesy. Particular attention is given to the Stokes' formula, its applications and limitations.

Chapter IV covers the actual methods used in this study of the local geoid. Data processing, accuracy and calculation accuracy are discussed. This chapter ends with an estimation of the accuracy of the local geoid based on data and calculation accuracies.

Chapter V analyzes the geoid calculation results. The calculated geoid is compared to GEOID93 and a GPS sea surface height experiment. Chapter V closes with some recommendations for future work and summarizes the thesis.

II. BACKGROUND

A. GENERAL

Geodesy is the branch of science concerned with the determination of the size and shape of the earth. One of the fundamental problems of physical geodesy is the determination of the mathematical surface of the earth or geoid. The earliest known references to the shape of the earth date back to the history of Mesopotamia, 30th century B.C., when the shape of the earth was thought to be a flat disk. The first scientific hypothesis that the earth was spherical is credited to Thales of Milet in 600 B.C. or Pythagoras in 550 B.C. (Dragomir et al. 1982)

It was from these early studies of the earth's shape and size that the study of the earth's gravity began. Galileo Galilei made the first scientific observations of gravity and developed his law of free falling masses in 1590. In 1687, Sir Isaac Newton published the law of universal gravitation in his "Philosopiar naturalis principia mathematica". (ibid.)

Sir George G. Stokes published his work "On the Variations of Gravity and the Surface of the Earth" in 1849, in which, he showed that the geoid could be determined by measuring gravity densely everywhere on the geoid's surface. (ibid.) The formula which Stokes derived allows the determination of the

separation between the geoid and a reference ellipsoid by measuring relative gravity differences or gravity anomalies. Stokes' formula is the basic foundation of gravimetric geodesy (Moritz 1974).

B. TERMS, CONCEPTS AND CONVENTIONS

1. Mean Earth Ellipsoids

Mean earth ellipsoids, also called reference ellipsoids, level ellipsoids or normal ellipsoids, are best fit ellipsoidal models for the geoid. An ellipsoid is a mathematically simple model of the geopotential whereas the geoid is the true geopotential. The geoid is represented by heights relative to a reference ellipsoid. There are several normal ellipsoids but only one geoid. Figure 7 gives a comparison of a reference ellipsoid to a sphere. Mean earth ellipsoids deviate from a sphere by approximately 21 km and the geoid deviates only ± 100 m from an ellipsoid.

Reference ellipsoids and their gravity field are defined by four values taken from the actual earth. The mean equatorial radius, a, is the ellipsoid's semimajor axis. The flattening of the polar axis, f, is the deviation of the ellipsoid from a sphere. The flattening is given by:

$$f = \frac{b-a}{a} \qquad (2\text{-}1)$$

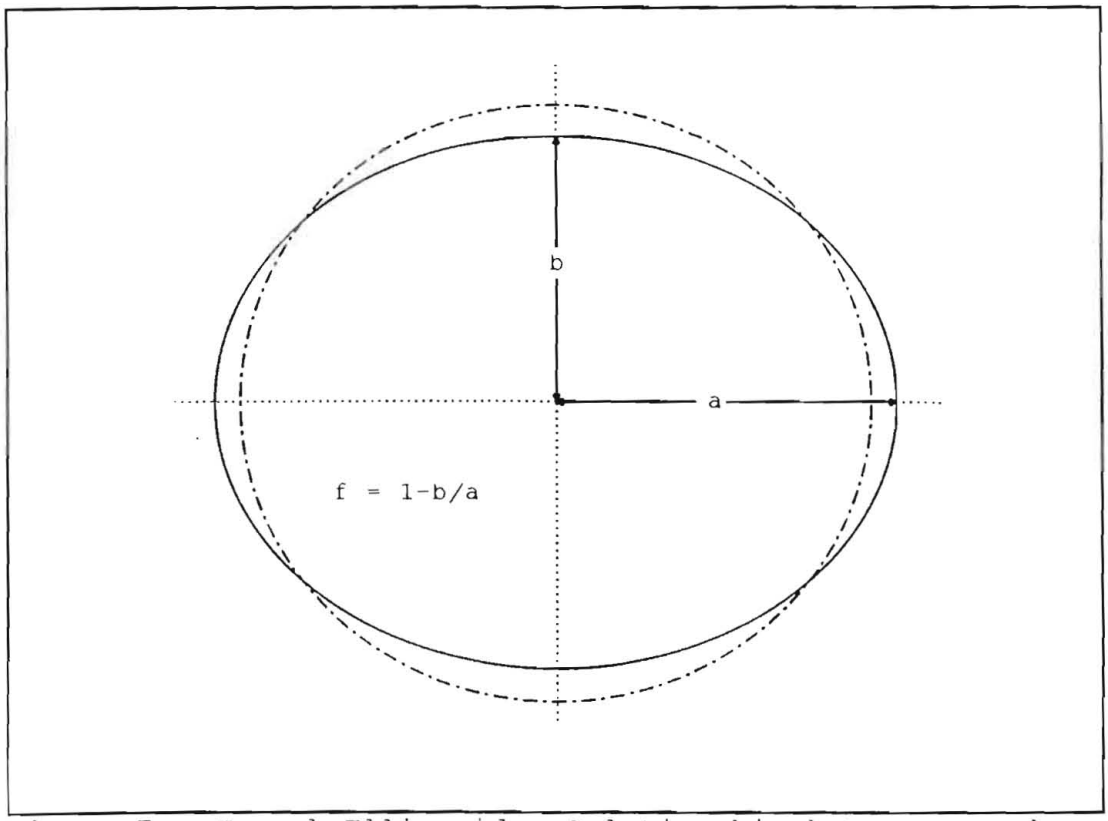

Figure 7. Normal Ellipsoid: Relationship between a sphere and ellipsoid showing the semimajor axis, a, semiminor axis, b, and the flattening, f. Dash line is sphere, solid line is ellipsoid

where b is the semiminor axis of the ellipsoid. The other parameters are the mass of the earth times the universal gravitational constant or the geocentric gravitational constant, GM, and the angular velocity of the earth, ω. (Heiskanen and Moritz 1967) The ellipsoid is also assumed to have a uniform density distribution (Fischer 1977).

The ellipsoid models are further constrained in that the center of the ellipsoid and the actual earth are collocated and the geopotential on the surface of the ellipsoid is equal to the geopotential on surface of the geoid. These constraints minimize the separations between the geoid and ellipsoid and allow simplifying assumptions, (linearity, zeroth and first order terms equal to zero), to be made in the derivation of formulas to calculate the geoid.

Values for the ellipsoid model parameters; a, GM, f and ω, are determined by the International Union for Geodesy and Geophysics, I.U.G.G., and then accepted as being exact values (Torge 1991). These reference systems consist of the normal ellipsoid and its gravity field. Table I is a list of some of the primary geodetic reference systems and their parameters.

TABLE I GEODETIC REFERENCE SYSTEMS

	GM	a	f	ω
	$[m^3/s^2]$ $x10^9$	[m]		[rad/s] $x10^{-5}$
Ell.1930:	398633	6378388	1/297.0	7.291551
GRS 1967:	398603	6378160	1/298.247	7.2921151467
WGS 1972:	398600.8	6378135	1/298.26	7.2921215
GRS 1980:	398600.5	6378137	1/298.2572	7.292115
WGS 1984:	398600.5	6378137	1/298.257223563	7.292115

2. Gravity

Gravity is actually an acceleration or body force. Weight is the force that results when a mass is acted upon by gravity. Gravity is given by:

$$\gamma = \frac{\mathbf{w}}{m} \qquad (2\text{-}2)$$

where γ is gravity, $\mathbf{w}$ is the weight or force and m is the mass. Gravity, as perceived on the surface of the earth, is composed of the gravitational and centrifugal accelerations of earth's mass and rotation:

$$\boldsymbol{\gamma} = \boldsymbol{f}_g + \boldsymbol{f}_c \qquad (2\text{-}3)$$

where f_g is the gravitational acceleration and f_c is the centrifugal acceleration. Centrifugal acceleration only affects a body which is rotating with earth. Gravitational acceleration is part of gravity but it is present whether a body is rotating or not. Masses which do not rotate with the earth, such as; satellites in orbit, feel the earth's gravitational acceleration but not the centrifugal acceleration.

The traditional unit of gravity is the gal, from Galileo, 1 gal = 1 cm/s^2. The gal is equal to 0.01 m/s^2 so that it is not strictly an SI unit. Another common unit for gravity is the milligal (mgal) 1 mgal = 0.001 gal. The mean gravity of the earth is 981 gal or 981,000 mgal. Gravity varies primarily with latitude and has mean values of 978 gal at the equator and 983 gal at the poles. (Bomford 1980) Within the Monterey vicinity, the gravity varies from -90 mgal to 150 mgal around an average value of 979,900 mgal. This is a total variation range of less than 0.025 percent of the mean. Appendix B covers methods of gravity measurement.

a. Normal gravity

Normal gravity is the gravity associated with an ellipsoid model of the geoid. Normal gravity is the combination of the model ellipsoid's gravitational acceleration and centrifugal acceleration. Figure 8 shows the

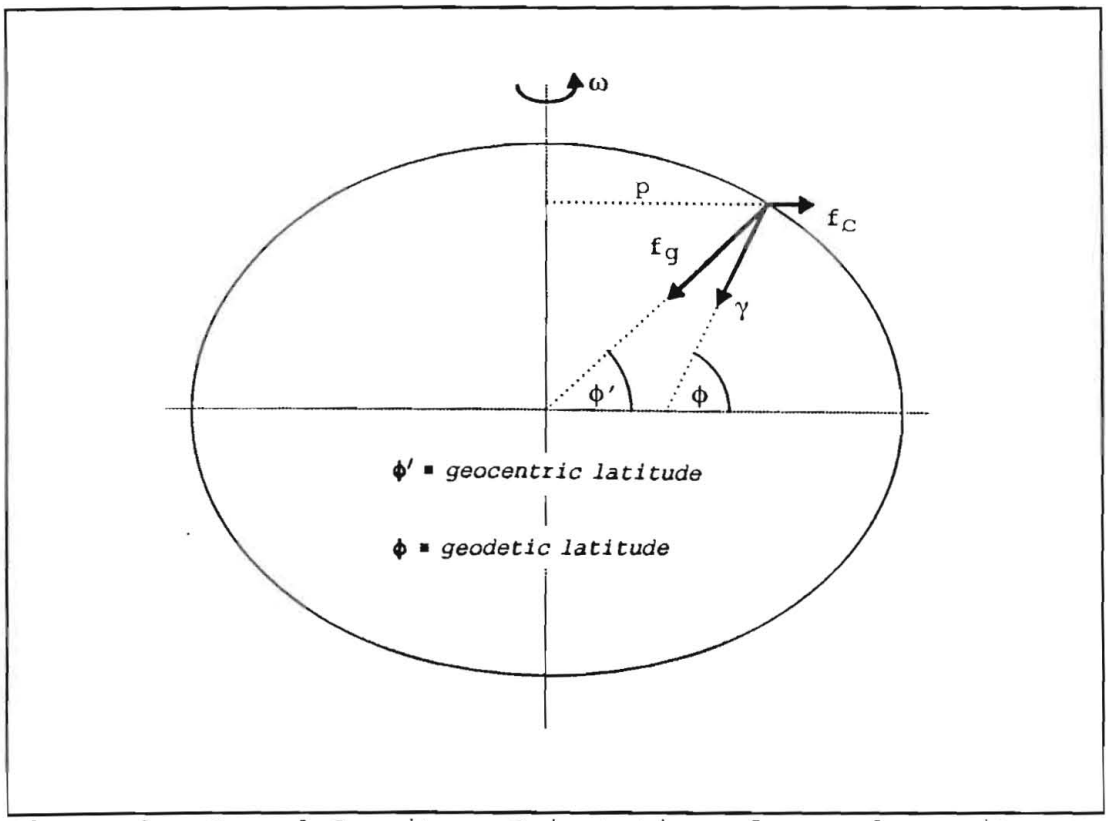

Figure 8. Normal Gravity: Orientation of normal gravity, γ, centrifugal acceleration, f_g, gravitational acceleration f, angular velocity, ω and rotation arm, p.

orientation of the accelerations on the surface of an ellipsoid. Normal gravity is γ, $\mathbf{f}_g$ is the gravitational acceleration and $\mathbf{f}_c$ is the centrifugal acceleration. The normal gravity of the GRS80 ellipsoid, in mgal, is given by:

$$\gamma = 9780327\ (1 + 0.005324\ \sin^2\phi - 0.000058\ \sin^2 2\phi) \quad (2\text{-}4)$$

where ϕ is the geographic latitude (Torge 1991). Equation 2-4 is the normal gravity formula or Cassini's formula.

b. Observed gravity

Observed gravity is the actual gravity of the earth measured on the surface of the earth. Observed gravity is designated, **g**, and is composed of the same accelerations as the normal gravity with the exception that they are the real values for the earth. Observed gravity represents a measurement of the earth's gravity potential.

c. Gravity Anomalies

Gravity anomalies represent perturbations in the gravity field which, in turn, represent perturbations in the geoid. Gravity anomalies are the differences between the magnitudes of normal gravity on the ellipsoid and observed gravity on the geoid. This is a peculiar definition because this difference is being taken of two vector quantities which are not collocated and the result is a scalar quantity. In Figure 9, ***g*** is gravity on the geoid and γ is the normal gravity on the ellipsoid. The gravity anomaly is given by:

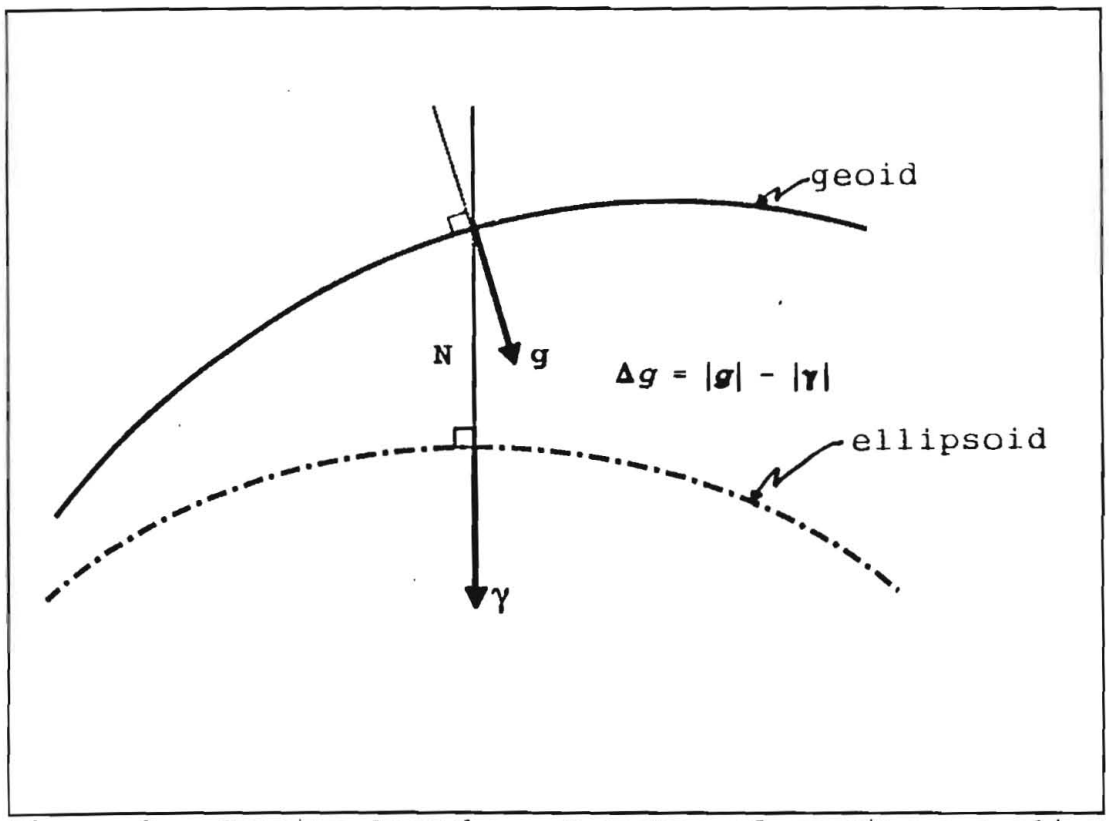

Figure 9. Gravity Anomaly: Geometry of gravity anomalies showing geoid undulation, N, observed gravity, g, normal gravity, γ.

$$\Delta g = |g| - |\gamma|. \qquad (2\text{-}5)$$

The angle between **g** and γ, the deflection of vertical, is kept small by proper determination of the reference ellipsoid and can be neglected. That is why gravity anomalies may be defined as the differences in magnitudes rather than vector differences.

d. Terrain Reductions

The assumptions made in the derivation of Stokes' formula require that gravity anomalies be on the surface of the geoid and that no masses are exterior to the surface of the geoid. Terrain reductions are the mathematical process of removing the effects of masses external to the geoid from gravity observations. Terrain reductions can be thought of as a two step process: first, the mathematical transfer of all masses to the interior of the geoid and second, movement of the gravity measurement from the physical surface of the earth to the surface of the geoid. These two steps, together, make up the terrain reduction.

There are many types of terrain reductions based on the method used to remove the effect of the terrain above the geoid. The proper reduction to apply is based on the intended use of the anomaly. Due to their small indirect effect, atmospherically corrected, free-air anomalies with a terrain

correction applied (also known as Helmert anomalies) are appropriate for geoid determinations (Milbert 1991). · The indirect effect is caused by the transferring of the mass of the terrain from above the geoid to below the surface of the geoid. This changes the gravity potential of the geoid and displaces the geoid. This displacement can be quite large, up to 100 m, depending on the terrain reduction method used (Heiskanen and Moritz 1967).

3. The Geoid

The geoid is an equipotential surface defined by the actual gravity potential of the earth. The geoid is one of an infinite number of surfaces of constant potential and is identified as the geopotential surface which most closely coincides with the mean surface of the earth's oceans.

The actual gravity potential field of the earth is not uniform; it is distorted by density variations which exist in the earth. These distortions cause corresponding distortions in the geoid called geoid undulations. Figure 10 represents the effects of density variation on the geoid. In Figure 10, the negative and plus signs indicate variations in the density structure of the earth, N represents the geoid undulation and the smooth ellipse the surface of a reference ellipsoid.

Differences between a particular normal ellipsoid and the geoid are the geoid heights, geoid undulations or geoid-

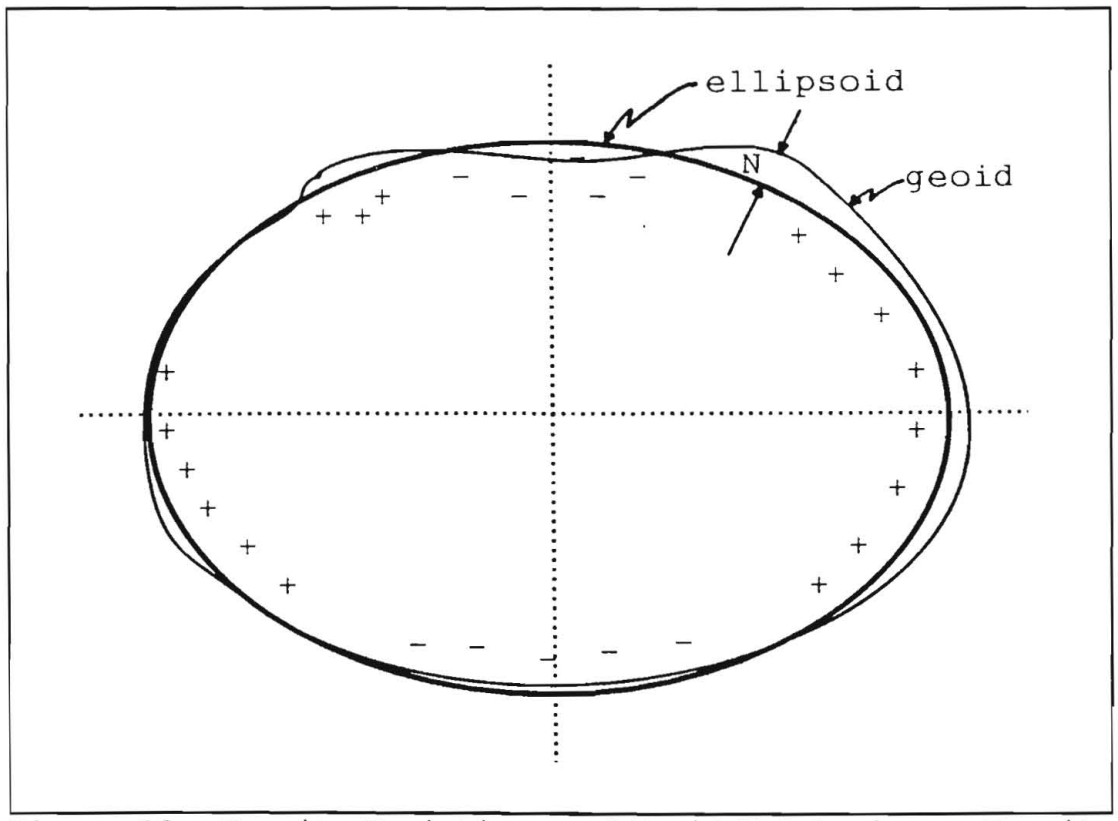

Figure 10. Density Variations and Geoid Undulations: Density variations (+,-) in the earth's crust causes corresponding geoid undulations, N.

ellipsoid separations. Geoid undulations are given as heights above or below a particular reference ellipsoid. Compared to a mean semimajor axis of 6,378,000 m, a ±100 m range gives a total variation of less than 0.004 percent between the geoid and ellipsoid. In the vicinity of the Monterey Bay the geoid undulation, as modeled by the OSU91A geopotential model, varies from -32 m in the northeast to -36 m in the southwest relative to the GRS80 ellipsoid see Figure 1.

4. Heights

Height measurements are made up of three elements; a reference surface, a direction vertical to the reference surface and a distance measured along that vertical. Geodesy differentiates between three types of heights; orthometric, geoid and ellipsoid. The primary difference between these heights is the surface that each of them uses for a reference. Orthometric heights are the heights which use mean sea level or the geoid as their reference surface. Orthometric heights are the heights used on maps when the terrain heights are given in MSL. Ellipsoid heights are the heights referenced to an ellipsoid model of the geoid. Geoid heights are actually ellipsoid heights and are the differences between a ellipsoid model of the geoid and the actual geoid. Ellipsoid heights,

h, and orthometric heights, H, are related by the geoid undulation:

$$H = h + N \tag{2-6}$$

where N is the geoid undulation see Figure 11.

C. CURRENT GEOID MODELS

1. General

Geoid models can be broken into three categories based on the extent of the geoid they model. The first are global models which attempt to model the geoid over the entire surface of the earth. Global geoid models are usually in the form of coefficients for a spherical harmonic expansion representing the geopotential. Global geoid models are also called geopotential models. The next category of geoid models are regional geoid models which cover parts of the geoid up to continental scales. These models attempt to best fit the geoid in their area and ignore errors outside their boundaries. The final category are local geoids which try to determine the geoid, in a confined area of interest, to very high resolution and accuracy.

2. Global Geoid Models

Global geoid models can be broken into two subcategories based on the types of information used in their calculation. Global models calculated using only satellite

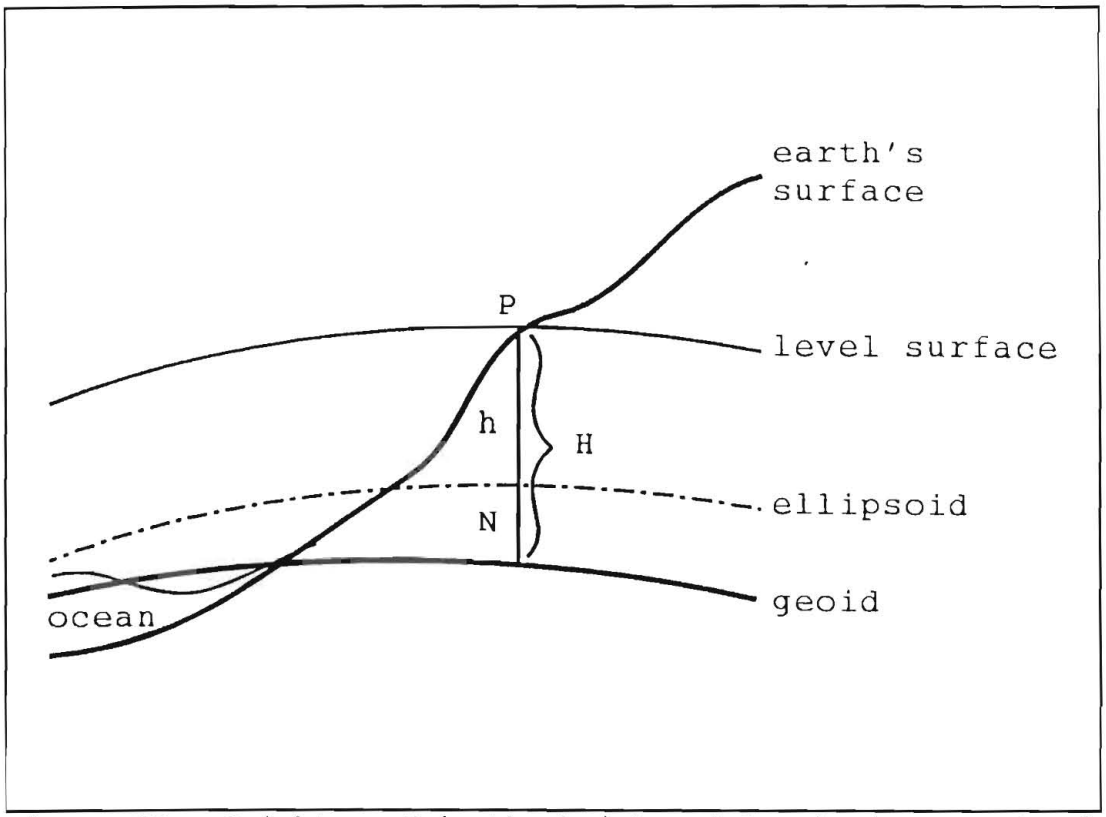

Figure 11. Heights: H is the height of P relative to MSL, h is the height of P relative to an ellipsoid, and N is the geoid-ellipsoid separation.

observation data are called satellite-only geoid solutions. These models generally contain only the low order spherical harmonics since satellite observation data does not include high spatial frequency information about the gravity field. (Seeber 1993) Examples of this type of model are the Goddard Earth Models (GEM) GEM-9, GEM-L2, GEM-T1, and GEM-T2 (Mainville et al. 1992; Rapp 1993). The GEM-T models were developed in preparation for the launch of the TOPEX/Poseidon mission.

Global geoid models may also combine satellite altimetry data, surface gravimetry data and satellite observation data. These models generally have better spatial resolution, which comes from the inclusion of the surface and altimetry data. Consequently, they have higher degrees of harmonic expansions and more coefficients. Recent examples of this type are the GEM10B, GEM-T3, GRIM4C1, and OSU91A. (ibid.)

Generally, the greater the number of coefficients a model has, the more accurate the model is since it contains shorter wavelength information of the gravity field. The shortest wavelength a given harmonic model can determine is given by:

$$\lambda = \frac{2\pi R}{k} \qquad (2\text{-}7)$$

where λ is the resolution, R is the radius of the earth and k is the degree of the harmonic expansion.

The OSU91A geoid model is a spherical harmonic expansion complete in degree and order to 360 with 130,682 coefficients calculated using satellite and surface data (Rapp et al. 1991). OSU91A can give "...geoid undulations to a resolution of 50 km with a predicted global accuracy of 57 cm (Rapp 1993)." The accuracy of the predicted undulation varies from region to region depending on the gravity data coverage which was available for the calculation of the model in that area. OSU91A's best accuracy is over the oceans. Where to degree 50 it is accurate to 14 cm. (Rapp 1992)

3. Regional Geoid Models

Regional geoid models are calculated by combining the solution of a global geopotential model and dense gravity data from the region of interest. The basic method is to remove the long wavelength information from the gravity data by subtracting the gravity anomalies predicted by the global geopotential model. The residual gravity data is then used to calculate small residual geoid undulations which are added to geoid undulations predicted from the global model. This method is known as the remove-calculate-restore technique and is the method which will be employed in calculating the Monterey Bay geoid.

A regional geoid for the United States, GEOID93, was calculated by NGS using the complete OSU91A geopotential model and 1.8 million gravity measurements. GEOID93 covers the

Continental United States, the limits being 24°-50°N, 125°-66°W (Milbert 1993). GEOID93 has displayed 10 cm accuracy over base lines of 100 km when compared to GPS surveys (ibid.). At shorter lengths, better accuracy has been seen; however, local variations due to long wavelength errors in the underlying global geoid may be up to one to two parts per million (PPM) (ibid.). A major thrust of this thesis will be the comparison of the local geoid as determined by GEOID93 and the calculated local geoid.

4. Local Geoid Models

Local geoid models can be calculated by the same remove-calculate-restore method as the regional models. Again, the primary difference is the extent of the geoid over which the errors are trying to be minimized. The short wavelength features of the geoid are generally modeled better in local geoid but only over a restricted area of interest. Local geoids are generally done for a specific purpose where the leveling requirements exceed the available geoid model. Preparation for the construction of the super collider required a local geoid accurate to a few millimeters (Leick et al. 1992). Precise telemetry control networks such as at the Air Force Flight Test Center located at Edward's Air Force Base, California also require accurate local geoids (Perrott 1993). Geodetic leveling of tide gauges require precise determination of the geoid so that ellipsoidal heights of

tidal datums from GPS can be converted to orthometric heights (Ashkenazi et al. 1990). Mineral and oil surveying also use local geoid calculations to determine the possible presence of natural resource deposits.

III. MATHEMATICAL BACKGROUND OF GEOID CALCULATION

A. GENERAL

The basic problem of physical geodesy is the determination of the gravity potential function from perturbations in its derivative, gravity anomalies. The gravity potential determines the shape of the geoid. This chapter looks into the mathematical foundations of geoid calculation. Three relationships will be introduced: Stokes' integral, the fundamental equation of physical geodesy and Brun's formula.

Stokes' integral solves for the gravity potential function using gravity anomalies as the boundary condition on the geoid and integrating the gravity anomalies over the surface of the geoid. The fundamental equation of geodesy provides a relationship between gravity anomalies and perturbations in the gravity potential. Brun's formula relates geoid undulations to the perturbations in the gravity potential. Appendix C contains expanded derivations of these formulas and should be consulted for more detailed information.

B. POTENTIAL

1. Gravitational Potential

The gravitational potential, V, at a point is given by:

$$V = \frac{GM}{r} \tag{3-1}$$

where r is the distance between the mass, M and the field point and G is the universal gravitational constant. The gravitational potential is a scalar function and is continuous outside the point mass, r › 0, and by convention is zero at r = ∞. (Heiskanen and Moritz 1967)

The gravitational acceleration at the field point is the negative gradient of the gravitational potential:

$$\boldsymbol{f}_g = -\nabla V. \tag{3-2}$$

This relationship between the gravitational acceleration and the gravitational potential is graphically shown in Figure 12. The gravitational acceleration will always be perpendicular to surfaces of constant potential.

If the mass is contained within a surface, such as the geoid, the gravitational acceleration can be integrated over the surface, by Gauss's theorem and gives:

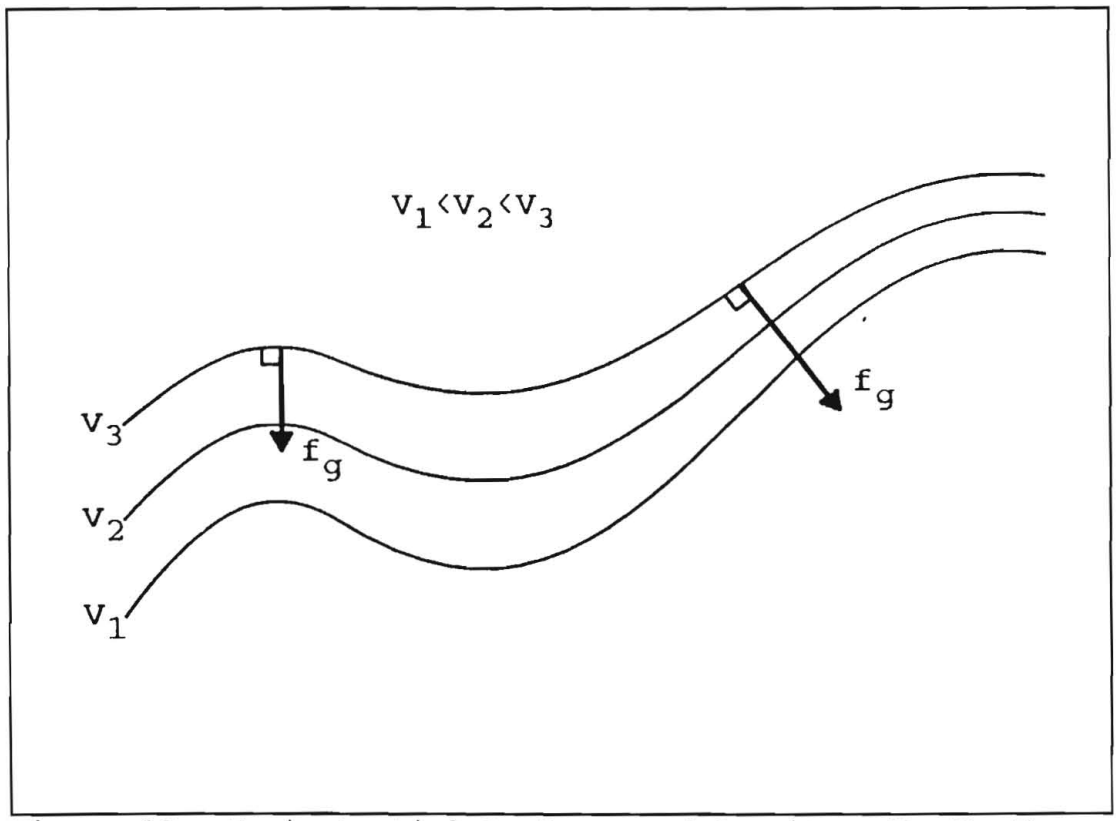

Figure 12. Equipotential Surfaces and Gravity: V_1, V_2, V_3 are the geopotential value on each surface, f_g is the gravitational acceleration.

$$\nabla^2 V = -4\pi G\rho \qquad (3\text{-}3)$$

where ∇^2 is the Laplacian operator. Equation 3-3 is known as Poisson's equation. If the calculation point is outside the mass, $\rho = 0$, and the equation becomes Laplace's equation:

$$\nabla^2 V = 0. \qquad (3\text{-}4)$$

The solutions to Laplace's equation are called harmonic functions. (Jackson 1975)

Equations 3-3 and 3-4 show that the gravitational potential is a harmonic function outside a surface enclosing all masses but not inside the surface. Several characteristics of harmonic functions can be seen by examining the behavior of the simple harmonic function, $1/r$. The harmonic functions goes to zero as r goes to infinity. Harmonic functions are continuous and have continuous derivatives where they satisfy Laplace's equation.

Stokes' theorem states that a harmonic function outside a surface is uniquely determined by the function's values on the surface (Heiskanen and Moritz 1967). In geodesy, this means that the gravitational potential can be determined by measuring gravity, the derivative of the potential, on the surface of the geoid. Determining the geopotential function is called the first boundary value

problem of geodesy and is done by Poisson's integral (ibid.). Equation 3-4 is true for the gravitational potential once all the topography above the geoid has been removed or shifted to the interior of the geoid via the terrain reduction.

2. Centrifugal Potential

The centrifugal acceleration on the surface of the ellipsoid is:

$$f_c = p\omega^2 \tag{3-5}$$

where p is the distance from the axis of rotation and ω is the earth's angular velocity. The centrifugal potential represents the amount of work done by the centrifugal acceleration in moving a body a distance, p, outward from the axis of rotation. The centrifugal potential is given by:

$$\Phi = \frac{1}{2}p^2\omega^2. \tag{3-6}$$

Unlike the gravitational potential, the centrifugal potential does not satisfy Laplace's equation outside the mass and is not representable by an harmonic series. However, the centrifugal potential is an analytic function and can be easily handled separately from the determination of the gravitational potential. (Dragomir et al. 1982)

3. Gravity Potential

The gravity potential of the reference ellipsoid, the normal potential, is the sum of the normal gravitational and centrifugal potentials,

$$U_0 = V+\Phi . \qquad (3-7)$$

where U_0 is the potential of the reference ellipsoid. Normal gravity is then,

$$\gamma = -\nabla U_0 . \qquad (3-8)$$

By definition, the normal potential on the reference ellipsoid surface is equal to the potential of the geoid:

$$U_o = W_o . \qquad (3-9)$$

On the geoid, the actual potential is:

$$W_o = U_G+T \qquad (3-10)$$

where W_o is the actual potential on the geoid, U_G is the potential of the ellipsoid displaced to the geoid and T is the disturbing potential. This defines the perturbed potential as the difference between the model potential U_o displaced to the geoid and the true potential W_o on the geoid. These

relationships between the normal potential and true potential are based on the assumption that the ellipsoid parameters have been determined properly. The gravity of the geoid is defined by:

$$g = -\nabla W_0 \qquad (3\text{-}11)$$

where W_o is the potential of the geoid at its surface. The relationships in this section form the basis used to derive Brun's theorem, the fundamental equation of geodesy and Stokes' Formula.

C. BRUN'S FORMULA

Brun's formula relates the perturbations in the gravity potential to the undulations in the geoid. Brun's formula is:

$$N = \frac{T}{\gamma} \qquad (3\text{-}12)$$

where N is the geoid-ellipsoid separation, T is the perturbing potential and γ is normal gravity. The importance of Brun's formula is that it gives a relationship between the disturbances in the potential function and the distance which the disturbance displaces the surface of the geoid. (Heiskanen and Moritz 1967)

D. THE FUNDAMENTAL EQUATION OF GEODESY

The fundamental equation of geodesy provides the relationship between gravity and the gravity potential, the two fundamental elements of geodesy. It links disturbances in the gravity field to disturbances in the gravity potential or the perturbing potential. In the previous section, Brun's formula was shown to relate the disturbing potential to the geoid undulation. The shortcoming of this is that it is physically difficult to measure the potential. However, the gravity potential determines the gravity field which is relatively easy to measure. The spherical form of the fundamental equation of geodesy is:

$$\Delta g = -\frac{2}{r}T - \frac{\partial}{\partial r}T. \qquad (3\text{-}13)$$

where Δg is the gravity anomaly caused by the disturbing potential T and r is the geocentric radius (ibid.). The fundamental equation of geodesy, 3-13, is actually a boundary condition for the gravity potential function because Δg is determined on the geoid. The importance of equation 3-13 is that it gives the anomalous potential and the vertical gradient of the anomalous potential, both of which are difficult to measure as a function of the gravity anomaly (which is easy to measure).

E. STOKES' FORMULA

The Stokes formula calculates the geoid undulation at a geographic position by integrating the gravity anomalies over a surface see Figure 13. Stokes' formula combines the fundamental equation of geodesy and Brun's formula to give the geoid undulation from gravity anomalies. The spherical form of Stokes' formula is:

$$N(\phi,\lambda) = \frac{R}{4\pi\gamma}\iint_{\sigma}\Delta g S(\psi)\, d\sigma \qquad (3\text{-}14)$$

where $N(\phi,\lambda)$ is the geoid undulation, Δg is the gravity anomaly in the solid angle $d\sigma = \sin\psi d\psi d\lambda$ and $S(\psi)$ is the Stokes' function:

$$\begin{aligned} S(\psi) &= \sum_{n=2}^{\infty} \frac{2n+1}{n-1} P_n(\cos\psi) \\ &= \frac{1}{\sin(\frac{\psi}{2})} - 6\sin\frac{\psi}{2} + 1 - 5\cos\psi \\ &\quad - 3\cos\psi \ln(\sin\frac{\psi}{2} + \sin^2\frac{\psi}{2}). \end{aligned} \qquad (3\text{-}15)$$

where p_n is the Legendre polynomial. Figure 14 shows $S(\psi)$ and $\frac{1}{2}\sin(\psi)S(\psi)$ as a function of ψ. Stokes' formula in the form of equation 3-14 assumes that the mass of the ellipsoid is equal to the actual mass of the earth, the center of the masses are collocated and the potentials are equal, $W_0=U_0$.

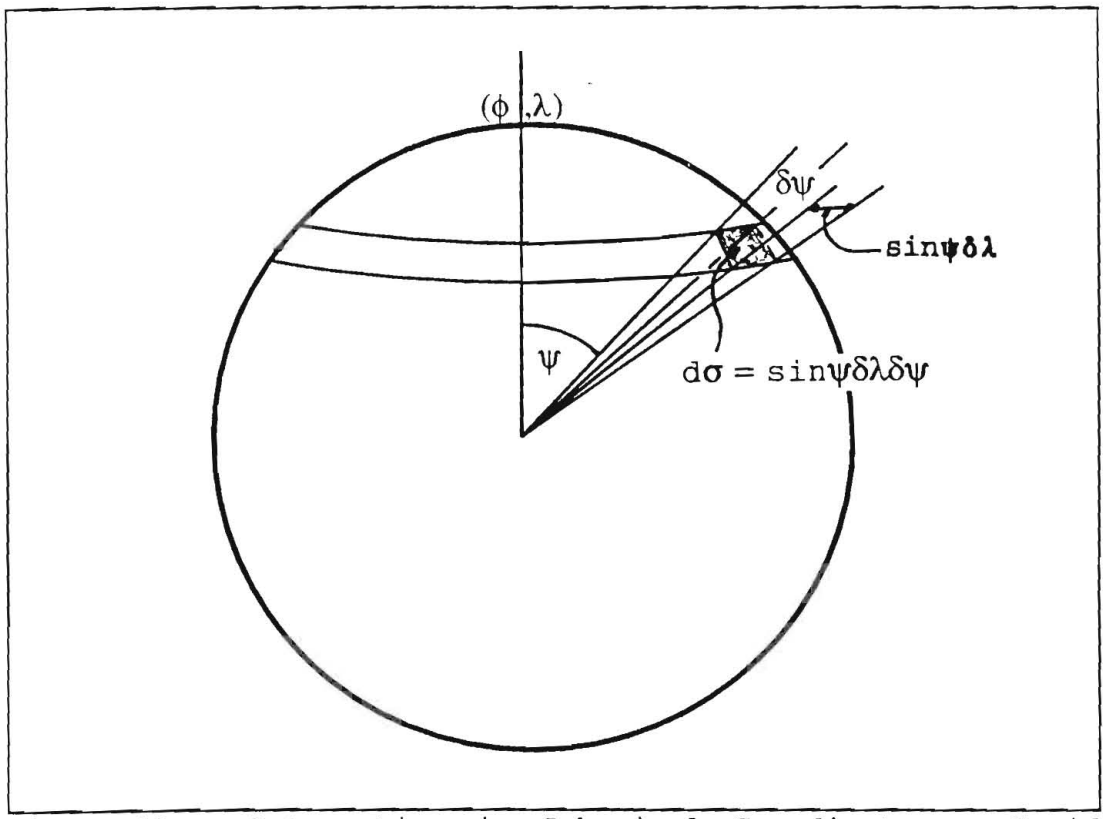

Figure 13. Integration in Spherical Coordinates: Geoid undulation is calculated at position (ϕ,λ) by integration of gravity anomalies via Stokes' formula over the sphere.

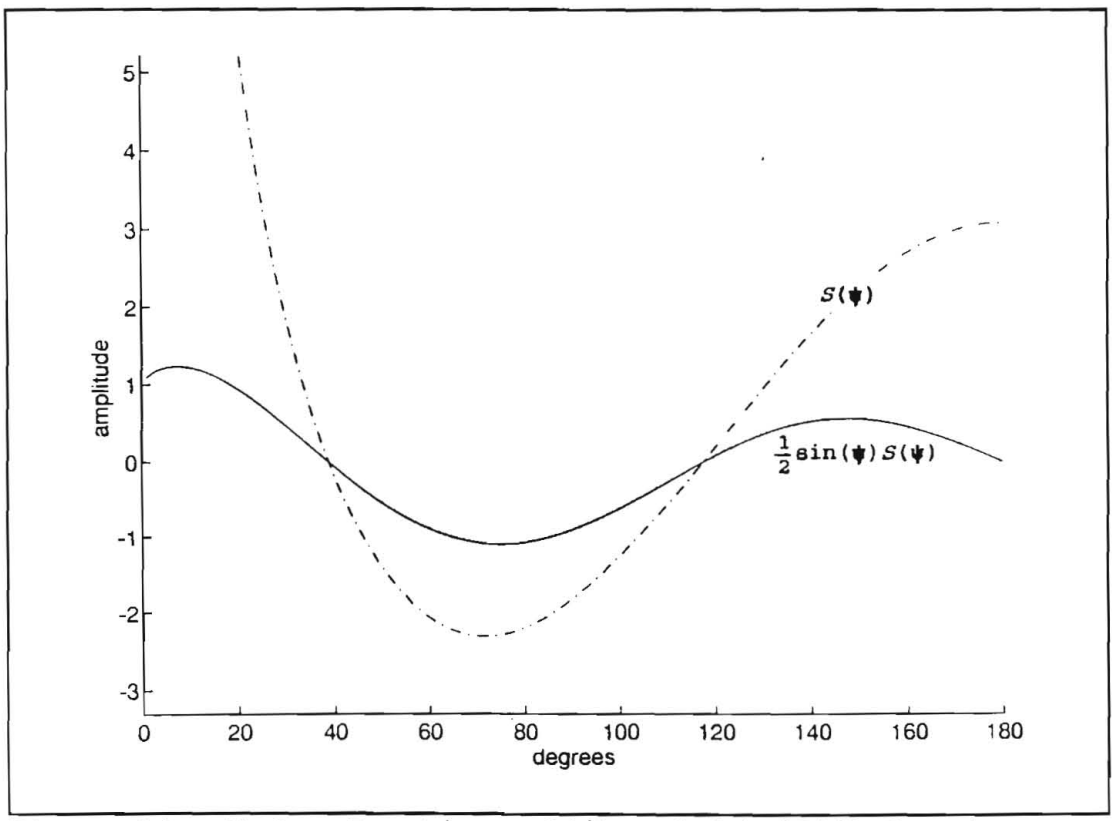

Figure 14. Stokes Function: $S(\psi)$ and $\frac{1}{2}\sin\psi S(\psi)$ for the range $0^{\circ}<\psi\leq 180^{\circ}$.

1. Limitations

The derivation of Stokes' formula followed several assumptions which lead to limitation on its application and accuracy. The assumptions are:

1. All masses are internal to the surface of the geoid.
2. The integration of Stokes' formula covers the entire earth.
3. The geoid is nearly a sphere so that the Stokes' formula has been derived and can be used in a spherical form.

The first assumption leads to the need for terrain reductions which mathematically remove masses outside the geoid. Theoretically, the second means that gravity must be known at every point over the entire earth which is not possible. However, the average gravity anomaly over increasingly larger areas, approaches zero, so the effect of distant gravity on the local undulation is less than gravity in the area of calculation (Bomford 1980). Thus, if a dense gravity survey is available locally, Stokes' integral may be applied with distant gravity which has been sampled less frequently. The error incurred by the third assumption is on the order of the deviation between the geoid and a sphere which is the flattening, f, $\epsilon \approx N \times 0.003$ (Dragomir et al. 1982).

2. Applications

Evaluations of the Stokes integral are suited for local geoid determinations such as the Monterey Bay, when a global geopotential model can be combined with a local dense gravity survey. The global model supplies the long wavelength information in the geoid so that the integration of Stokes' formula can be carried out over residual gravity anomalies and a smaller integration area. (Bomford 1980; Mainville et al. 1992) The formula representing this process is:

$$N_T = N_{GM} + \frac{R}{4\pi\gamma}\iint_{\sigma}(\Delta g - \Delta g_{GM})\sin(\psi)\,S(\psi)\,d\sigma \qquad (3\text{-}16)$$

where N_T is the total geoid undulation, N_{GM} is the global geoid undulation, Δg represents the local gravity anomalies and Δg_{GM} the global gravity anomalies (Mainville 1992). The removal of the long wavelength data in the local gravity anomalies occurs in the (Δg - Δg_{GM}) prior to evaluation of Stokes' integral. The long wavelength information is then restored by adding the N_{GM} term following the integration.

IV. METHODS

A. GENERAL

Figure 15 is a schematic of the data flow and processing used in determining the local Monterey geoid. This figure indicates that there are three types of data used in local geoid calculations; local gravity observations, terrain elevation and data derived from a global geopotential model.

The local gravity data are gravity anomalies which have been reduced from gravity observations using the free air reduction (Appendix D). The terrain data is used in determining the terrain correction. The global geopotential model provides two types of data, global geoid undulations and mean gravity anomalies. These global data sets contain the long wavelength components of the geoid. The global gravity anomalies are subtracted from the local gravity anomalies leaving residual anomalies. This residual data set should then only contain the short wavelength data in the local gravity anomalies. From this residual gravity anomaly data, residual geoid undulations are calculated which are then added to the global geoid undulations to restore the long wavelength data.

The calculation of the terrain correction, the residual gravity anomalies and extraction of the global model data was

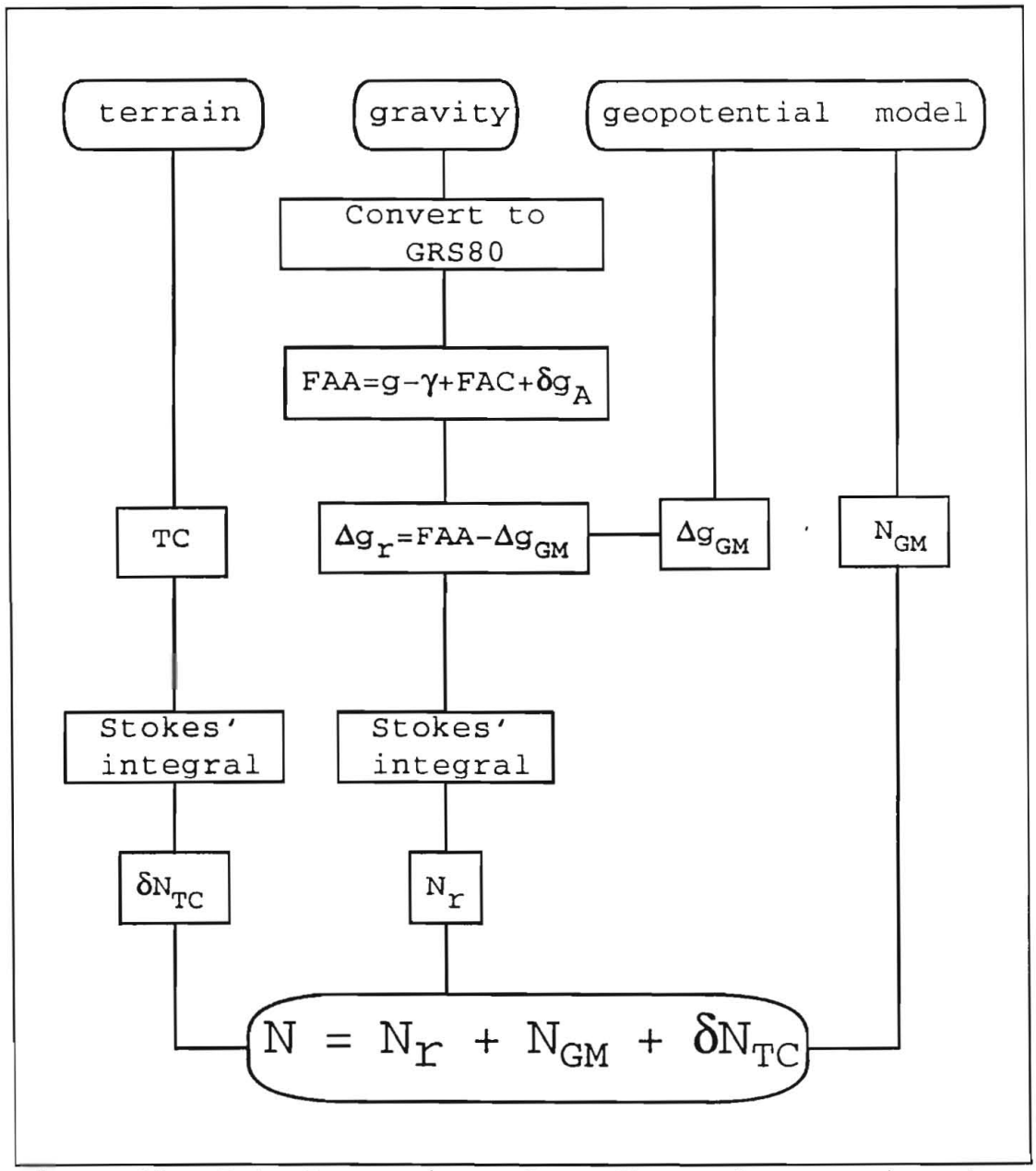

Figure 15. Data Processing: Data flow and processing steps in calculation of the Monterey Bay Geoid.

done using programs provided by Dr. Dennis Milbert of the National Geodetic Survey. The programs were written in FORTRAN and required only slight modification to run on a UNIX system. Appendix E contains a listing of the individual NGS programs and a description of the process they performed.

B. DATA

1. Gravity

a. Sources

The local gravity data used in this study came in the form of point gravity observations from three sources: 1,549 land gravity station observations from Defense Mapping Agency (DMA), 17,098 NGS land and ship gravity observation data from the National Geophysical Data Center Gravity CD-ROM (Hittleman et al. 1992) and lastly, 179 gravity observations within the Monterey Bay which came from two NPS bottom gravity surveys conducted in 1973. (Brooks 1973; Cronyn 1973) Figure 16 shows the gravity observations used in the calculation of the Monterey geoid.

b. Accuracy

All of the data sets included free-air anomalies calculated from gravity observation and station elevation. The accuracy of the data, the standard deviation of the measurements, was also contained in the data. The land data free-air anomalies had a given accuracy of 2 mgal or less. The oceanic data had a given accuracy of 3.5 to 4 mgal.

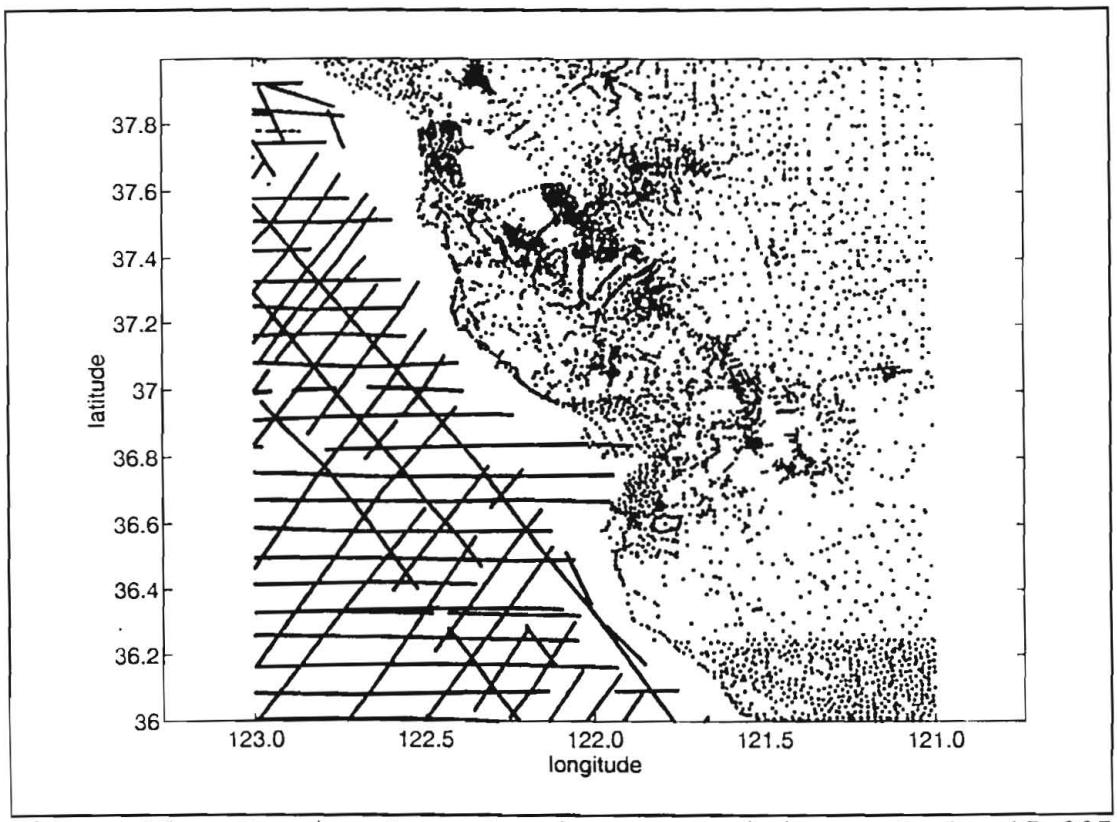

Figure 16. Gravity Data Stations: Positions of the 17,905 point gravity anomalies used in calculating the Monterey Bay geoid.

c. Preprocessing

The point gravity anomalies were converted into Helmert anomalies referenced to GRS80. The bulk of the preprocessing and editing was done through a series of FORTRAN and MATLAB programs written by the author. The three gravity data sets had to be corrected from their various reference systems to the GRS80 (DMAAC 1987) system to match the gravity anomalies and geoid heights calculated from the global geopotential model. A specific series of programs were developed to correct and edit each set of gravity data separately.

The reduction of observed gravity to Helmert anomalies require further corrections to the free-air anomalies for the effects of the atmosphere and terrain. Helmert gravity anomalies are given by:

$$\Delta g_H = g_{obs} - \gamma + FAC + \delta g_A + TC \qquad (4\text{-}1)$$

where g_{obs} is observed gravity γ is normal gravity FAC is the free-air correction, δg_A is the atmospheric correction and TC is the terrain correction.

The atmospheric correction corrects for the gravitational attraction of the mass of the atmosphere above a gravity station. The geocentric gravitational constant, GM, of GRS80 includes the mass of the atmosphere. Gravity measurements made on the surface of the earth must be

increased to remove the effect of the atmosphere. The atmospheric correction in mgal is given by:

$$\delta g_A = 0.87 \exp(-0.116 h^{1.047}) \qquad (4\text{-}2)$$

where h is the station elevation in kilometers (ibid). At sea level the correction is 0.87 mgal and it varies less than 0.15 mgal over the area of interest so that a constant 0.87 mgal may be added to all the point gravity anomalies with negligible error.

Biases between the data sets were evaluated by a point-by-point comparison of individual points which were collocated with gravity stations in the other sets. The NGS and DMA data did not show a bias. Figure 17 shows the position of the DMA and NPS data points used to determine the value of the bias in the NPS data. Figure 18 shows the same points as Figure 17 with their free-air gravity anomaly values on the vertical axis and latitude on the horizontal axis. The two curves in Figure 18 are polynomial fits for the two data subsets. The upper curve was generated by the NPS data and the lower by the DMA data. Differencing the two curves gives an approximate bias of 13 mgal which was subtracted from the NPS data.

After each gravity anomaly data set had been processed into atmospherically corrected, free-air anomalies referenced in the GRS80 system, the sets were combined. The

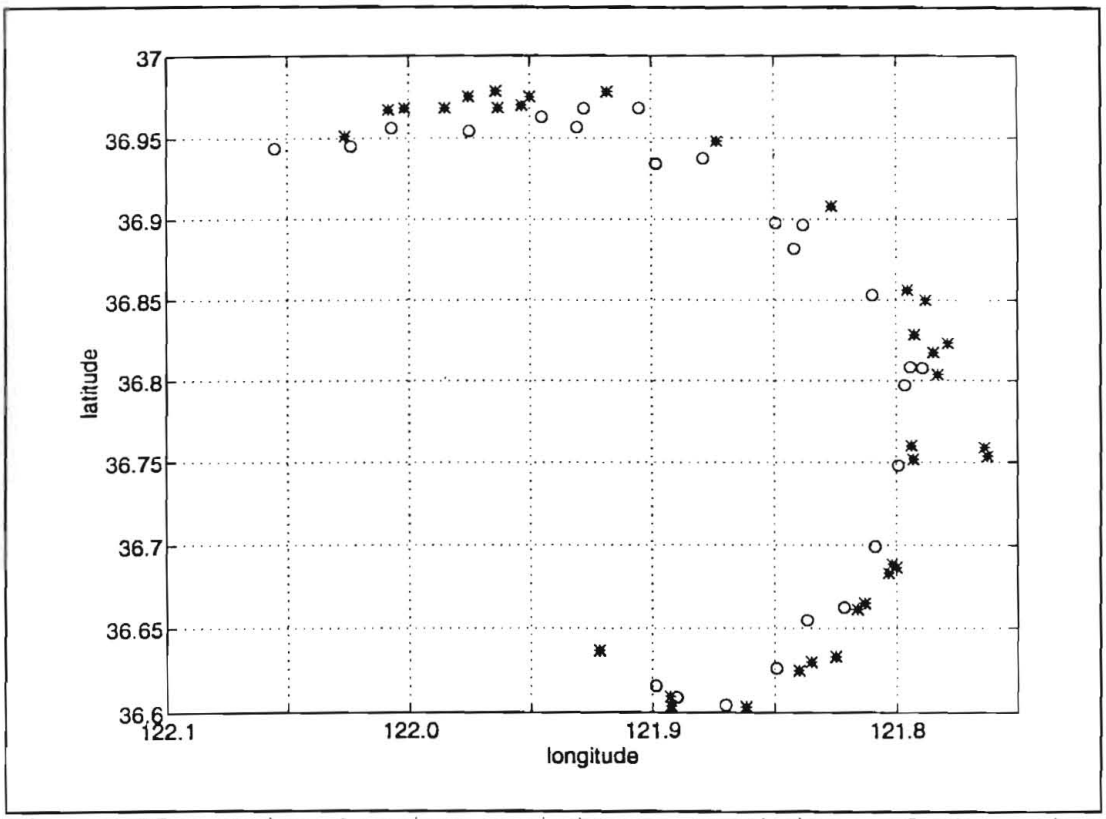

Figure 17. Point Gravity Positions: Positions of the point gravity values used in the determination of bias in NPS data. * DMA data, o NPS data.

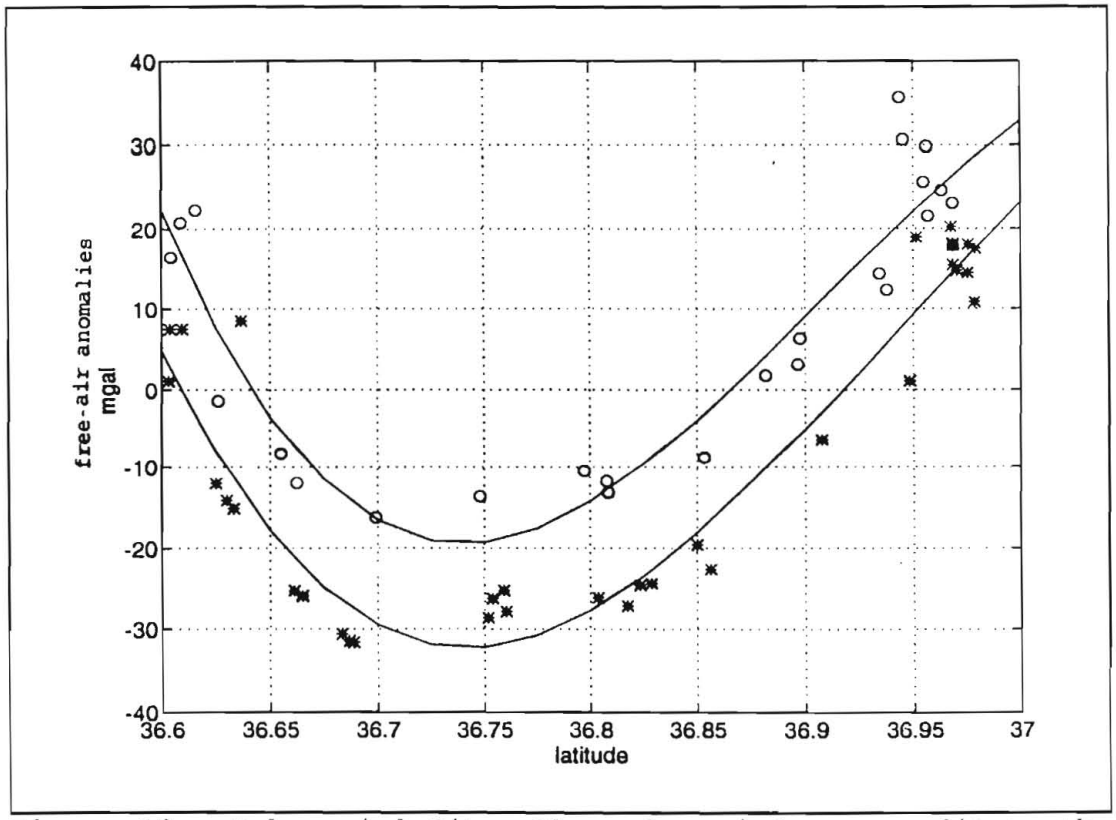

Figure 18. Polynomial Fit: The polynomial curves fit to the gravity data shown in Figure 17. The NPS data yielded the upper curve and the DMA data, *, the lower curve.

complete set contained 17,905 atmospherically corrected free-air anomalies which were then gridded at 2.5′ x 2.5′ using SURFER™ (Golden Software, Inc. 1989) over a 2° by 2° block centered on the Monterey Bay.

The gridding method used a quadrant search and a minimum curvature method with a maximum allowable error of 0.005. These gridding parameters were chosen because they eliminated some of the adverse effects caused by the variable density data. The presence of ship track data in the oceans caused a terracing effect in the gridded data when a normal search pattern was used. A normal search pattern takes the closest points to the gridding point. A quadrant search forces the process to find a specified number of points from each quadrant around the gridding point.

Figure 19 is a contour plotting of the gridded gravity anomalies. The contours, in mgal, show the agreement between the free-air anomalies and the topography. The gravity anomalies ranged in value from -92.8 mgal to 147.7 mgal.

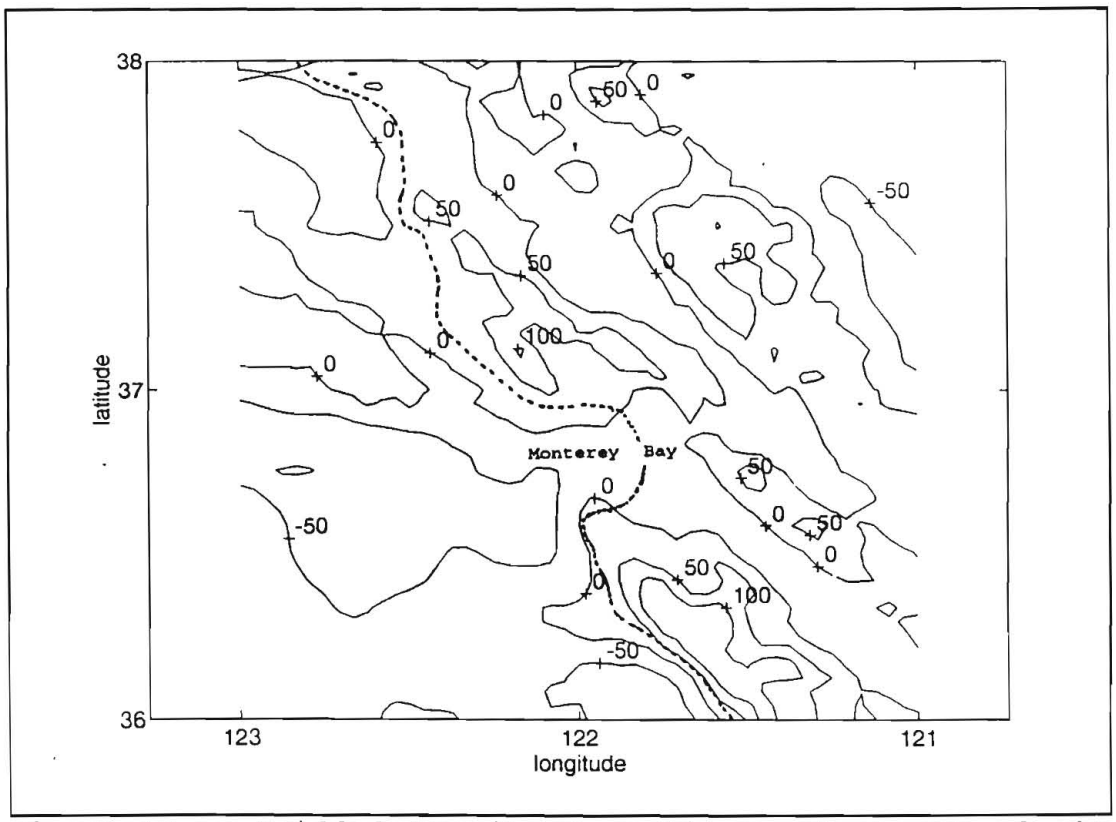

Figure 19. Gridded Gravity Anomalies: Contours of the gridded local free-air gravity anomalies in mgal.

2. Terrain

a. Sources

Terrain elevation data was from the Rocky Mountain Communications Incorporated (RMC) Three Arc Second Elevation Data CD-ROM. The RMC digital elevation data was originally produced from DMA digital terrain elevation records. (Rocky Mountain Comm, Inc. 1991)

b. Accuracy

The elevation data from the RMC CD-ROM has a resolution of 3" or approximately 100 m with the elevation given to the nearest meter.

c. Preprocessing

The terrain data was extracted from the RMC CD-ROM to a PC using a generic extraction program provided with the CD-ROM to copy 1^{o} blocks of 3" data. Each 1^{o} block was then regridded at 15" intervals using a program developed by Dr. Clynch. This program calculated the block average for each 15" area and the geographic position of the grid element. The program also converted from a DOS binary format to ASCII format so that the data could be transferred to a UNIX system. The 15" resolution represents a reasonable trade off between computer limitations and accuracy requirements of the terrain correction. Each 1^{o} block of 15" data was 1.9 MB in ASCII format. The individual 1^{o} by 1^{o} blocks were then constructed

into a single data set of 15" elevations covering an area between 34°N - 39°N and 123°W - 119°W.

3. Geopotential Model Data

a. Source

The OSU91A geopotential model was used as the source for the global geoid undulation and gravity anomalies. The full 360 degree and order expansion of the OSU91A geopotential model was used. The geopotential model coefficients and were provided by Dr. Richard Rapp of The Ohio State University.

b. Accuracy

The accuracy of the OSU91A geopotential model is 57 cm over 50 km. (Rapp 1992) This accuracy represents its RMS accuracy over the entire globe.

c. Preprocessing

The geoid undulations and gravity anomalies were extracted from the geopotential coefficients using the NGS program GRD360. This program provided the data in a format which was compatible with follow on applications. The geopotential is calculated from the normalized geopotential coefficients, $\overline{C_{nm}}$, $\overline{S_{nm}}$ by:

$$V_{GM} = \frac{GM}{r}\left[1+\sum_{n=2}^{n_{max}}\left(\frac{a}{r}\right)^n\sum_{m=0}^{n}\left(\overline{C_{nm}}\cos m\lambda+\overline{S_{nm}}\sin m\lambda\right)\overline{P_{nm}}(\sin\phi')\right] \qquad (4\text{-}3)$$

(Tscherning et al. 1983) where V_{GM} is the global model geopotential, GM is the geocentric gravitational constant, a is the semimajor axis of the reference ellipsoid, γ is the mean gravity of the reference ellipsoid, n_{max} is the number of coefficients in the model, r, λ and ϕ' are the geocentric radius, longitude and latitude of the point, $\overline{C_{nm}}$, $\overline{S_{nm}}$ are the fully normalized potential coefficients and $\overline{P_{nm}}(\sin\theta)$ are the fully normalized associated Legendre polynomials. The perturbing potential is determined by subtracting the normal potential of the GRS80 ellipsoid. The gravity anomalies and geoid undulations are then determined by Brun's formula and the fundamental equation of geodesy. Figure 20 is a contour plot of the global gravity anomalies with contours in mgal. The smooth, long wave nature of the global anomalies contrasts with the contours of the local gravity. Figure 1 was the geoid undulations extracted from the model.

When the global geopotential model gravity anomalies are removed from the local gravity anomalies, Figure 19, the range of the residual gravity anomalies becomes -80.8 mgal to 128.4 mgal. Although the range had not been reduced much, the northeast to southwest tilt was removed see Figure 21. This tilt was a long wavelength feature and its removal allows the use of a smaller integration area. Using the full 360 degree expansion of the OSU91A should remove all wavelengths greater than 1^{o} or 112 km.

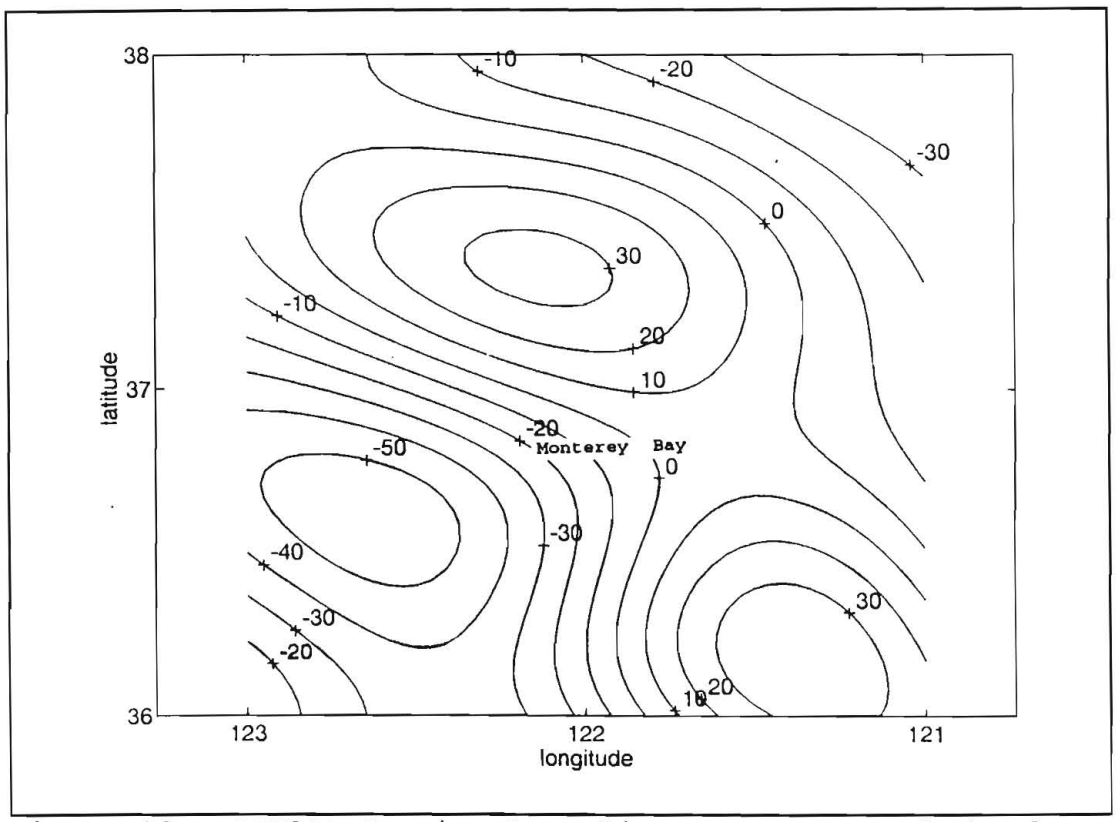

Figure 20. OSU91A Gravity Anomalies: Contours of the free-air anomalies from the OSU91A geopotential model in mgal.

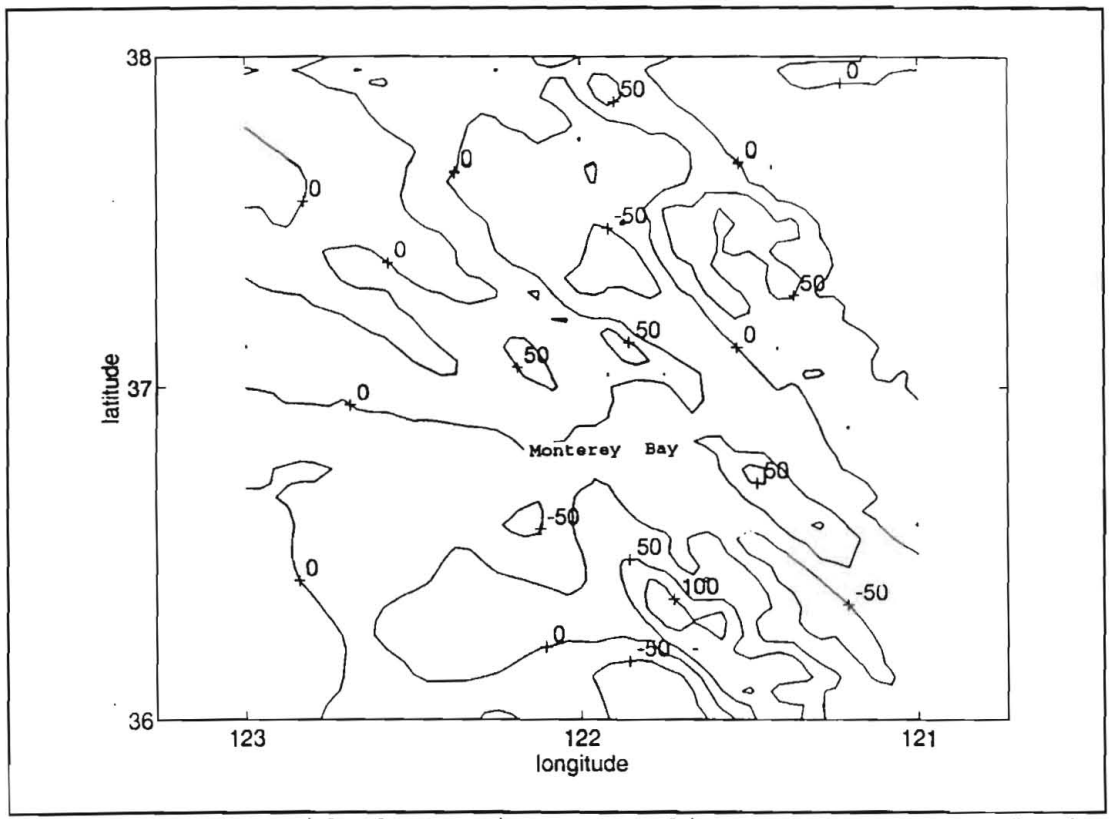

Figure 21. Residual Gravity Anomalies: Contours of the residual gravity anomalies in mgal.

C. CALCULATIONS

1. FFT Methods

The NGS programs used to calculate the terrain correction and the Stokes' integral utilizes fast Fourier transform (FFT) techniques. The application of FFT provides an efficient means of evaluating the convolution integrals involved in geodesy (Schwarz et al. 1990). FFT allows the large amounts of gridded geophysical data to be convolved in a single step rather than integrating at each point in the data. This permits a substantial savings in computer time with little loss of accuracy.

The use of FFT requires careful consideration of the data sampling and extent of data coverage used in the integrations. In order to resolve the long wavelengths contained in the geoid, data used in FFT's should technically extend to infinity. It is not possible to have an infinite data set which leads to the phenomenon known as leakage. Leakage is caused by the use of finite data sets which are not capable of resolving wavelengths which are longer than the data set and the discontinuities in the data when the values suddenly drop to zero. (ibid.)

Aliasing is a phenomenon which occurs with FFTs when the sampling rate is not high enough to resolve the short wavelengths of in the data. Aliasing is the appearance of low frequency data which is actually caused by data that contains

information at a higher spatial frequency than the sampling rate could resolve. The Nyquist frequency is the highest frequency which a sampling interval can resolve. Nyquist frequency is:

$$f_N = \frac{1}{2\Delta x} \qquad (4\text{-}4)$$

where Δx is the spatial resolution of the data. To avoid aliasing, data should be sampled at a rate at least twice as high as the highest frequency. (ibid.)

The highest spatial frequency components in the geoid are caused by the local topography (Forsberg 1984). The Monterey Submarine Canyon is the sharpest topography in the area of interest. The width of 10 km at the Bay's mouth suggests that the canyon would cause a geoid undulation with a wavelength of approximately 10 km. The local gravity is gridded at 2.5 minutes or 4.63 km which should resolve any undulation caused by the canyon.

The leakage is controlled by removing the long wavelength information in the raw gravity anomalies. The long wavelength information is removed by subtracting the gravity anomalies from the global geoid model. Leakage is also controlled in the gravity and terrain by tapering and padding the data sets. Tapering is the process of smoothly reducing the edge of the data to zero. Padding adds a border of zeros to the data set. The terrain and residual gravity data were

tapered using a ten percent split cosine bell taper and padded 50 percent. Figure 22 is a plot of the taper used. Leakage with gravity data tends to be less of a problem than is other fields because the spectrum of gravity tends to decay smoothly (Schwarz 1990).

The result of this process is a 4° by 4° grid with the central 2° by 2° grid containing data. The geoid will be calculated from this 4° by 4° grid with only a central 0.5° by 0.5° area considered a valid solution.

Following the preprocessing, the terrain correction and Stokes' integral were calculated by the programs provided by NGS. These programs utilized the Cooley-Tukey FFT algorithm.

2. Terrain Correction

The terrain correction should not be confused with the terrain reduction. The terrain reduction is the complete process of removing the effects of masses external to the geoid from observed gravity. The terrain correction is a part of the terrain reduction. It corrects the measured gravity for the effects of terrain undulations above and below the gravity station. The terrain correction always increases observed gravity. Consider a gravity station on the side of a mountain, Figure 23, the mass of the mountain above the station will have a gravitational attraction upward reducing observed gravity. The lack of crustal material below the

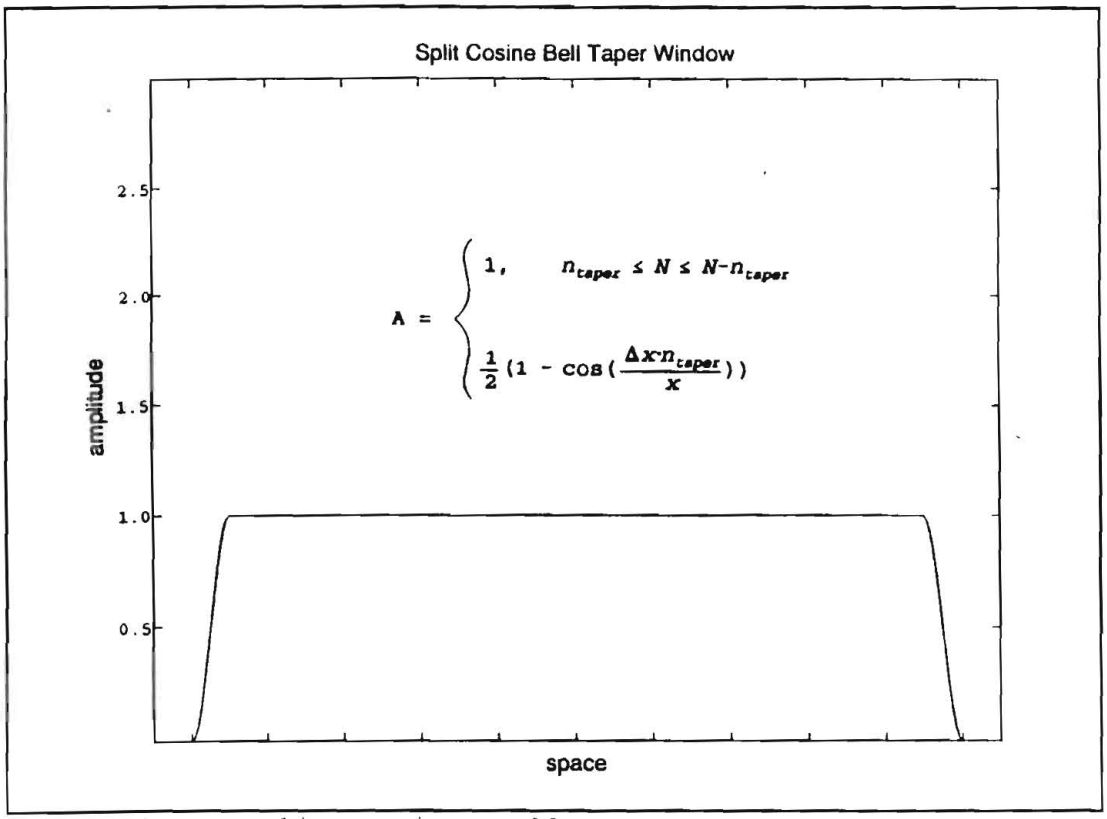

Figure 22. Split Cosine Bell Taper: A is the amplitude weighting, Δx is the grid resolution, n_{taper} is the number of grid elements tapered and x is the size of the grid.

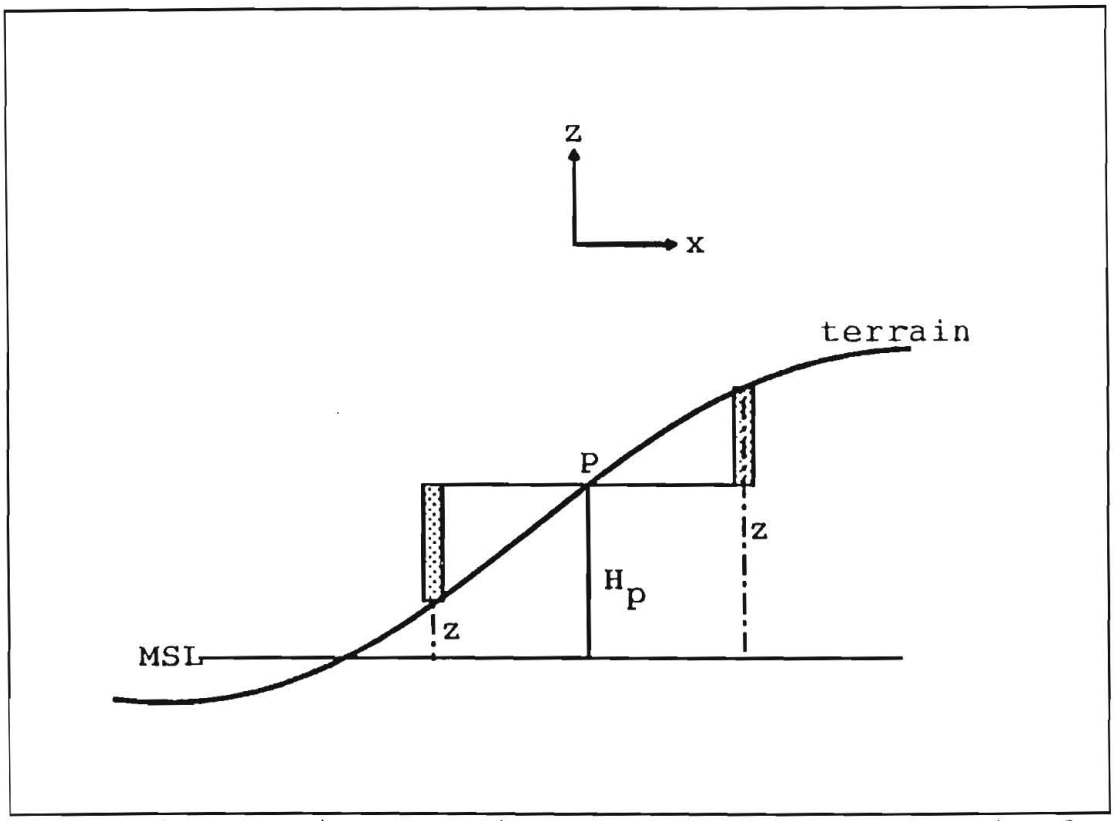

Figure 23. Terrain Correction: Corrects observed gravity for the slopes in the topography, Z is the terrain elevation and h_p is the elevation of the gravity station.

gravity station will form a mass deficiency below the station and reduce the observed gravity. To correct these effects the terrain correction must increase the value of the observed gravity. The terrain correction is given by:

$$TC = G\rho \iint_{z\,x} \frac{(z-H_p)}{r^3} dzdx \qquad (4\text{-}5)$$

where z is the terrain elevation and H_p is the elevation of the gravity station (Forsberg 1984). The amplitude and spatial frequency of the terrain correction represents the ruggedness of the terrain. It amplifies the ruggedness of the terrain and falls off rapidly away from mountains. The terrain correction is usually an order of magnitude smaller than the free-air correction. (ibid.)

a. Linear Approximation of the Terrain Correction

Linear approximation of the terrain correction simplifies the calculation and allows the use of FFT techniques. In all but the most rugged of terrain the linear approximation will give sub mgal accuracies when coupled with a high resolution digital terrain model. (ibid.) The error between the exact terrain correction and the linear approximation can be bound by looking at the worst case example of a gravity observation taken on the top of a cone shaped mountain. The error in the linear approximation for this is:

$$\Delta TC = 2\pi G\rho H(\sin\theta - \tan\theta) \qquad (4\text{-}6)$$

where H is the height of the gravity station and θ is the slope of the cone shaped mountain (ibid.) Putting in worst case values for the local area, H = 1500 m and $\theta = 15^{o}$ gives a relative error of 0.0015 mgal. This indicates that the linear approximation can be used in the local area.

b. Terrain Resolution Requirements

Schwarz (Schwarz et al. 1990) found that "...for RMS accuracies better than one mgal...the terrain has to be sampled at spacings of 0.5 kilometers or less, in areas of rough topography". Their results came from the Kananaski region of the Canadian Rocky Mountains which has elevation ranges from 1400 m to over 3400 m. This would indicate that using a 15" (450m) grid for the Monterey geoid calculation should accurately determine the terrain corrections to less than 0.5 mgal. Using a finer grid would at most give an improvement of 0.2 - 0.3 mgal with substantial increases in computer memory requirements. (ibid.)

c. Calculation

The NGS program, FTC2, was used to calculate the terrain correction from a grid of 15" by 15" terrain elevation data program. FTC2 uses a linear approximation and constant terrain elevation grid spacing in calculating the terrain correction. Processing of the entire tapered and padded

terrain data set, required approximately 40 minutes on a UNIX work station. The output of the terrain correction was a 15" by 15" grid of terrain corrections in mgal covering the entire terrain data set plus the 50 percent taper. A sub set of this grid was taken which was the 1° by 1° area, 37.3°N - 36.3°N, 237.5°E - 238.5°W, centered on the Monterey Bay. Figure 24 shows a three-dimensional plot of the terrain correction. The maximum values and spatial frequencies are found in the mountainous areas. The high spatial frequency is a result of the $1/r^3$ kernel of the terrain correction. The maximum value is approximately 24 mgal with the values tapering to zero over the water.

The 1° by 1° grid of terrain corrections was padded, tapered and the Stokes integral evaluated over it to determine the effect of terrain correction on geoid undulations. This processing revealed that the maximum effect was 3 cm or less within Monterey Bay and the total variation over the Bay was less than 1.5 cm and less than 1 cm for the majority of the Bay. Figure 25 is a contouring of the terrain correction undulation with contours in meters. Because of this small variation in the area of interest, it was decided to use a constant value of 2 cm for the terrain correction undulation and add that to the residual undulation rather than adding the mgal values to the point gravity anomalies. The calculation can be split in this manner because the Stokes integral is a linear process.

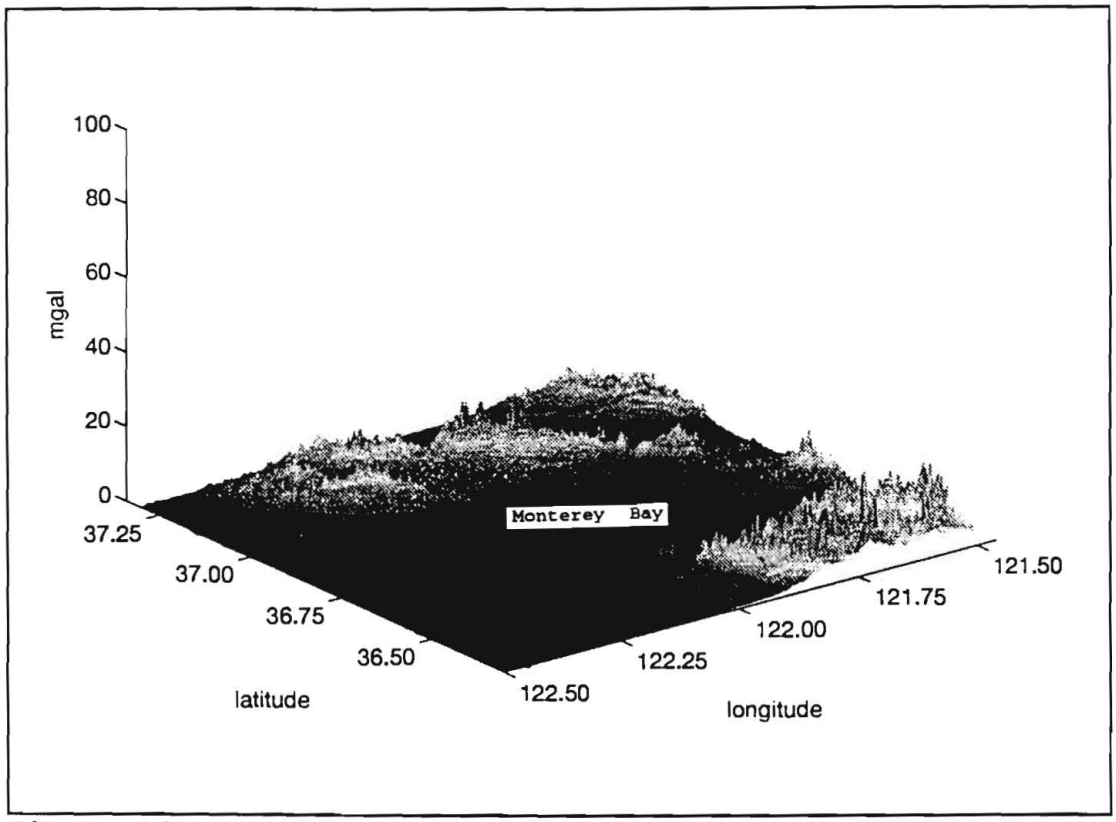

Figure 24. The Terrain Correction: 3-D plot of the calculated terrain correction, emphasizes the ruggedness of the terrain by its magnitude and spatial frequency.

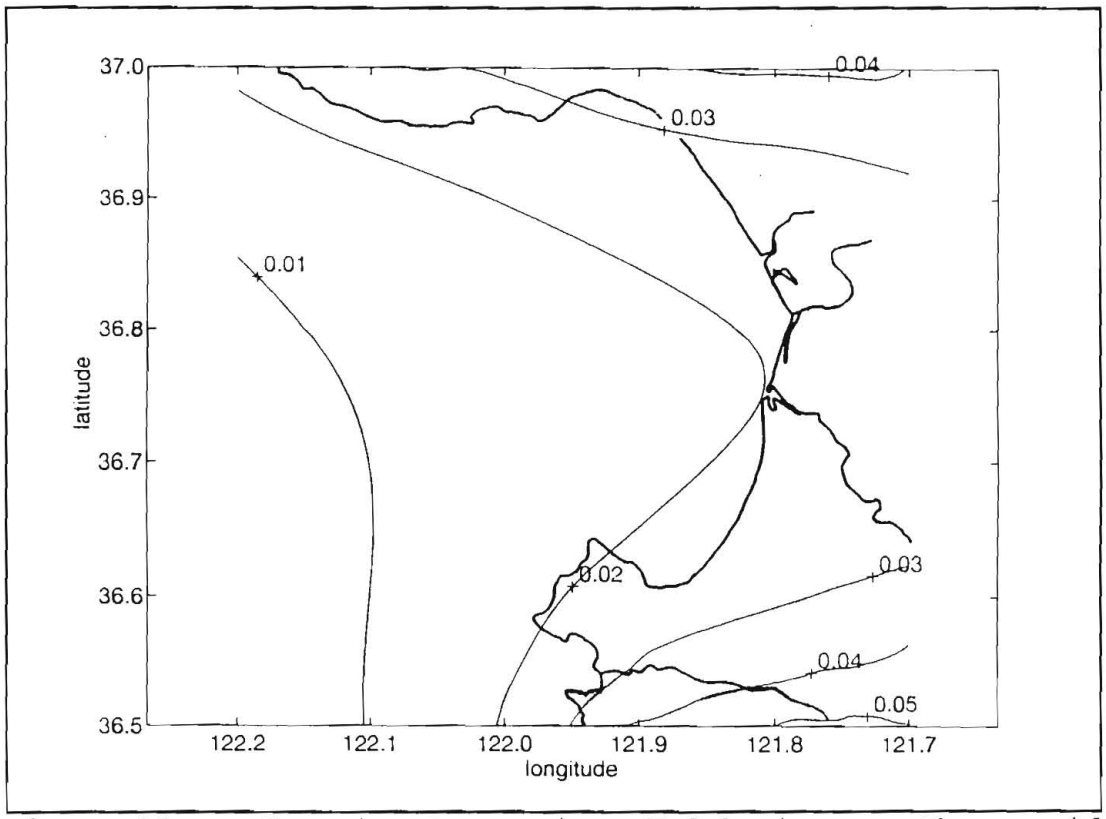

Figure 25. Terrain Correction Undulation: The geoid undulation effects calculated from the terrain correction, contours in meters.

3. Geoid Undulations

The actual calculation of the geoid was carried out in a series of steps. First, a residual geoid is calculated from the residual anomalies which contains only short wavelength data. To the residual geoid, the constant terrain correction undulation of 2 cm was added. The complete geoid was then constructed by adding the long wavelength features from the OSU91A geopotential model geoid undulations.

The residual geoid undulations were computed by the NGS programs MAKSTO and RESGEO. MAKSTO uses the padded and tapered residual anomaly grid in calculating the Fourier transform of the Stokes function on the grid. The output is a grid of the transformed Stokes function or kernel. Stokes' formula is diverges at $\psi = 0$ so that the gravity anomaly of the calculation point is skipped by setting the value of the kernel equal to zero. The effect of the skipped gravity anomaly is added separately in the RESGEO Program.

The RESGEO program calculates the residual geoid heights using the inputs of the padded and tapered residual anomaly grid and the grid of the transformed Stokes function from MAKSTO. RESGEO convolves the residual anomaly grid and Stokes kernel in the frequency domain and calculates the effect of the inner zone, $\psi = 0$, skipped in MAKSTO in the space domain. The effect of the inner zone gravity anomaly is calculated by:

$$N_i \approx \frac{\Delta x/2}{\gamma} \Delta g \qquad (4-7)$$

where Δx is the grid element size and Δg is the gravity anomaly of that element. These are then added and output to a grid of residual geoid heights. Figure 26 is a plot of the calculated residual geoid height with contours in meters. The residual geoid height ranged from -0.63 m to 1.13 m. The total local geoid was then constructed by adding the residual geoid undulation, the terrain correction undulation of 2 cm and the geopotential model geoid undulation.

D. SOLUTION STABILITY

To determine if a large enough data grid was used in the calculation of the geoid the stability of the solution was checked by examining the relative difference between solutions using different data set coverage. Two separate geoids were calculated, one using a 1° by 1° grid of gravity data and the second using a 2° by 2° grid of gravity data. These solutions were then differenced over the 1° block centered on Monterey Bay. Figure 27 shows the difference between the two solutions where the 1° by 1° solution has been subtracted from the 2° by 2° solution. What Figure 27 shows is that there are substantial differences between the solutions on the edges, especially where data from mountainous areas was neglected by the 1° solution. The large difference in the northeast corner

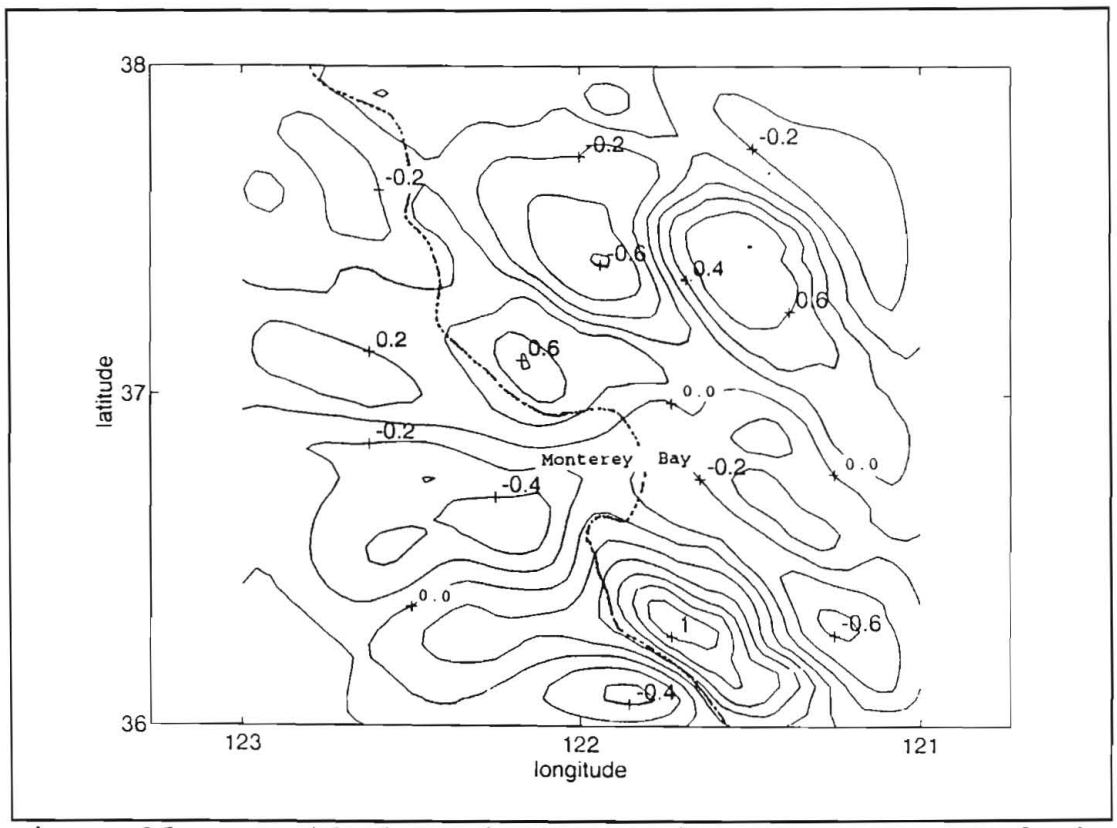

Figure 26. Residual Geoid Undulations: Contours of the residual geoid in meters.

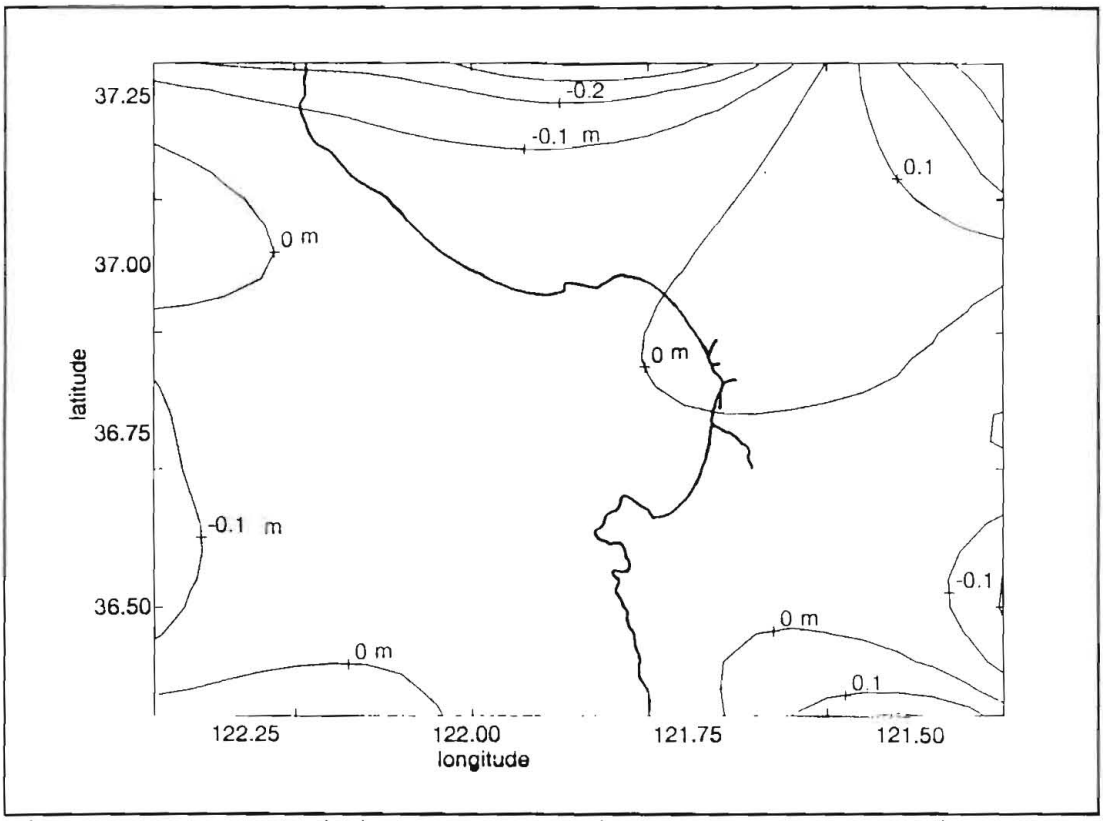

Figure 27. Stability of Solution: Contoured difference between two geoids, one calculated from a 2 deg x 2 deg grid of gravity data minus one from a 1 deg x 1 deg grid in meters.

is caused by the Diablo Mountain Range which is just beyond the 1° block.

The stability analysis shows that the solution is stable in the central region and that the use of a 2° by 2° grid of data should be sufficient to calculate the geoid in the center half degree block of the area. This is not a general result and may not hold in a location with more variation in the gravity/topography. The net result of Figure 27 is that increasing the spatial coverage of the data used to calculate the geoid in Monterey Bay is not necessary.

E. ERROR PROPAGATION

The accuracy of the final geoid undulation is determined by the propagation of errors from the gravity anomaly grid through the Stokes integral. The primary source of error in the calculation of a local gravity anomaly grid is often the lack of a uniform, dense gravity survey. (Moritz 1974) This leads to interpolation errors when mean gravity anomalies are calculated in areas with sparse gravity measurements; such as, ocean areas. The transition from an area of dense data coverage to less dense data coverage, such as in the southeast corner of Figure 16, can also cause errors in the gridded values. This effect was examined in a paper by Smith (Smith and Wessel 1990) and may be an explanation for some of the differences between the calculated geoid and GEOID93 which will be discussed in Chapter V. When a dense, uniform

distribution of gravity data is available, as in the Monterey Bay and surrounding area land surveys, the primary source of error becomes the measurement error in the gravity data.

The propagation of the anomaly error through the Stokes integral was examined by Moritz (ibid.). The variance of the geoid undulations caused by errors in the gravity anomaly data is given by:

$$\sigma_N^2 = \frac{\Delta x^2 \sigma_{\Delta g}^2}{4\pi\gamma^2} \int_{\psi_o}^{\sigma} [S(\psi)]^2 \sin\psi d\psi \qquad (4\text{-}8)$$

where σ_N is the standard deviation of the geoid undulations, Δx is the grid element size of the gravity anomaly grid, $\sigma_{\Delta g}$ is the standard deviation of the mean gravity anomalies. The integral is undefined at $\Psi = 0$ so Ψ_o which neglects the first grid element or the inner zone is used as the lower integration limit. (ibid.) The value of the integral is dominated by the value at the lower bound and the lower bound is determined by the grid resolution, Δx.

When a geopotential model of degree k is available to remove long wavelength effects, equation 4-8 is changed to:

$$\sigma_N^2 = \frac{\Delta x^2 \sigma_{\Delta g}^2}{4\pi\gamma^2} \left[\sum_{n=k}^{n_o} \frac{2(2n+1)}{(n-1)^2} \right] \qquad (4\text{-}9)$$

where $n_o \approx R\pi/\Delta x$, R is the radius of earth and the integral has been expanded in Legendre polynomials, equation 3-15 (ibid.). For the local application with $\sigma_{\Delta g} \approx 4.0$ mgal, $\Delta x \approx$ 5 km and k = 360, the error on the geoid undulation from the errors in the gravity measurements is $\sigma_N \prec 2$ cm.

Other sources of error include the addition of a constant value for the terrain correction undulation and neglecting the indirect effect. The error from adding a constant 2 cm to the geoid undulations to model the terrain correction results in a maximum error that is bound by the amount of variation in the terrain correction in the area of interest. The maximum variation in Monterey Bay is less than 1.5 cm so the error is estimated to be less than 1.5 cm.

The indirect effect is a consequence of the terrain reduction. The shifting of mass from the exterior of the geoid to the surface of the geoid changes the potential of the geoid. This change in potential displaces the geoid in the same fashion as the perturbing potential. The indirect effect is given by:

$$\delta N = -\frac{\pi G\rho}{\gamma} h^2 \leq -6x10^{-8}h^2 \qquad (4\text{-}10)$$

where h is the terrain elevation in meters (Heiskanen and Moritz 1967). The indirect effect can be neglected in the local geoid calculation with the error being less than 1 cm and zero over the water. These error sources combine to give a theoretical error estimate of less than 3.5 cm on the geoid undulations of the local geoid.

V. RESULTS AND CONCLUSIONS

A. GENERAL

In this chapter, the results obtained during the work will be reviewed. This will primarily be done by interpretation of the various figures which help illustrate the results. The differences between the local geoid and GEOID93 will be examined to see how well they match in the local area. The results of a GPS sea surface height experiment will be compared to the calculated local geoid heights. Finally, some conclusions will be made about the results and recommendations for improvement and further study.

B. RESULTS

For clarity, the final results are broken in to two geoids; the Monterey geoid which is the 2° by 2° block centered on Monterey Bay and the Monterey Bay geoid which is the half degree block centered on Monterey Bay. The Monterey geoid will be used to point out some of the more general features in the local geoid which are not as clear in the smaller Monterey Bay geoid. The perimeter of the Monterey geoid should be treated as a qualitative only.

1. Monterey Geoid

Figure 28 is a 2° by 2° block, 36.0^0N-37.8^0N, 123.0^0W-121.0^0W, roughly centered on Monterey Bay. Figure 28 is the

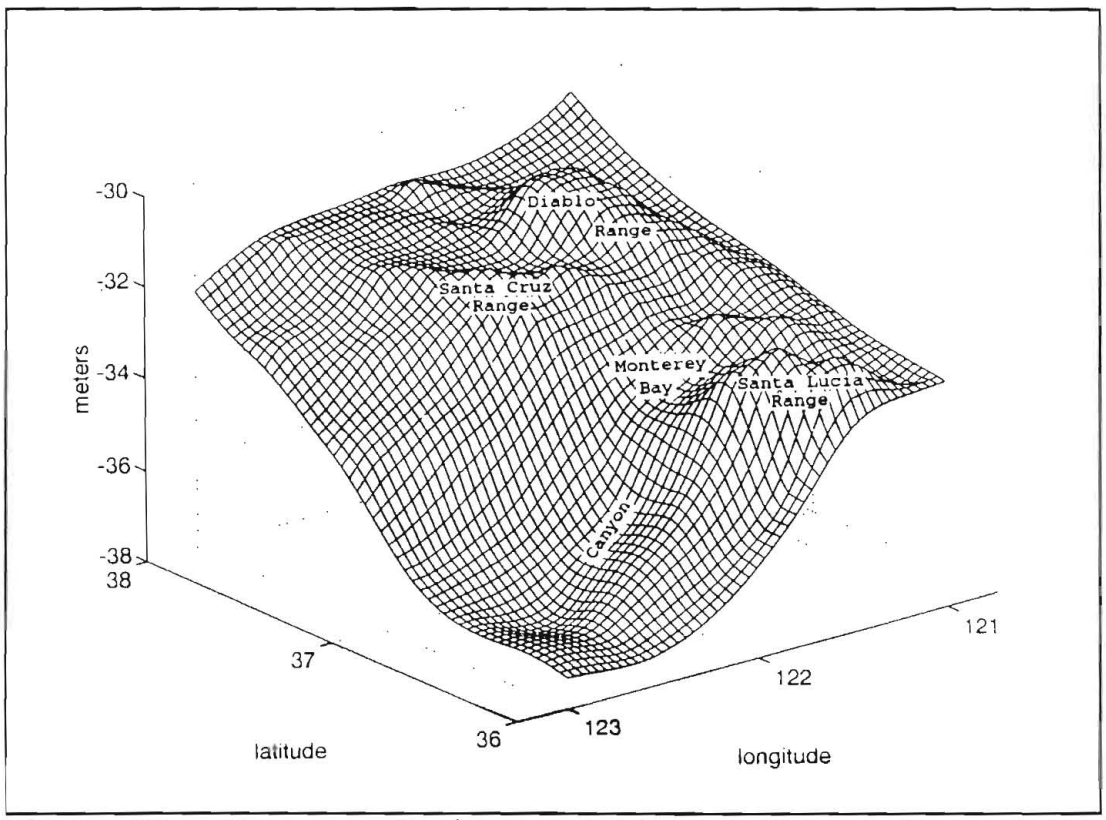

Figure 28. Monterey Geoid Undulations: The surface of the calculated geoid for the 2°x2° data area.

surface of the Monterey geoid referenced to the GRS80 ellipsoid. The figure shows a general slope in the geoid from the northeast to the southwest which is consistent with its location on the continental slope.

The local effects of the terrain show up as lumps in the geoid surface. The local mountains cause local perturbations in the geoid which mimic the actual topography. The effects of the Santa Cruz and Santa Lucia mountain ranges are clearly visible in the figure. A comparison of Figures 3 and 28 show that the local geoid from GEOID93 and the calculated geoid are very similar. Differences can be seen along the edges where tapering the gravity data caused a corresponding tapering of the undulations in the calculated geoid.

2. Monterey Bay Geoid

The Monterey Bay geoid is the surface of the calculated geoid within the geographic limits of 37^0N-36.5^0N, 122.2^0W-121.7^0W. The estimated theoretical accuracy of the Monterey Bay geoid is 3.5 cm or better with a 5 km resolution. Figure 29 is a three dimensional plot of the Monterey Bay geoid and Figure 30 is a contour plot. The general slope within the Monterey Bay is oriented north to south with the south lower. In the southwest portion of the bay the slope

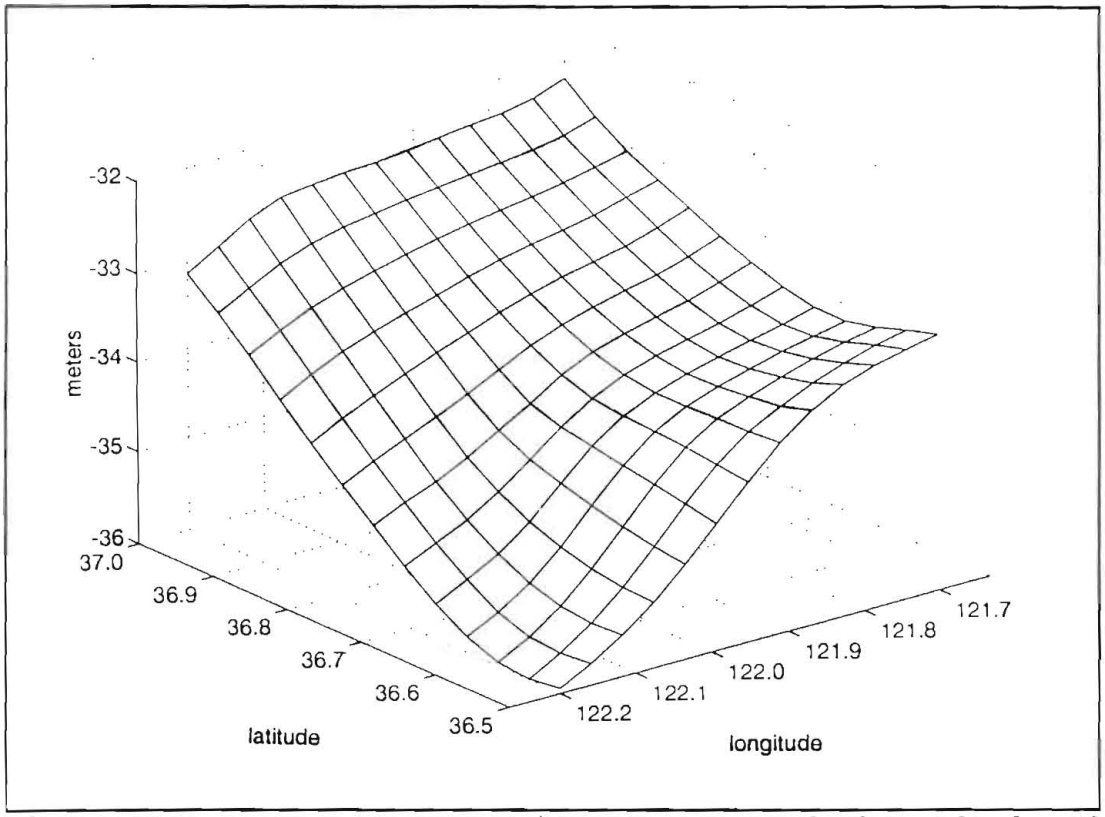

Figure 29. Monterey Bay Geoid: Surface of the calculated geoid for the .5° x .5° area centered on the Monterey Bay.

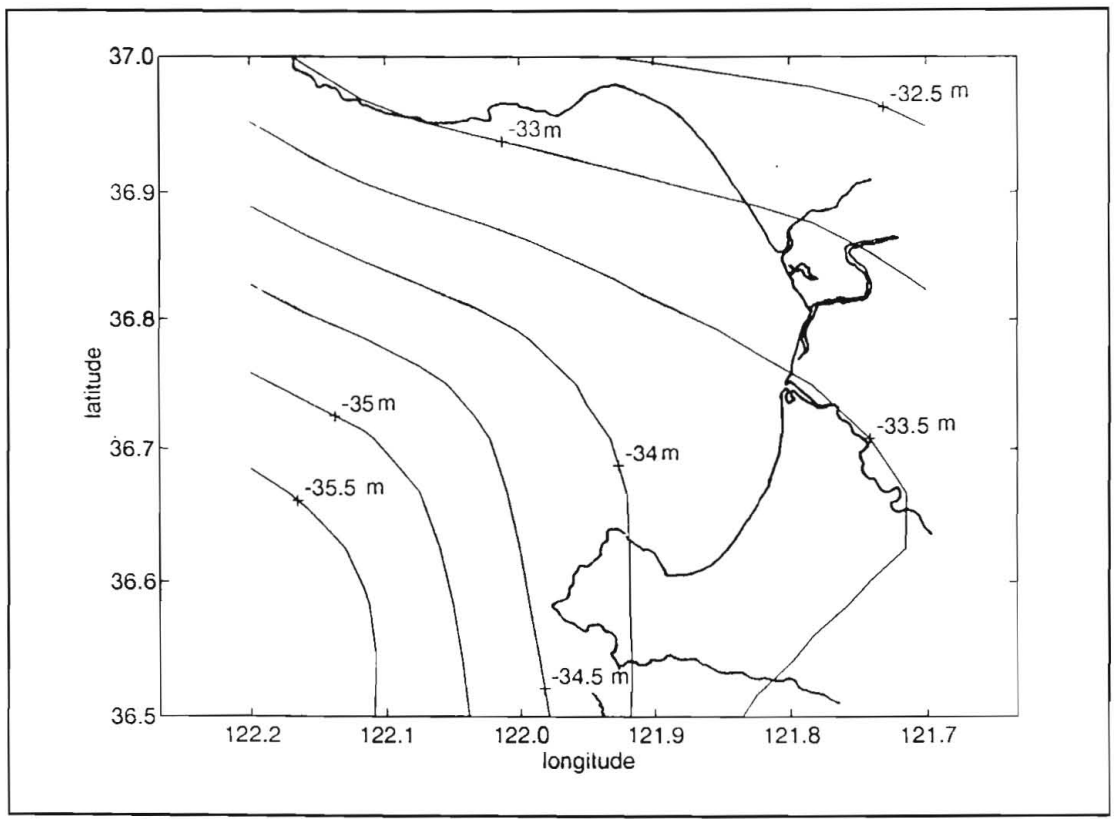

Figure 30. Monterey Bay Geoid: Contours of the Monterey Bay geoid in meters.

begins to become more east-west to parallel the continental slope. The sharp elbowing of the contour lines in the southeast corner is caused by the Santa Lucia Mountains. The Monterey Submarine Canyon does not appear to cause an undulation in the geoid which is measurable by the gravimetric method utilized. This means that to 3.5 cm any sea surface topography associated with the canyon will be the effect of the interactions between the ocean and the topography.

C. COMPARISON WITH GEOID93

To compare the local solution for the geoid with the regional geoid, GEOID93, the two geoids were differenced, calculated geoid minus GEOID93, on the 2° by 2° grid 36°N - 38°N, 123°W - 121°W and the differences contoured in Figure 31. Figure 31 emphasizes the edge effects and the effects of sparse gravity data. The area in the southeast with differences of 20 - 40 cm coincides with an extended area of sparse point gravity data see Figure 16. This suggests that differences in the gridding process for the gravity data may have dealt with the problem of variable density data differently or that different gravity data sets were used for the calculation of GEOID93. (Milbert priv. comm. 1994) The change in the density of gravity coverage can degrade the accuracy of a gridding process by causing edge effects in the gridded gravity data (Smith and Wessel 1990). GEOID93 gravity data was gridded using a minimum curvature spline in tension

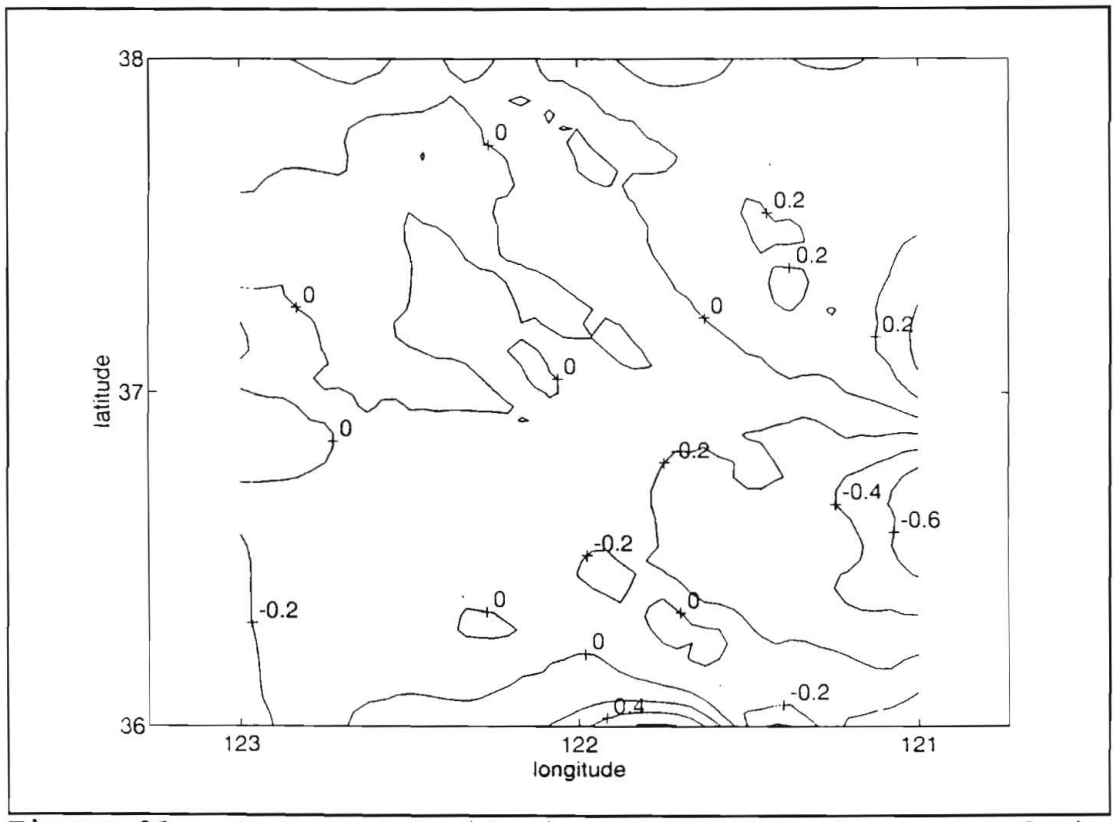

Figure 31. Monterey Geoid minus GEOID93: Contours of the difference in the Monterey Geoid and GEOID93 geoid surfaces in meters. 2° x 2° area centered on Monterey Bay.

with a tension value of 0.75 (Milbert 1991). The gridding process used for the local geoid used a minimum curvature with maximum allowable error 0.005 to calculate the gridded gravity anomalies.

Comparing the contour plots of the Monterey Bay geoid, Figure 30, and the GEOID93 contours for the same area, Figure 32, indicates that there is generally good agreement between the two geoid models. The only clear differences are a slight displacement in the contours and sharper elbowing in the 33.5 m contour of the Monterey Bay geoid.

To examine the differences closer the two geoid models were point by point differenced, calculated geoid minus GEOID93 and the contours of the difference are plotted in Figure 33. A relative slope across the Bay between the two geoids becomes apparent in Figure 33. This relative slope between the two geoids qualitatively matches the anomalous sea slope seen in a GPS transect of the Bay (Appendix F).

D. COMPARISON WITH GPS SEA SURFACE HEIGHTS

A GPS sea surface topography experiment was conducted October 26, 1993 on board the *R/V Pt. Sur*. Appendix F contains additional information on the experiment. The experiment was conducted to investigate the residual sea surface topography between the tide gauges in Santa Cruz and Monterey. Figure 34 shows the transect GPS stations occupied

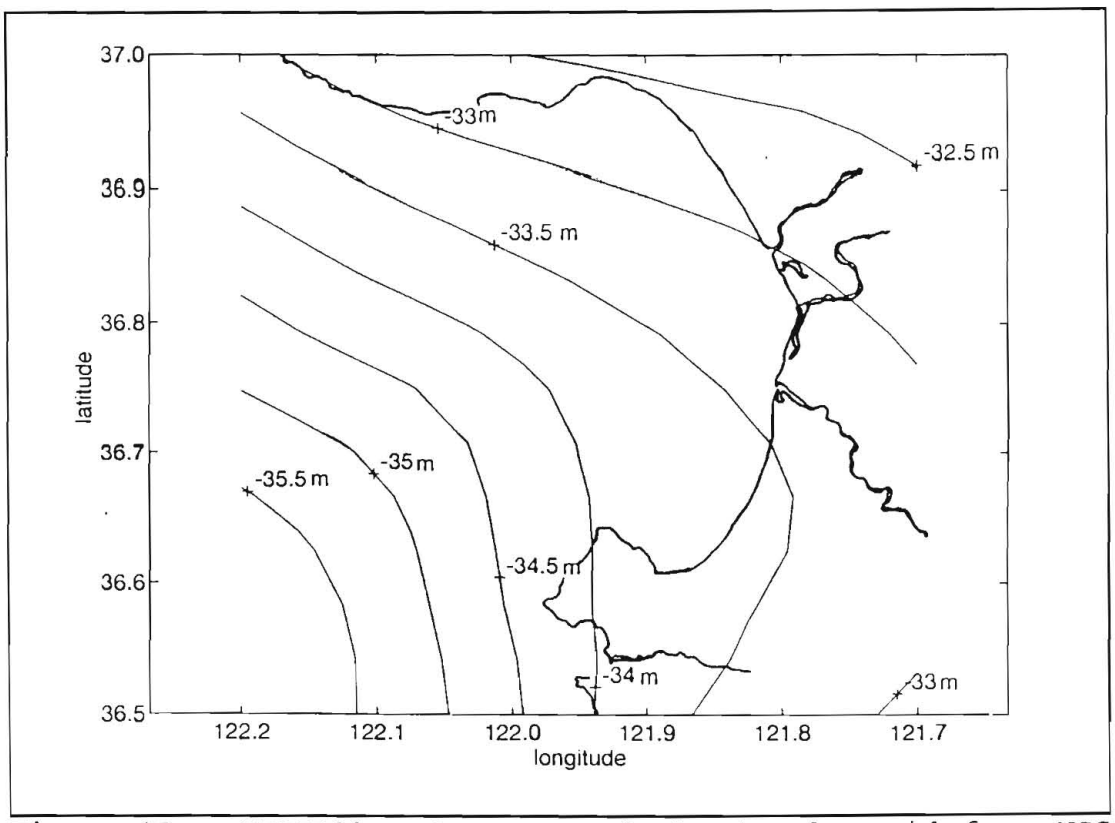

Figure 32. GEOID93: Contours of the local geoid from NGS GEOID93 geoid model in meters.

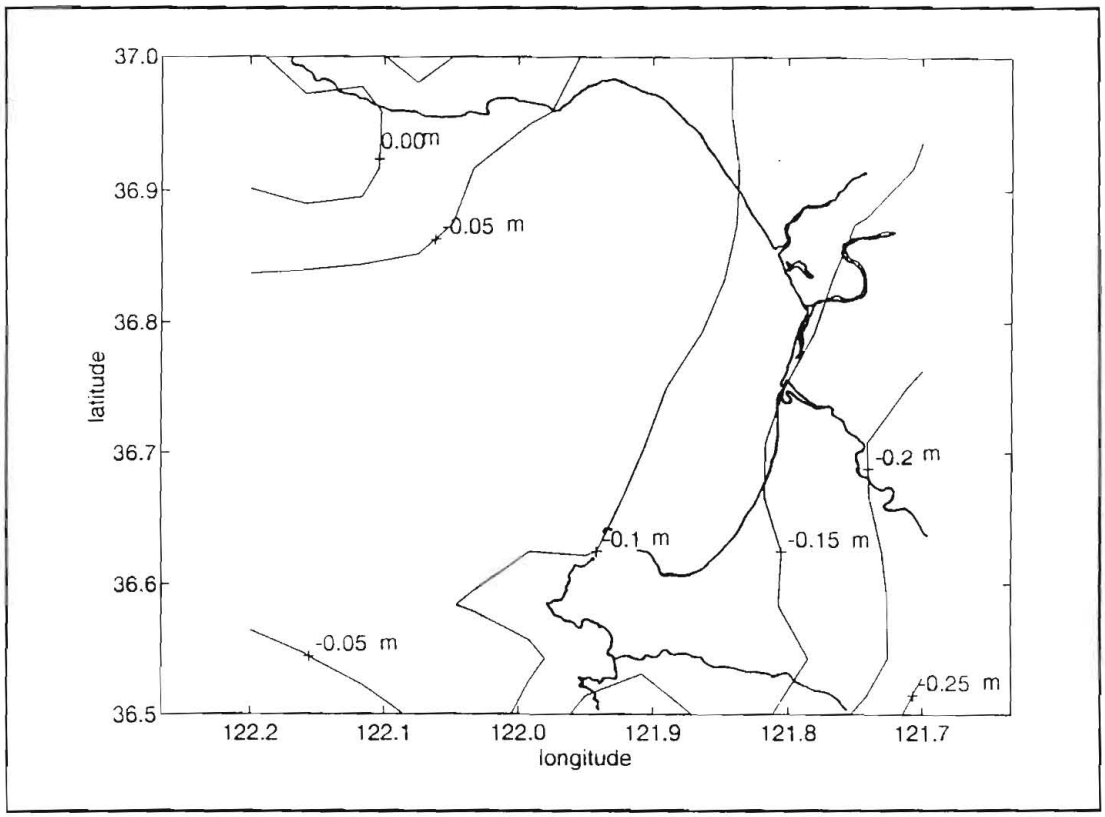

Figure 33. Monterey Bay Geoid minus GEOID93: Contours of the relative separation of the two geoid models in meters.

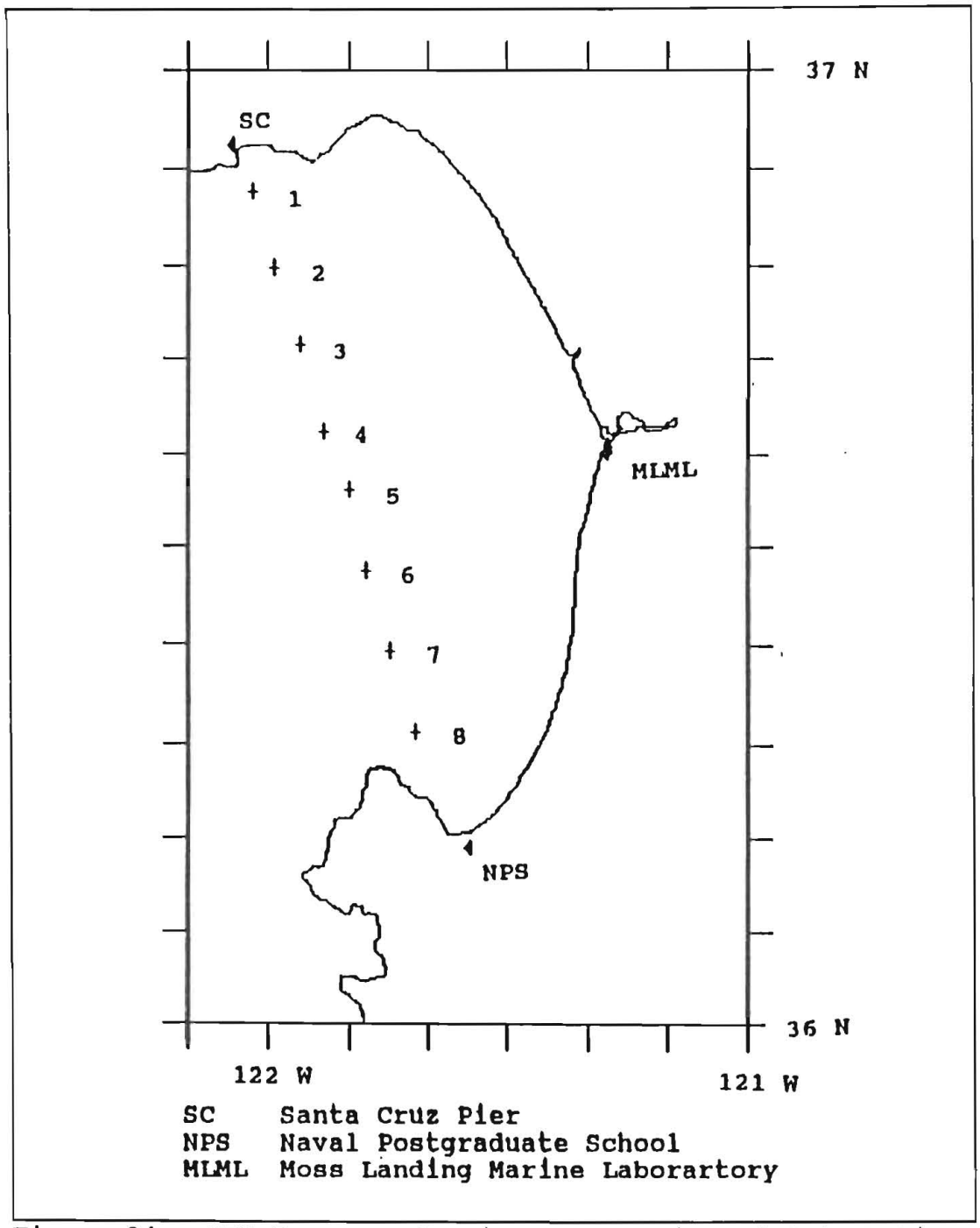

Figure 34. GPS Transect Stations: Location of GPS stations occupied during the GPS sea surface topography experiment. Plus signs indicate transect stations triangles GPS base stations.

during the experiment. A residual slope, Figure 35, was found in the sea surface which agrees qualitatively with the slope shown in Figure 33.

The sea surface shown in Figure 35 was determined from the GPS heights measured by a GPS antenna mounted in a small fiberglass boat deployed from the *Pt. Sur*. From the GPS heights the antenna height, tide height geoid heights and inverse barometric effect were subtracted to give the residual sea surface topography:

$$SST = GPS-HI-TIDE-IBAR-N \qquad (5\text{-}1)$$

where SST is the residual sea surface topography, HI is the height of the antenna above the waterline, TIDE is the tidal heights, IBAR is the inverse barometric effect and N is the geoid height at the station. Figure 35 shows the residual sea surface at the stations along the tract and standard deviation of the calculated mean sea level. A bias of 4.5 cm between the Monterey and Santa Cruz solutions has been removed from the GPS heights. If all of the corrections in equation 5-1 to the GPS heights were correct, the residual sea surface should have been a horizontal line of zero height, or given heights related to oceanographic processes.

The residual sea surface contained a slope from north to south in the Bay, Figure 35, which did not appear to be associated with oceanographic or meteorological processes occurring. The slope produced a 10 to 15 cm difference

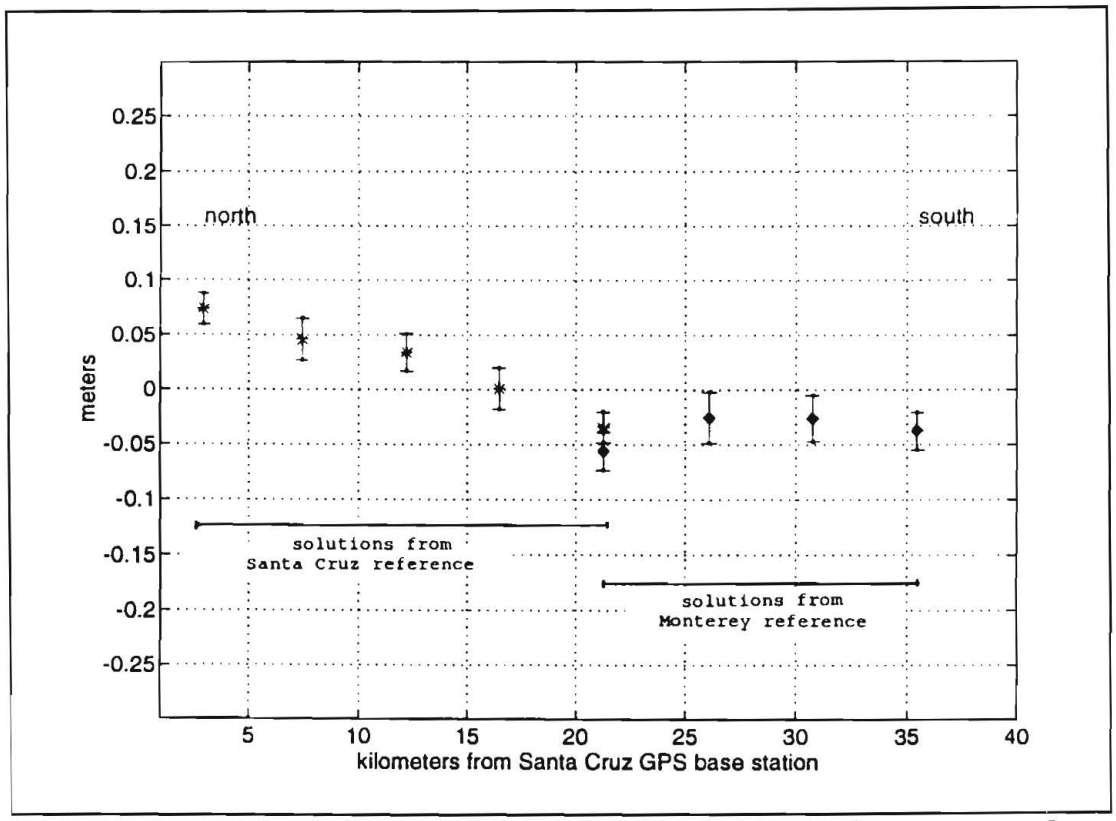

Figure 35. Relative MSL from GEOID93: The relative sea surface topography from the GEOID93 geoid. * and ◆ indicate sea surface height, bars indicate the one sigma accuracy.

between the north and south ends of the transect. In terms of a geostrophic current, this would indicate a flow of approximately 20 cm/s out of the bay.

To see if this slope could be attributed to a local geoid feature, the Monterey Bay geoid heights calculated in this study were used to correct the profile along the GPS transect. Figure 36 is the result of substituting the Monterey Bay geoid heights for the GEOID93 heights in equation 5-1. The same corrections were applied in both cases. Stations one through four now fall within 3 cm of the horizontal, zero height line. The southern stations do not show comparable agreement. They are offset up to 9 cm above the zero line. The net result is a reversal of the residual slope seen in Figure 35. The slope is concentrated between stations four through six indicating possible interaction between the tide and the Canyon.

E. CONCLUSIONS

A local geoid for Monterey Bay was calculated using dense local gravity data, gridded terrain elevations and the OSU91A geopotential model. The modeling of the near shore geoid is complicated by the inherent slope in the geoid caused by the proximity of the continental slope and the discontinuity in the data at the shoreline. This study attempted to combine several sets of data to fill in the near shore gap in Monterey Bay. The calculation of the geoid was done with FORTRAN

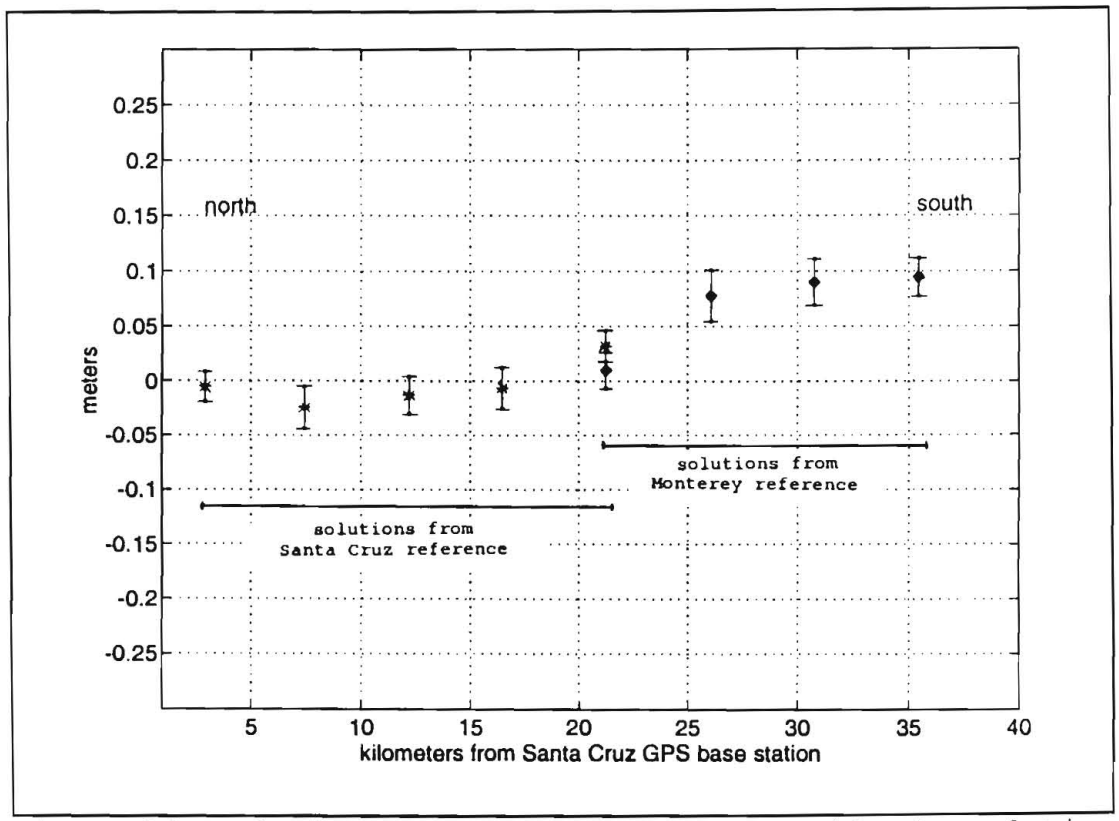

Figure 36. Relative MSL from Monterey Bay Geoid: The relative sea surface topography from to the Monterey Bay Geoid. *, ♦ indicate sea surface height, bars indicate one sigma accuracy.

computer programs received from NGS which ran on a UNIX system.

The estimated accuracy and resolution of the local geoid was 3 cm and 5 km, respectively. Although this accuracy could not be independently checked within the time constraints of this thesis, the calculated geoid showed excellent agreement with GEOID93 in areas endowed with high density gravity data. Comparisons with the regional geoid and a GPS survey of the mean sea level in Monterey Bay showed that the method used accurately modeled the local geoid in area covered with dense gravity data. Appendix G contains the latitude, longitude and geoid undulations calculated for the Monterey Bay geoid.

Further studies comparing the geoid and the mean sea surface in the Monterey Bay are suggested. This could be accomplished by either a GPS experiment such as the one discussed above or by analyzing the tide gauge records from Monterey and Santa Cruz. The effect of different gridding processes needs to be evaluated further and an optimum method selected. Additional gravity data should be requested from DMA to increase the density of the area in the southeast 1° block and the effect of additional data on the geoid studied.

APPENDIX A. GLOSSARY

Terms:

- **Ellipsoid Heights** - heights measured from a reference ellipsoid. Geoid heights are given as ellipsoid heights.
- **Equipotential/Level Surface** - a surface over which the gravity potential is constant and gravity is perpendicular.
- **Free-air Correction** - the correction applied to observed gravity values to mathematically move them vertically from the surface of the earth to the geoid, MSL. The free-air correction corrects for the vertical gradient of gravity only.
- **Geocentric Gravitational Constant** - the product of the earth's mass and the universal gravitational constant, GM, for WGS84 and GRS80 the GM includes the mass of the atmosphere.
- **Geocentric Radius** - the radial distance from the center of the earth
- **Geopotential** - the gravity potential of earth.
- **Geoid** - the equipotential surface of the earth's gravity field which most closely represents the mean sea level.
- **Geoid Undulations** - height differences between a reference ellipsoid and the geoid, also geoid heights and geoid-ellipsoid separations.
- **Gravimetry** - gravity observation of the surface of the earth.
- **Gravitational Potential** - the potential energy at a point caused by the proximity of a mass.
- **Gravity** - acceleration which is the combination of the gravitational acceleration and centrifugal acceleration.
- **GRS** - Geodetic Reference System ellipsoid reference systems: GRS80, GRS67
- **Normal Ellipsoid** - an ellipsoidal model the geoid, also reference or mean earth ellipsoid.

- **Normal Gravity** the model gravity of an ellipsoid reference system.
- **Orthometric Heights** - height measured from the geoid or mean sea level.
- **Terrain Correction** - correction applied to observed gravity values to correct for the effect of terrain undulations above and below a gravity station.
- **WGS** - World Geodetic System, DoD ellipsoid reference systems: WGS84, WGS72

APPENDIX B. METHODS OF GRAVITY MEASUREMENT

A. PENDULUMS

The original method used to measure absolute gravity was with reversible pendulums. The period of a pendulum was calibrated at a common location, such as Potsdam, Germany, where an absolute reference gravity value had been established. The gravity a particular site could then be calculated from the difference between the pendulum's period at the measurement site and the pendulum's period at the calibration site. The limitations to this method were that the exact length of the pendulum arm was difficult to determine, the instruments were difficult to transport and the calculations involved were complex. The maximum accuracy of the pendulum method was reached in the 1950's and is approximately 0.2 mgal on land. (Bomford 1980)

B. FREE FALLING MASSES

The earliest method of observing gravity was by the observations of free falling masses. It was Galileo's observation of free falling masses that lead to Newton's formulation of the law of universal gravitation. (Dragomir et al. 1982) In this method the times and distances over which a mass falls is converted into an acceleration which is

gravity. While this is potentially the most accurate and straight forward means of determining gravity, it is a difficult method to properly employ. (Bomford 1980) The difficulty with the method of free falling bodies is that the apparatus is difficult to transport and requires nearly one week to complete a single gravity measurement. However, the accuracy of that measurement is 0.003 to 0.005 mgal (ibid.).

C. STATIC GRAVIMETERS

Static gravimeters were developed because of the difficulties in performing dynamic gravity measurements with the pendulum and free fall methods. The term static is used because, unlike the dynamic methods, a displacement is measured not a motion. Static gravimeters measure gravity by comparing gravity to a constant force supplied by a spring, gas pressure, or torsion of metal or quartz fibers. Static gravimeters are generally small and very transportable but not as accurate as the devices which use dynamic methods. A modern static gravimeter can measure differences in gravity to an accuracy of 0.1 mgal. (ibid.) This accuracy is not suited for absolute gravity determinations but is accurate enough for the relative gravity measurements needed for the evaluation of Stokes integral. (Moritz 1974) Despite their accuracy limitation, static gravimeters have seen increasing use because they can mass produce gravity anomaly measurements for use in Stokes' formula.

D. SATELLITES

1. Satellites Used in Geodesy

The launching of the Soviet satellite Sputnik-1 in 1957 ushered in the use of artificial satellites to measure the gravity field of the earth. The motion of a satellite within the gravity field contains information about the gravity field. This is the basis of the dynamical method of satellite geodesy. (Seeber 1993) The main advantage of satellites is the global coverage which they can provide. They are especially useful in determining the basic parameters of the earth such as the mean size, mass and flattening. The first parameter determined using observation data of Sputnik-2 and Explorer-1 was the value for the flattening of the earth. (ibid.) The determination of the general shape of the geoid is also possible with satellite observations; but, with low spatial resolution unless combined with satellite altimetry or surface gravimetry. (Mainville et al. 1992)

The satellites used in geodesy can be classified by whether they were specifically designed for geodetic missions or not. Some of the satellite systems which were designed specifically for geodetic missions are:

- ANNA-1B USA 1962
- PAGEOS USA 1966
- STARLETTE FRANCE 1975
- GEOS1-3 USA 1965, 1968, 1975
- LAGEOS USA 1976, 1992
- EGS JAPAN 1986

The ARISTOTELES geodetic satellite has been planned for the mapping of the gravity field and has a tentative launch date in 1997/98. (Rapp 1993)

Many satellites have been used for geodetic studies but relatively few were actually designed with geodetic applications in mind. Typical types of satellites which fit this description are navigation satellites such as TRANSIT and GPS, and satellites with radar altimeters such as SEASAT, GEOSAT, ERS-1, and TOPEX/POSEIDON. (Seeber 1993)

Satellites can also be classified on whether they are active or passive. Passive satellites are simply targets for ground based observations and are covered with a reflective surface. Active satellites transmit energy and receive reflected energy or can just collect energy emitted by the surface of the earth. Laser reflecting satellites are one example of the passive type of satellite and radar altimeter satellites are an active type. Some of the more important satellites are listed in the table below from Seeber. (ibid.)

TABLE B-I SATELLITES USED IN GEODESY

Passive satellites	Active satellites
ECHOI, II	ANNA-1B
PAGEOS	GEOS-3
STARLETTE	SEASAT-1
LAGEOS	NNSS satellites
EGP (AJISAI)	NAVSTAR-GPS satellites
ETALON	GEOSAT
	ERS-1
	TOPEX-POSEIDON

2. GPS

The application of GPS to physical geodesy studies comes from its ability to accurately determine the three dimensional position of a point referenced to the WGS 1984 reference ellipsoid. If the ellipsoid height, h, of a point is accurately determined by GPS and the height of the point above mean sea level, H, is known, the separation between the geoid and ellipsoid, N, can be found by:

$$N = h - H \qquad \text{(B-1)}$$

This assumes that the orthometric height, H, has been determined by some means such as geodetic leveling. (Perrott 1993)

3. Satellite Radar Altimeters

Satellites with radar altimeters, such as TOPEX/Poseidon, collect information by reflecting electromagnetic energy off the surface of the earth and measuring the length of time between the transmission and reception of the signal. When the orbit altitude of the satellite is accurately known, the measured distance can be converted into information about the height of the terrain below the satellite.

When the reflected energy is from the surface of a body of water, such as the ocean, then it is the sea surface topography that is measured. Figure B-1 shows the general arrangement of satellite altimetry. In the figure, h is the height of the satellite above the ellipsoid, h_s is the height of the satellite above the surface of the ocean and η is the deviation of the ocean surface from the geoid or the dynamic height. Repeat measurements of the same location in the ocean allows the time variability to be eliminated and the geoid directly determined. Brun's formula can then be used to determine the disturbing potential. (McAdoo and Marks 1992)

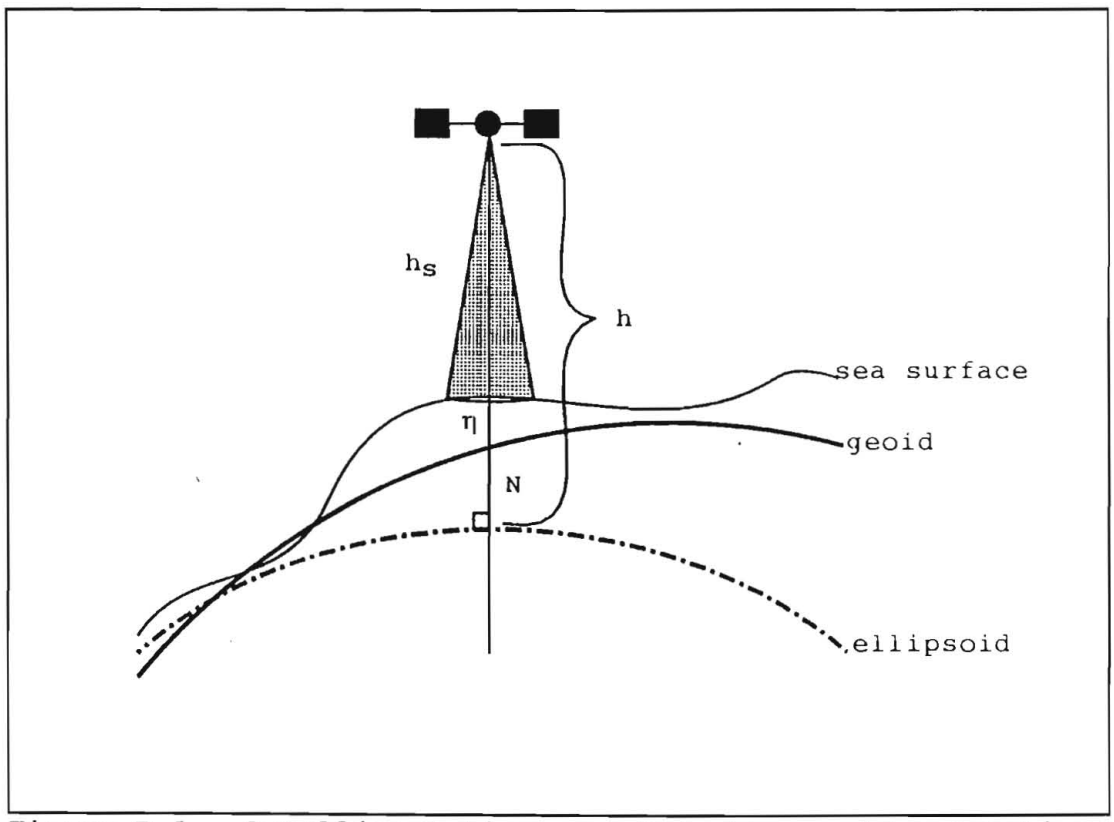

Figure B-1. Satellite Altimetry: N is the geoid undulation, η the sea surface topography, h_s the radar range and h the ellipsoid height of the satellite.

APPENDIX C. MATHEMATICAL BASIS OF CALCULATION

A. BRUN'S FORMULA

On the geoid:

$$W_G = U_G + T_G \qquad \text{(C-1)}$$

where W_G is the potential of the ellipsoid at point G and T_G is the anomalous potential at point G. (Figure C-1) We also have the relationships from the definition of the normal ellipsoid.

$$W_G = W_0 = U_0 = U_E \qquad \text{(C-2)}$$

which will allow us to derive Brun's formula.

The potential of the ellipsoid, U_o displaced to the geoid is:

$$U_G \approx U_E + \left(\frac{\partial U_o}{\partial n}\right)_E N + \ldots \qquad \text{(C-3)}$$

where the partial derivative of U_o with respect to, n, is the gradient of the normal potential along the normal, n, to the

ellipsoid. The gradient of the normal potential is the same as the normal gravity, γ, giving:

$$U_G = U_E - \gamma N \qquad \text{(C-4)}$$

Substituting into equation C-1,

$$W_G = U_E - \gamma N + T_G \qquad \text{(C-5)}$$

and applying the relationship of equation C-2 between the normal potential on the ellipsoid and the true potential on the geoid gives:

$$N = \frac{T}{\gamma} \qquad \text{(C-6)}$$

which is Brun's formula. (Heiskanen and Moritz 1967)

B. The Fundamental Equation of Geodesy

1. General Form of the Fundamental Equation

In Figure C-1, g is gravity on the geoid and γ is the normal gravity on the ellipsoid. The gravity anomaly is:

$$\Delta g = |g| - |\gamma| \qquad \text{(C-7)}$$

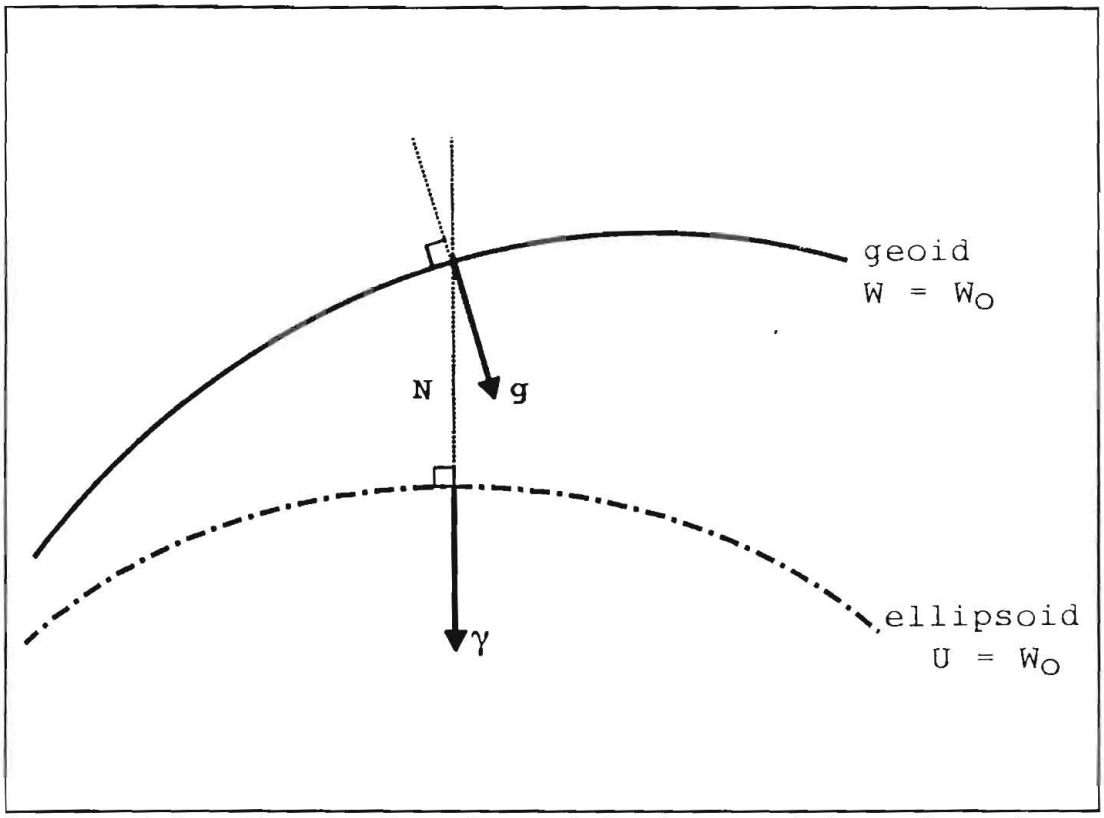

Figure C-1. Brun's Formula: Relative position of surfaces and accelerations used in deriving Brun's formula; γ is the normal gravity, g observed gravity, N the geoid undulation.

the angle between **g** and γ, the deflection of vertical, is kept small by proper determination of the reference ellipsoid and can be neglected.

Substituting the magnitudes of the negative gradients of the potentials gives:

$$\Delta g = -\nabla W_G + \nabla U_E \qquad \text{(C-8)}$$

and then replacing the true potential by the sum of the model and perturbing potentials gives:

$$\Delta g = -\nabla U_G - \nabla T_G + \nabla U_E. \qquad \text{(C-9)}$$

The vertical gradient can be replaced by:

$$\frac{\partial}{\partial h} = \frac{\partial}{\partial n} \qquad \text{(C-10)}$$

because the verticals of the geoid and ellipsoid nearly coincide and the height, h, is measured along the vertical. Equation C-9 becomes:

$$\Delta g = -\frac{\partial}{\partial h} U_G - \frac{\partial}{\partial h} T + \frac{\partial}{\partial h} U_E \qquad \text{(C-11)}$$

Substituting equation C-4 into equation C-10, we have

$$\Delta g = \frac{\partial}{\partial h} \gamma N - \frac{\partial}{\partial h} T. \qquad \text{(C-12)}$$

Now applying Brun's formula, C-6 and the fact that the vertical gradient of N is zero gives:

$$\Delta g = \frac{T}{\gamma}\frac{\partial \gamma}{\partial h} - \frac{\partial}{\partial h} T \qquad \text{(C-13)}$$

which is the fundamental equation of physical geodesy. (ibid.)

2. Spherical form of the fundamental equation

The spherical approximations are:

$$\frac{\partial}{\partial h} = \frac{\partial}{\partial r} \qquad \text{(C-14)}$$

$$\gamma = \frac{GM}{r^2} \qquad \text{(C-15)}$$

where r is the radius vector to a point and r is the radius of a sphere chosen so that it has the same GM as the reference ellipsoid. Then Brun's formula and the fundamental equation become:

$$N = \frac{T}{\gamma} \qquad \text{(C-16)}$$

$$\Delta g = -\frac{2}{r} T - \frac{\partial}{\partial r} T. \qquad \text{(C-17)}$$

C. STOKE'S FORMULA

1. Derivation

If equation C-17 is multiplied by $-r^2$ the result is:

$$-r^2\Delta g(r) = \frac{\partial}{\partial r}(r^2T). \qquad \text{(C-18)}$$

With the upward continuation of gravity (Dragomir et al. 1982) equation C-18 can be integrated with respect to r:

$$-\int_{\infty}^{r} r^2\Delta g(r)\,dr = r^2T - \lim_{r\to\infty} r^2T \qquad \text{(C-19)}$$

where the limit of r^2T goes to zero because the potential, T, goes to zero, external to all mass as r goes to infinity. This gives the result:

$$r^2T = -\int_{\infty}^{r} r^2\Delta g(r)\,dr \qquad \text{(C-20)}$$

Substitution of the equation for the upward continuation of gravity (Dragomir et al. 1982) for Δg gives:

$$r^2T = \frac{R^2}{4\pi}\int_{\infty}^{r}\left[\iint_{\sigma}\left(\frac{r^2-R^2}{q}-\frac{1}{r}-\frac{3R}{r}\cos\psi\right)\Delta g\,d\sigma\right]dr \qquad \text{(C-21)}$$

Where q is the spherical distance, r is the geocentric radius and R is the mean radius of the geoid. On the surface of the geoid, r = R and integrating with respect to r gives:

$$T(\phi,\lambda) = \frac{R}{4\pi}\iint_{\sigma}\Delta g S(\psi)\,d\sigma \qquad \text{(C-22)}$$

where $T(\phi,\lambda)$ is the anomalous potential at geographic position (ϕ,λ) on the geoid, Δg is the gravity anomaly in the element area $d\sigma$ and $S(\psi)$ is the Stokes' function:

$$S(\psi) = \sum_{n=2}^{\infty}\frac{2n+1}{n-1}P_n(\cos\psi) \qquad \text{(C-23)}$$

The geoid undulation at (ϕ,λ) is then given by the substitution of Brun's formula into equation C-23.

$$N(\phi,\lambda) = \frac{R}{4\pi\gamma_M}\iint_{\sigma}\Delta g S(\psi)\,d\sigma \qquad \text{(C-24)}$$

APPENDIX D. TERRAIN REDUCTION

A. GENERAL

The application of Stokes' formula is based on the assumption that all mass is interior to the surface of the geoid. The mathematical removal of the topography exterior to the geoid is the terrain reduction. Terrain reductions can be thought of as a two step process; first, the mathematical transfer of all masses to the interior of the geoid and second, movement of the gravity measurement from the physical surface of the earth to the surface of the geoid. These two steps, together, make up the terrain reduction. There are many types of terrain reductions based on how they handle the problem of masses external to the geoid. A book on physical geodesy such as Bomford 1980, Heiskanen and Moritz 1967, should be consulted for an in depth analysis of the various types of terrain reductions.

The process of transferring the mass of the terrain from above the geoid to below the surface of the geoid changes the gravity potential of the geoid (Heiskanen and Moritz 1967). This change is called the indirect effect; and, depending on the method used, can be quite large, up to 100 meters for the Bouguer reduction. The indirect of Helmert reduction is

small, on the order of 1 m change in the geoid for 3000 m of average elevation. This makes them desirable for use in calculating the geoid (Milbert 1991). The Helmert reduction is composed of the free-air correction and the terrain correction.

B. FREE-AIR REDUCTION

The free-air reduction corrects the gravity measurement, taken on the surface of the earth to the surface of the geoid. It ignores the density of the intervening crustal material and is based solely on the vertical gradient of gravity and the elevation of the gravity station. The free-air correction is given by a Taylor series expansion of the vertical gradient of gravity truncated at the first term:

$$FAC = \frac{\partial \gamma}{\partial r} h \qquad \text{(E-1)}$$

where h is the elevation of the gravity station. For surface gravity measurement, the gradient of gravity is considered a constant over the range of station elevations:

$$\frac{\partial \gamma}{\partial r} = 0.3086 \frac{mgal}{m} \qquad \text{(E-2)}$$

giving:

$$FAC = 0.3086 h \qquad \text{(E-3)}$$

where h is in meters. (DMAAC 1987) The free-air correction is positive for gravity stations above MSL because it is the effect of moving the gravity station closer to the center of the earth.

Free-air anomalies are obtained by applying the free-air correction to the difference between the gravity observed at the gravity station and the normal gravity:

$$\Delta g_{FAA} = g_{obs} - \gamma + FAC \qquad \text{(E-4)}$$

where Δg_{FAA} is the free-air anomaly, g_{obs} is the observed gravity and γ is the normal gravity.

APPENDIX E. GEOID CALCULATION PROGRAMS

FOURT - Cooley-Tukey FFT subroutine, included for MAKSTO, RESGEO and FTC2 programs.

FTC2 - Terrain correction via FFT. Takes input of constant resolution gridded elevation data, calculates gravimetric terrain correction on grid and returns gridded terrain corrections in same grid size as input elevation grid. Does not use grid element of calculation point.

GRD360 - Calculates the geoid undulations and gravity anomalies from global geopotential model. Recognizes OSU86, OSU89, OSU91 and JGM2 models. Subtracts the normal potential of the GRS80 reference ellipsoid. Has options for resolution, area of coverage, number of degrees of spherical harmonic used.

GTAPER - Tapers and pads standard grid using split cosine bell taper. Amount of tapering and padding is chosen interactively and is based on percentages of grid resolution and grid size.

MAKSTO - Calculates the Fourier transform of Stokes' function on an input grid of residual gravity anomalies. Skips grid element at calculation point by setting the kernel, Stokes' function, equal to zero.

RESGEO - Computes the residual geoid undulations from the residual anomaly grid. Calculates the undulation effect of the gravity anomaly of the grid element at the calculation point in the space domain.

APPENDIX F. GPS SURVEY OF MONTEREY BAY SEA SURFACE TOPOGRAPHY

A. INTRODUCTION

A Naval Postgraduate School oceanographic cruise was conducted October 26th through the 29th, 1993 aboard the *R/V Pt. Sur*. On October 26th, a transect of the Monterey Bay was conducted from north to south between the cities of Santa Cruz and Monterey. See Figure F-1. The purpose of the transect was to determine the sea surface topography (SST) using the NAVSTAR Global Positioning System. The actual sea surface height was determined using GPS in differential mode with two ground reference stations. In this paper, SST is defined as the deviation of the sea surface from the geoid remaining after the GPS heights have been corrected for the inverse barometric effect, geoid undulations and tides.

The transect was oriented as close as possible to the imaginary line connecting the Santa Cruz and Monterey tide gauges. The positions of the stations occupied by the *Pt. Sur* are shown in Figure F-1 as plus signs and the positions of the two reference stations are triangles. The number of stations to be occupied was determined by the time available to complete the transect and the desired spacing. The position of station five was chosen to coincide with the center of the

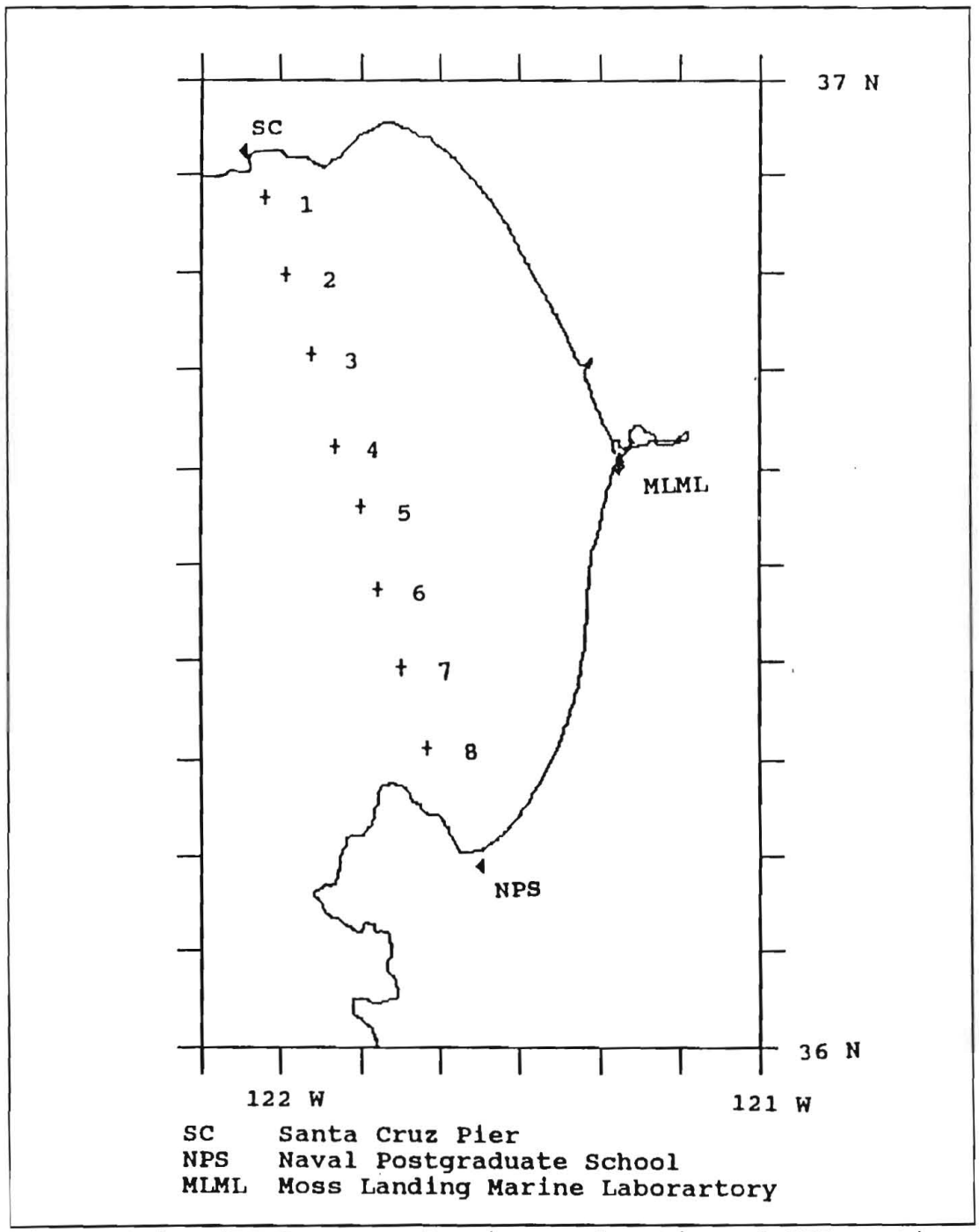

Figure F-1. GPS Transect Stations: Location of GPS stations occupied during the GPS Sea Surface Topography experiment. Plus signs indicate transect stations, triangles GPS base stations.

Monterey Submarine Canyon. The rest of the points were selected by evenly spacing them at approximately 4.5 km around station five.

During the transect, a small, unmanned boat was deployed from the *Pt. Sur* at each station. A GPS antenna was mounted on the small boat and connected to a GPS receiver on the *Pt. Sur* by a tow line and a 60 m low loss antenna cable. The combination of the antenna mounted on the small boat and the GPS receiver on the *Pt. Sur* will be referred to as the rover receiver. The GPS receiver calculated and recorded the three dimensional position of the antenna. Simultaneously, the ground reference stations recorded range corrections to be combined with the rover's solutions during post processing. The three GPS receivers utilized were Ashtech-Z12 GPS receivers on loan from Ashtech Incorporated, Sunnyvale, California.

B. BACKGROUND

The actual sea surface, η, can be modeled in simplified form as:

$$\eta = \text{tides} + \text{geoid} + \text{IBAR} + \text{oc/air-sea} \qquad \text{(F-1)}$$

where tides are the ocean tides, geoid is the geoid height at the station, IBAR is the inverse barometric effect and oc/air-sea represents currents, wind waves, etcetera. In the above

equation, the geoid is the only time invariant term while the other terms are temporal in nature and represent forces which will cause the sea surface to deviate from the geoid. Assuming that the geoid is known to high accuracy, the residual SST can be used to detect and study oceanic processes such as currents, eddies and up/down welling. Conversely, if the oceanographic phenomenon are known or removed through time averaging the geoid can be studied. Rearranging the terms of equation F-1:

$$\text{oc/air-sea} = \eta - \text{hi} - \text{tide} - \text{geoid} - \text{IBAR} \qquad \text{(F-2)}$$

The oc/air-sea term corresponds to the residual SST, η is the height determined by GPS, tided heights came from the NOAA tide gauge on Monterey Municipal Wharf number two and the inverse barometric effect was calculated from pressure data collected by the *Pt. Sur* SAIL system. Local geoid undulations were computed from a regional geoid model, GEOID93, (Milbert 1993) for North America supplied by the National Geodetic Survey (NGS).

C. DATA PROCESSING/EDITING:

GPS:

GPS three dimensional positions were recorded at two second epoch. The rover receiver recorded data for approximately 15-20 minutes at each station by the rover

receiver. The collection time at station five was doubled to 40 minutes. The two reference stations recorded continuously during the experiment. The GPS data was processed using the Ashtech PNAV 2.0-beta software. Following this processing, the data contained the GPS week time, the three- dimensional position of the rover antenna relative to the WGS84 reference ellipse, a formal error estimate for each data point, PDOP, and the number of satellites used in the solution. The data was in two sets: one for the solutions calculated from the Monterey reference site and another from the Santa Cruz reference site. These sets were then further broken into individual data sets for each station of the transect.

The GPS data was first edited to remove data points which were collected before the small boat was deployed. The next editing removed points where discontinuities in solution PDOP and/or the formal error estimates occurred. These generally coincided with a change in the number of satellites being used in the solution. Last, the data outliers were edited by removing all points which were more than three standard deviations from the average vertical position for a station. This removed several spikes in the data but did not effect the average station vertical positions above the 0.5 cm level.

The station sea surface heights were calculated by taking the average height of the best solution at the station, based on an examination of point-by-point differencing with an overlap of solutions at station five. To convert the GPS

heights to the North American Datum 1983 (NAD83), 58.9 cm were subtracted from the WGS84 GPS height to correct for the local datum. Figure F-2 is a schematic of reference system adjustments required to get comparable heights.

GEOID:

To remove the effect of the geoid on the sea surface, the NGS GEOID93 was used. Geoid heights were determined using the geoid interpolation program which is part of the GEOID93 software. Using latitude and longitude as inputs, the program results are given as geoid heights referenced to NAD83. The geoid height was calculated for each station from the mean station latitude and longitude.

TIDES:

Tidal effects were removed using the Monterey tidal record for the time period of the experiment. Tide records for Monterey were requested and received from NOAA. The data set contained time and tidal heights referenced to the tide gauges' staff zero. To adjust these values to tidal heights in the NAD83 reference, a common bench mark was found which was referenced in the tidal datum and also referenced in NAD83. One such bench mark was located for this project which was used to adjust the Monterey tides. The geoid height at the tide gauge was also be subtracted from the raw tidal heights.

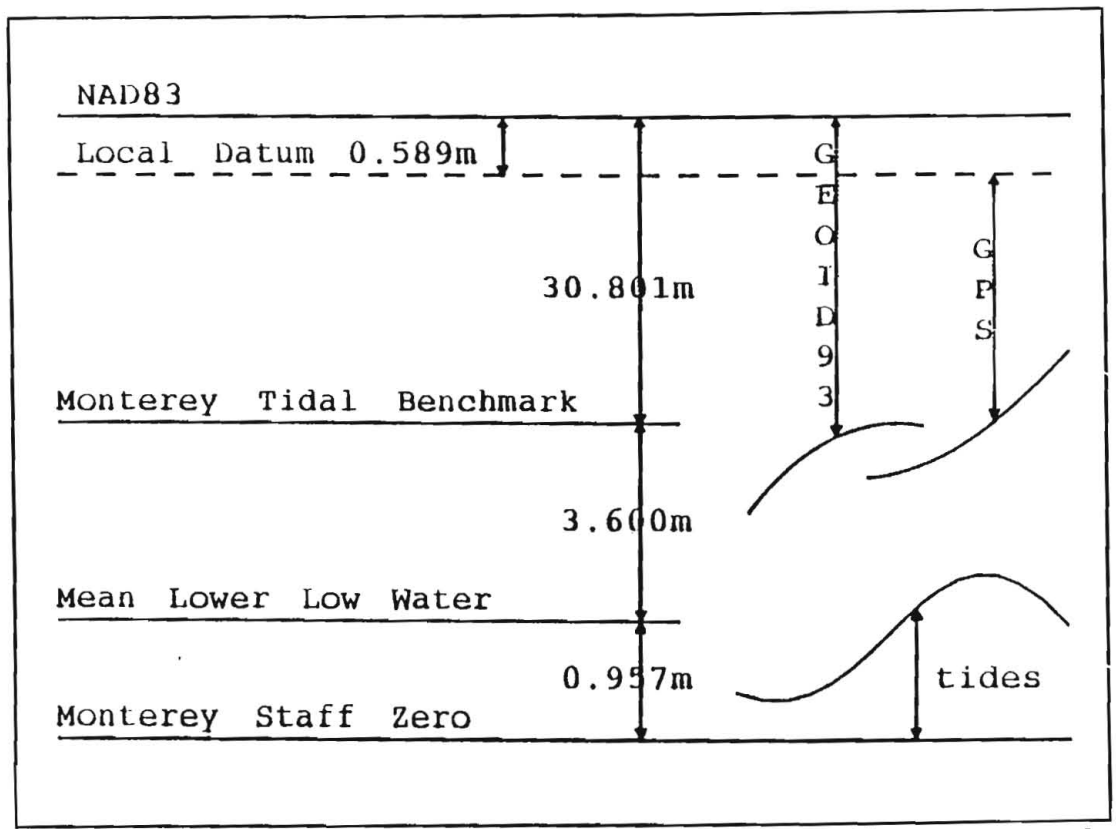

Figure F-2. Local Datum Adjustments: Height adjustments made to measurements in GPS sea surface experiment.

INVERSE BAROMETRIC EFFECT:

The effect of atmospheric pressure differences on sea level is called the inverse barometric effect. As the name suggests, the water level reacts inversely to the atmospheric pressure. For example, in the center of a high, the water level will be depressed and the opposite will occur in a low pressure system. An extreme case is the severe low pressure system of a hurricane; then the effect is called a storm surge. The relationship between the air pressure and sea level is one cm/mbar. The effect was calculated by the following equation:

$$IBAR = -0.01 \text{ m/mbar } (\text{station pressure} - 1013.3) \quad \text{(F-3)}$$

Station pressure was measured by the *Pt. Sur* SAIL system. The value, 1013.3 mbar is the standard atmospheric pressure. This is by far the smallest correction with a maximum absolute value of only 5.5 cm. (Pond and Pickard 1983)

D. RESULTS:

Figure F-3 is a plot of the residual SST, as defined by equation 2. An antenna height of 46 cm has also been subtracted from the GPS heights in Table F-I. The antenna height was only crudely determined, ±4 cm, because it was originally planned that the experiment would only attempt to measure relative sea surface height. The asterisks and

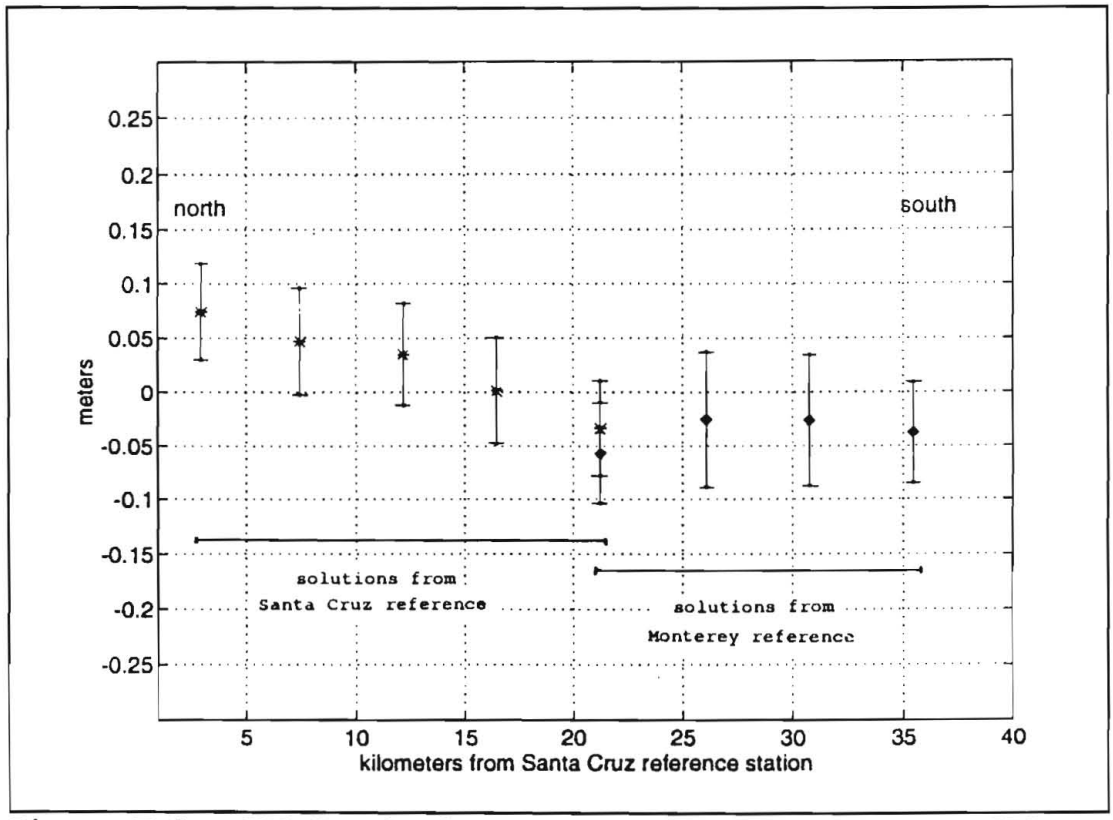

Figure F-3. GPS Sea Surface Topography: Monterey Bay GPS sea surface topography relative to NAD83. * and ◆ indicate sea surface height with bars indicating the one sigma accuracy.

diamonds are the sea surface heights at each station with the bars indicating accuracy at one sigma.

The one sigma value is for the accuracy of the mean sea level measurement. The accuracy of the antenna height determination is not contained in the plotted error of Figure F-3. The GPS measurements have an estimated accuracy of three centimeter based on the relative accuracy of the reference station positions. The mean error of the mean sea level was calculated by:

$$\sigma_{MSL} = \frac{\sigma_\eta}{\sqrt{\frac{N}{3}}} \qquad \text{(F-4)}$$

where σ_η is the standard deviation of the GPS heights and N is the total number of points used to find the mean sea level at a station. The total number of points is divided by three, which is the approximate number of points per swell period. Figure F-4 is the relative sea surface across the bay. A 4.5 cm bias between the Monterey and Santa Cruz solutions has been removed by adding half to the Santa Cruz heights and subtracting half from the Monterey heights. The bars indicate the accuracy calculated by equation F-4. The 3 cm error in the relative positioning of the base stations and the antenna height accuracy are no longer part of the error because the plotted surface is relative only. The bias is believed to have been caused by relative ionospheric delays between the

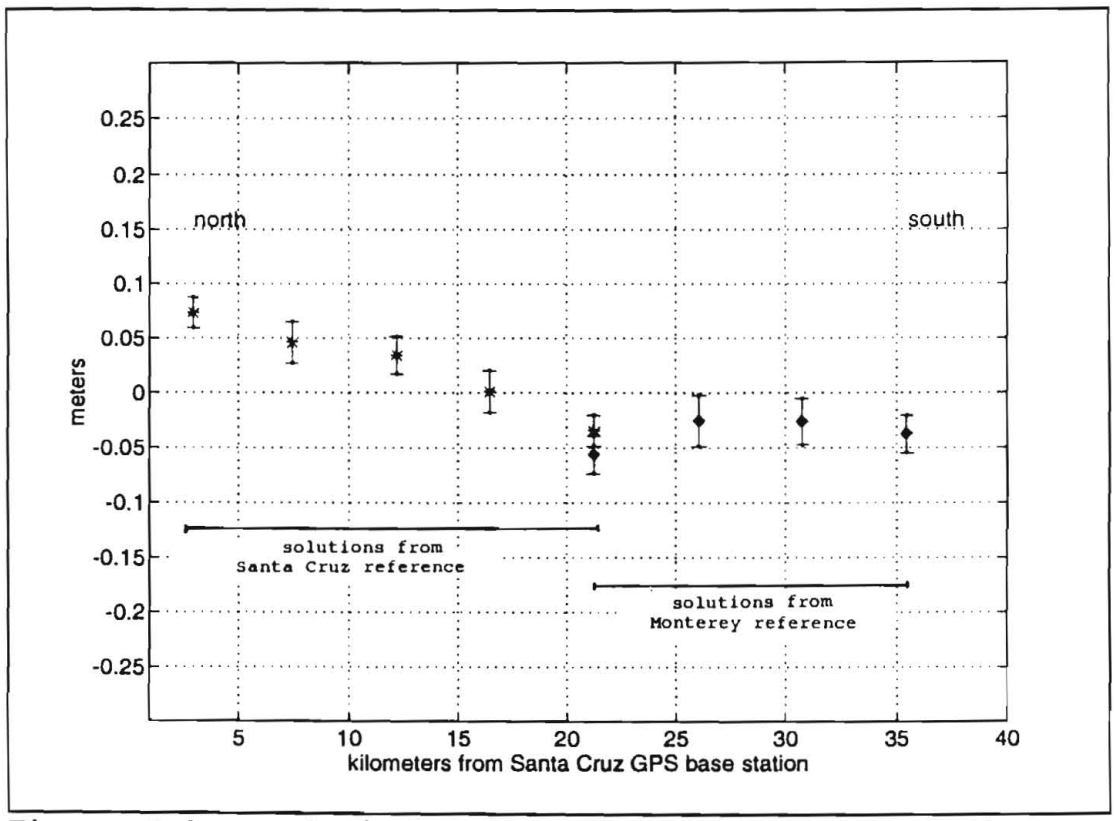

Figure F-4. Relative SST from GEOID93: The relative sea surface topography using GEOID93. * and ◆ indicate sea surface height with bars indicating the one sigma accuracy.

two base stations which were not properly solved for in the processing.

The relative difference between stations one and eight in Figure F-3 is approximately 10 cm. This would relate to an approximate geostrophic flow of 20 m/s out of the bay. However, the currents from the Acoustic Doppler Current Profiler (ADCP), did not show the presence of such a flow. (Figures F-5 and F-6) These currents would actually cause a slope in the opposite direction in the northern half of the bay and no slope in the southern half. There is a lesser slope detected south of the canyon where the ADCP currents are more or less along the transect; however, the overall slope does not appear to be the result of currents in the bay.

The possibility of the slope being the result of wind stress was investigated by examining the wind conditions prior to and during the experiment. During that period, the winds were light and from the north-northwest (350^{o} @5 kts). These winds were not strong enough to cause a set-up and if they were, it would have been in the opposite direction of the observed slope.

Since the currents and wind do not supply answers to the cause of the slope the author feels that some of the cause is the use of the Monterey tidal heights to model the tide along the entire transect. While the accuracy of the tidal measurement at the tide gauge is accurate enough, using that measurement ten to 40 km away may not. If this is the

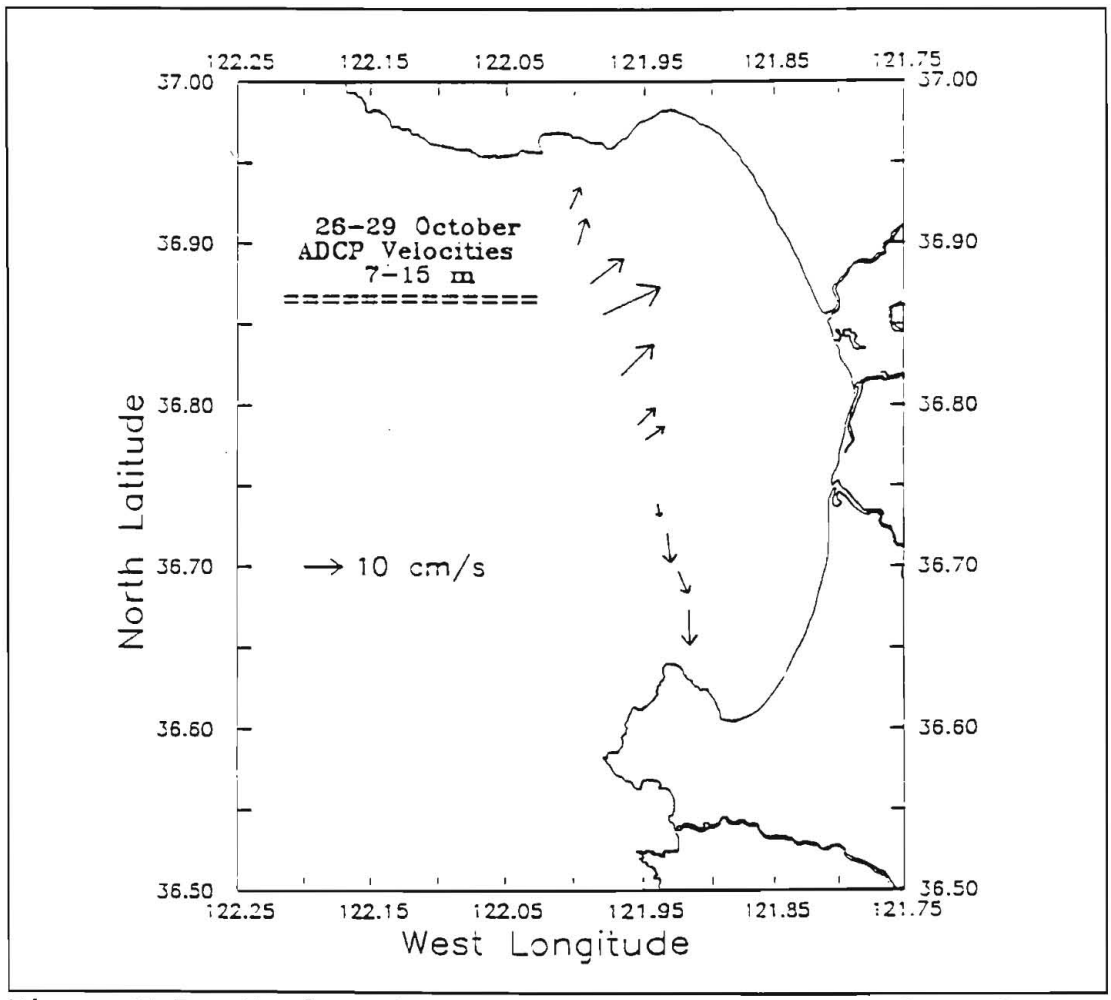

Figure F-5. Surface Currents: Surface currents from the *Pt. Sur* Acoustic Doppler Current Profiler during GPS transect.

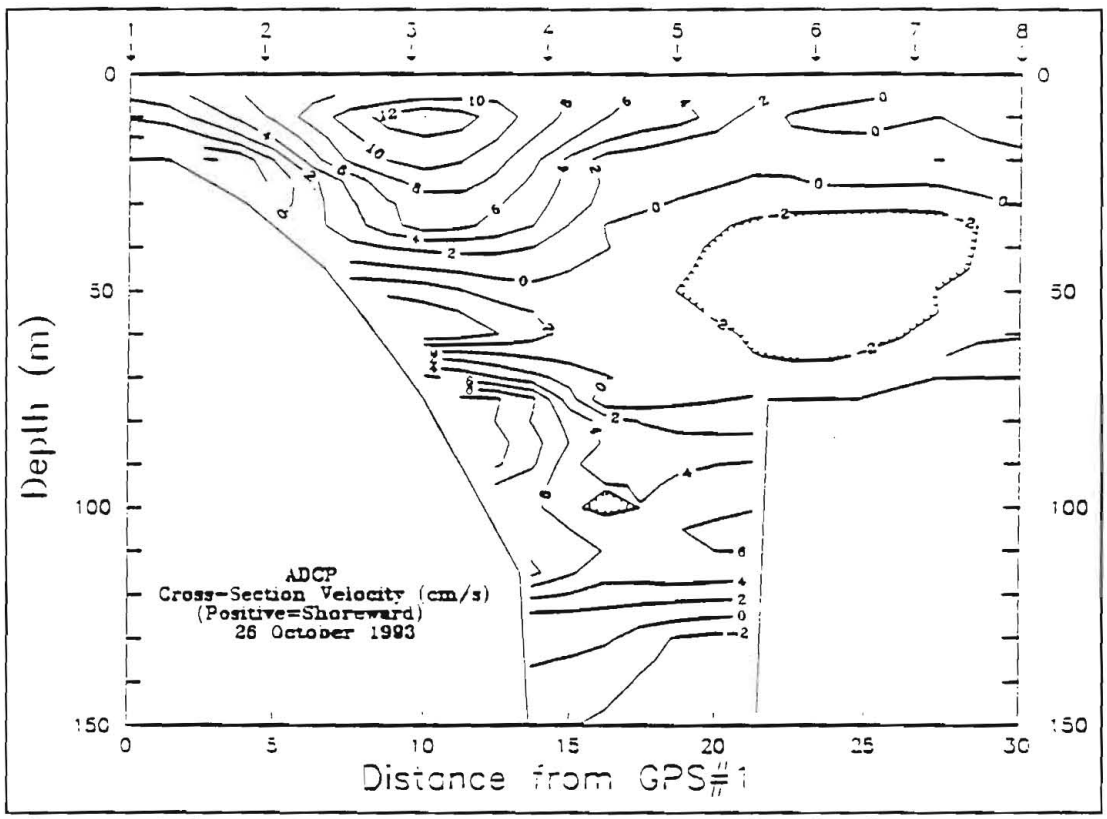

Figure F-6. Currents: Currents at depth from *Pt. Sur* Acoustic Doppler Current Profiler during GPS transect.

situation, the slope then represents the error caused by assuming the tide is a level surface across the bay. The first step to confirm this would be to reference the Santa Cruz and Monterey tide gauges in a common datum and compare their tidal records.

Verification of the local geoid should also be done in conjunction with the leveling of the tide gauges. This is the thesis research of the author and when complete the results will be reapplied to this experiment.

E. SUMMARY

This project used the method of kinematic differential GPS to measure the near-shore sea surface topography to a 3 cm level of accuracy. Following corrections for the geoid, tide and atmospheric pressure the residual sea surface topography was accurate seven to 8 cm in an absolute frame and three to 4 cm in a relative frame. A 10 cm relative slope across the bay was detected which did not appear to be linked with the currents in the bay or air-sea interactions.

Follow on experiments using this technique should concentrate on observing varied tide phases to confirm the presence of the slope. If absolute measurements are required, finer determination of the rover antenna's height above the surface of the water will be needed. Experiments may also look into the range at which this technique can be used away from the shore and still get data of sufficient accuracy.

Table F-I is the data summary for the experiment. Column one is the station number. Column two is the distance from the Santa Cruz base station in Kilometers. Columns three and four are the station data recording times, start and stop, respectively in GMT. Columns five and six are the mean station position. Column seven is the mean GPS height of the Santa Cruz solution. Column eight is the one sigma value for column seven as calculated by equation F-4. Column nine is the Monterey solutions for mean GPS height and column ten is their one sigma value. Column 11 is the Monterey tidal heights. Column 12 is the inverse barometric effect. Column 13 is the GEOID93 geoid heights. All heights, columns seven through 13, are given in meters referenced to NAD83. Columns seven and nine include the 46 cm antenna height which was subtracted for plotting Figures F-3 and F-4.

TABLE F-I GPS SEA SURFACE EXPERIMENT DATA

Station	Distance	$Time_1$	$Time_2$	Lat	Long
	[km]	[GMT]	[GMT]	[°N]	[°W]
1	2.95	16.7778	17.1056	36.9380	122.0099
2	7.43	17.5083	17.8006	36.8989	121.9966
3	12.19	18.2278	18.5967	36.8581	121.9800
4	16.47	18.9494	19.2611	36.8188	121.9661
5	21.25	19.9317	20.5867	36.7802	121.9498
6	26.08	20.9667	21.3300	36.7373	121.9393
7	30.76	21.7700	22.0789	36.6969	121.9243
8	35.45	22.5550	22.9128	36.6576	121.9079

GPS_{scz}	σ	GPS_{mty}	σ_{MSL}	Tide	IBAR	GEOID93
[m]	[m]	[m]	[m]	[m]	[m]	[m]
-31.66	0.014	000000	00000	0.87	-0.055	-32.989
-32.05	0.019	000000	00000	0.74	-0.054	-33.226
-32.50	0.017	-32.45	0.017	0.54	-0.052	-33.446
-32.90	0.019	-32.85	0.022	0.35	-0.049	-33.641
-33.32	0.014	-33.29	0.017	0.07	-0.037	-33.761
-33.58	0.022	-33.51	0.023	-0.10	-0.031	-33.849
000000	00000	-33.60	0.021	-0.17	-0.026	-33.865
-33.60	0.036	-33.54	0.017	-0.15	-0.027	-33.818

APPENDIX G. MONTEREY BAY GEOID HEIGHTS

(ref. GRS80)

36.5°N-37.0°N/122.2°W-121.7°W

LAT [deg N]	LONG [deg W]	HEIGHT [m]
37.0000	122.2000	-33.1517
37.0000	122.1583	-32.9506
37.0000	122.1167	-32.7464
37.0000	122.0750	-32.6017
37.0000	122.0333	-32.5606
37.0000	121.9917	-32.5251
37.0000	121.9500	-32.5104
37.0000	121.9083	-32.4807
37.0000	121.8667	-32.4452
37.0000	121.8250	-32.4082
37.0000	121.7833	-32.3757
37.0000	121.7417	-32.3103
37.0000	121.7000	-32.1881
36.9583	122.2000	-33.4483
36.9583	122.1583	-33.2580
36.9583	122.1167	-33.0791
36.9583	122.0750	-32.9528
36.9583	122.0333	-32.8709
36.9583	121.9917	-32.8165
36.9583	121.9500	-32.7653
36.9583	121.9083	-32.7252
36.9583	121.8667	-32.6857
36.9583	121.8250	-32.6458
36.9583	121.7833	-32.6074
36.9583	121.7417	-32.5528
36.9583	121.7000	-32.4486
36.9167	122.2000	-33.7707
36.9167	122.1583	-33.5865
36.9167	122.1167	-33.4223
36.9167	122.0750	-33.2964
36.9167	122.0333	-33.1971
36.9167	121.9917	-33.1129
36.9167	121.9500	-33.0386
36.9167	121.9083	-32.9734
36.9167	121.8667	-32.9182
36.9167	121.8250	-32.8642
36.9167	121.7833	-32.8059
36.9167	121.7417	-32.7326
36.9167	121.7000	-32.6539

LAT [deg N]	LONG [deg W]	HEIGHT [m]
36.8750	122.2000	-34.1187
36.8750	122.1583	-33.9307
36.8750	122.1167	-33.7671
36.8750	122.0750	-33.6350
36.8750	122.0333	-33.5234
36.8750	121.9917	-33.4153
36.8750	121.9500	-33.3073
36.8750	121.9083	-33.2110
36.8750	121.8667	-33.1346
36.8750	121.8250	-33.0752
36.8750	121.7833	-33.0078
36.8750	121.7417	-32.9076
36.8750	121.7000	-32.8132
36.8333	122.2000	-34.4627
36.8333	122.1583	-34.2718
36.8333	122.1167	-34.1076
36.8333	122.0750	-33.9623
36.8333	122.0333	-33.8235
36.8333	121.9917	-33.6900
36.8333	121.9500	-33.5566
36.8333	121.9083	-33.4375
36.8333	121.8667	-33.3433
36.8333	121.8250	-33.2691
36.8333	121.7833	-33.1949
36.8333	121.7417	-33.0853
36.8333	121.7000	-32.9632
36.7917	122.2000	-34.7703
36.7917	122.1583	-34.5997
36.7917	122.1167	-34.4529
36.7917	122.0750	-34.2979
36.7917	122.0333	-34.1313
36.7917	121.9917	-33.9573
36.7917	121.9500	-33.7780
36.7917	121.9083	-33.6385
36.7917	121.8667	-33.5330
36.7917	121.8250	-33.4372
36.7917	121.7833	-33.3583
36.7917	121.7417	-33.2518
36.7917	121.7000	-33.1229

LAT [deg N]	LONG [deg W]	HEIGHT [m]
36.7500	122.2000	-35.0578
36.7500	122.1583	-34.9053
36.7500	122.1167	-34.7753
36.7500	122.0750	-34.6015
36.7500	122.0333	-34.3984
36.7500	121.9917	-34.1837
36.7500	121.9500	-33.9581
36.7500	121.9083	-33.7972
36.7500	121.8667	-33.6822
36.7500	121.8250	-33.5880
36.7500	121.7833	-33.4977
36.7500	121.7417	-33.3841
36.7500	121.7000	-33.2593
36.7083	122.2000	-35.3512
36.7083	122.1583	-35.1936
36.7083	122.1167	-35.0395
36.7083	122.0750	-34.8311
36.7083	122.0333	-34.5708
36.7083	121.9917	-34.3055
36.7083	121.9500	-34.0715
36.7083	121.9083	-33.9035
36.7083	121.8667	-33.7855
36.7083	121.8250	-33.6921
36.7083	121.7833	-33.6038
36.7083	121.7417	-33.4998
36.7083	121.7000	-33.3824
36.6667	122.2000	-35.6139
36.6667	122.1583	-35.4429
36.6667	122.1167	-35.2587
36.6667	122.0750	-35.0051
36.6667	122.0333	-34.6811
36.6667	121.9917	-34.3672
36.6667	121.9500	-34.1225
36.6667	121.9083	-33.9504
36.6667	121.8667	-33.8342
36.6667	121.8250	-33.7401
36.6667	121.7833	-33.6502
36.6667	121.7417	-33.5611
36.6667	121.7000	-33.4656
36.6250	122.2000	-35.8255
36.6250	122.1583	-35.6522
36.6250	122.1167	-35.4257
36.6250	122.0750	-35.1289
36.6250	122.0333	-34.7751
36.6250	121.9917	-34.4290
36.6250	121.9500	-34.1484
36.6250	121.9083	-33.9533
36.6250	121.8667	-33.8257

LAT [deg N]	LONG [deg W]	HEIGHT [m]
36.6250	121.8250	-33.7235
36.6250	121.7833	-33.6265
36.6250	121.7417	-33.5472
36.6250	121.7000	-33.4713
36.5833	122.2000	-35.9581
36.5833	122.1583	-35.7736
36.5833	122.1167	-35.5291
36.5833	122.0750	-35.2164
36.5833	122.0333	-34.8530
36.5833	121.9917	-34.4871
36.5833	121.9500	-34.1708
36.5833	121.9083	-33.9439
36.5833	121.8667	-33.7867
36.5833	121.8250	-33.6649
36.5833	121.7833	-33.5561
36.5833	121.7417	-33.4651
36.5833	121.7000	-33.3921
36.5417	122.2000	-35.9879
36.5417	122.1583	-35.8024
36.5417	122.1167	-35.5670
36.5417	122.0750	-35.2676
36.5417	122.0333	-34.9168
36.5417	121.9917	-34.5508
36.5417	121.9500	-34.2125
36.5417	121.9083	-33.9451
36.5417	121.8667	-33.7491
36.5417	121.8250	-33.5810
36.5417	121.7833	-33.4549
36.5417	121.7417	-33.3492
36.5417	121.7000	-33.2725
36.5000	122.2000	-35.9406
36.5000	122.1583	-35.7663
36.5000	122.1167	-35.5466
36.5000	122.0750	-35.2809
36.5000	122.0333	-34.9610
36.5000	121.9917	-34.6104
36.5000	121.9500	-34.2566
36.5000	121.9083	-33.9195
36.5000	121.8667	-33.6471
36.5000	121.8250	-33.4495
36.5000	121.7833	-33.3294
36.5000	121.7417	-33.2496
36.5000	121.7000	-33.1711

LIST OF REFERENCES

Ashkenazi, F., G.A. Basker, and T.F. Baker, 1990: A geodetic investigation of the British sea slope anomaly. *Marine Geodesy*, **14**, 205-216.

Bomford, G., 1980: *Geodesy (4th Edition)*. Clarendon Press, 855pp.

Brooks, R.A., 1973: *A bottom gravity survey of the shallow water regions of southern Monterey Bay and its geological interpretation*. Masters Thesis, Naval Postgraduate School, Monterey, CA.

Cronyn, B.S., 1973: *Underwater gravity survey of northern Monterey Bay*. Masters Thesis, Naval Postgraduate School, Monterey, CA.

Defense Mapping Agency Aerospace Center(DMAAC), 1987: *WGS84 Ellipsoidal gravity formula and gravity anomaly conversion equations*. DMA Aerospace Center (DS(DSGA)), 10 pp.

Defense Mapping School (DMS), 1977: *The geoid*. DMS No. ST202, Fort Belvoir, BA, 18pp.

Dragomir, F.G., D.N. Ghitau, M.S. Mihailescu, and M.G. Rotaru, 1982: *Theory of the earth's shape*. Elsevier Scientific Publishing Company, 694pp.

Fischer, I., 1977: Mean sea level and the marine geoid - an analysis of concepts. *Marine Geodesy*, **1**, 37-59.

Forsberg, R., 1984: *A study of terrain reductions, density anomalies and geophysical inversion methods in gravity field modeling*. Air Force Geophysics Lab., TR-84-0174, 129pp.

Fu, L., 1983: Recent progress in the application of satellite altimetry to observing the mesoscale variability and general circulation of the oceans. *Review of Geophysics and Space Physics*, **21**, 1657-1666.

Fu, L., D.B. Chelton and V. Zlotnicki, 1988: Satellite altimetry: observing ocean variability from space. *Oceanography*, **1**, 4-11.

Golden Software, INC., 1989: *SURFER Reference Manual. Ver. 4.09*, 330 pp.

Heiskanen, W.A.,and H. Moritz, 1967: *Physical Geodesy*. W. H. Freeman and Company, 364pp.

Hittleman, A.M., R.E. Haberman, D. T. Dater, and L. Di, 1992: *Gravity Earth System Data, CD-ROM Users Manual. (alpha release)*, U.S. Dept. of Commerce, National Geophysical Data Center 109pp.

Jackson, J.D., 1975: *Classical Electrodynamics (2nd Edition)*. John Wiley & Sons, 848pp.

Leick, A., C. Aiken, and M. Carr, 1992: Super conducting super collider GPS networks. *Proceedings Sixth International Geodetic Symposium on Satellite Positioning*, **II**, 789-800.

Mainville, A., R. Forsberg, and M.G. Sideris, 1992: Global Positioning System testing of geoids computed from geopotential models and local gravity data: a case study. *Journal of Geophysical Research*, **97**, 11,137- 11,147.

McAdoo, D.C. and K.M. Marks, 1992: Gravity fields of the Southern Ocean from GEOSAT data. *Journal of Geophysical Research*, **97**, 3247-3260.

Milbert, D.G., 1991: GEOID90: a high-resolution geoid for the United States. *EOS*, **72**, 545-556.

Milbert, D.G., 1993: GEOID93 software and documentation. priv. comm. National Geodetic Survey.

Milbert, D.G., 1994: Telephone conversations between Dr. Dennis Milbert, N/EG18, National Geodetic Survey and the author, Jan - Mar 1994.

Moritz, H., 1974: *Precise gravimetric geodesy*. Dept. of Geodetic Science Report No. 219, The Ohio State Univ, 80pp.

Perrott, T.A., 1993: Final report. *The first super 1-inch geospatial data range, Edwards Air Force Base, California*. Defense Mapping Agency Aerospace Center, Dept. of Geodesy and Geophysics, 23pp.

Pickard, G.L.,and W.J. Emery, 1990: *Descriptive Physical Oceanography; An Introduction (5th edition)*. Pergamon Press 320pp.

Pond, S., and G.L. Pickard, 1983: *Introductory Dynamical Oceanography (2nd Edition)*. Pergamon Press , 329pp.

Rapp, R.H., Y.M. Wang, and N.K. Pavlis, 1991: The Ohio State 1991 geopotential and sea surface topography harmonic coefficient models. *Report No. 410*, The Ohio State Univ. 100pp.

Rapp, R.H., 1992: Computation and accuracy of global geoid undulation models. *Proceedings Sixth International Geodetic Symposium on Satellite Positioning Vol. II.* The Ohio State Univ. Columbus, OH, 865-872.

Rapp, R.H., 1993: Geoid undulation accuracy. *IEEE Trans. Geoscience and Remote Sensing*, **31**, 365-370.

Rocky Mountain Communications, INC., 1991: *3 arc second elevation data on CD-ROM.* Technical Reference 1, 9 pp.

Schwarz, K.P., M.G. Sideris, and R. Forsberg, 1990: The use of FFT techniques in physical geodesy. *Geophysical Journal International*, **100**, 485-514.

Seeber, G., 1993: *Satellite Geodesy*. Walter de Gruyter & Co., 532pp.

Smith, W.H.F., and P. Wessel, 1990: Gridding with continuous curvature splines in tension. *Geophysics*, **55**, 393-405.

Stokes, G.G., 1849: *On the variation of gravity on the surface of the earth*. Trans. Cambridge Philosoph. Soc., **8**, 672-695.

Torge, W., 1991: *Geodesy (2nd Edition)*. Walter de Grayter & Co., 264pp.

Tscherning, C.C., R.H. Rapp, and C. Goad, 1983: A comparison of methods for computing gravimetric quantities from high degree spherical harmonic expansion. *Manuscripta Geodaetica*, **8**, 249-272.

Vanicek, P., 1993: *The Geoid*. Dept. of Surveying and Engineering, Univ. of New Brunswick, 2pp.

Wunsch, C., and E.M. Gaposhkin, 1988: On using satellite altimetry to determine the general circulation of the oceans with application to geoid improvement. *Reviews of Geophysics and Space Physics*, **18**, 725-745.

INITIAL DISTRIBUTION LIST

		No. Copies
1.	Defense Technical Information Center Cameron Station Alexandria VA 22304-6145	2
2.	Library, Code 052 Naval Postgraduate School Monterey CA 93943-5002	2
3.	Oceanography Department Code OC/CO Naval Postgraduate School 833 Dyer Rd Rm 331 Monterey CA 93943-5122 Attention: Dr. Collins	2
4.	Meteorology Department Code MR/HY Naval Postgraduate School 589 Dyer Rd Rm 252 Monterey CA 93943-5114	1
5.	Oceanography Department Code OC/CL Naval Postgraduate School 833 Dyer Rd Rm 215 Monterey CA 93943-5122 Attention: Dr. Clynch	2
6.	Meteorology Department Code MR/SY Naval Postgraduate School 589 Dyer Rd Rm 252 Monterey CA 93943-5114 Attention: Dr. Sirayanone	1
7.	Commander Naval Meteorology Oceanography Command Stennis Space Center MS 39529-5000	1

8. Commanding Officer 1
Naval Oceanographic Office
Stennis Space Center
MS 39529-5001

9. Commanding Officer 1
Naval Oceanographic and Atmospheric
Research Laboratory
Stennis Space Center
MS 39529-5004

10. Library 1
Scripps Institution of Oceanography
P.O. Box 2367
La Jolla, CA 92037

11. Chief, Nautical Charting Division (N/CG2) 1
National Oceanic and Atmospheric
Administration
Rockville, MD 20852

12. NOAA Library 1
7600 Sand Point Way NE
Building 3
Seattle, WA 98115

13. Library 1
Moss Landing Marine Lab
California State Colleges
Sandholdt Road
Moss Landing, CA 05039

14. The Ohio State University 1
Department of Geodetic Science and Surveying
404 Cockins Hall
1958 Neil Avenue
Columbus OH 43210-1247
Attention:
Dr. R.H. Rapp

15. National Geodetic Survey, NOAA 1
N/CG18
Rockwall Bldg
11400 Rockville Pike
Rockville MD 20852
Attention:
Dr. D.G. Milbert

16. Defense Mapping Agency Headquarters — 2
8613 Lee Highway
Fairfax VA 22031-2137
Attention:
Dr. K. Wooden
Mr. J. Slater

17. Defense Mapping Agency Aerospace Center — 3
Department of Geodesy and Geophysics (MS L-41)
3200 South Second Street
St. Louis MO 63118-3399
Attention:
Mr. Kenneth Burke
Mr. John Rees
Mr. R. Cramer

18. NOAA/NOS — 1
Tidal Analysis Branch(N/OES22)
SSMC4, Room 7109
1305 East-West Highway
Silver Spring, MD 20910-3233
Attention:
Mr. S. Gill

19. Ashtech Inc. — 1
1170 Kifer Road
Sunnyvale, CA 94086
Attention:
Mr. X. Qua

20. Naval Surface Weapons Center-Dahlgren Laboratory — 1
Dahlgren, VA 22448
Attention:
Mr. A. Evans(K10)

21. Defense Mapping Agency Systems Center — 1
12100 Sunset Hills Road #200
Reston, VA 22090-3221
Attention:
Mr. Ben Roth (MS J2)

22. Department of Oceanography — 1
Florida State University
B169
Tallahassee, FL 32306
Attention:
Dr. W. Sturges

23. HQ DMA/DH STOP A-6 — 1
8613 Lee Highway
Fairfax, VA 22031-2137
Attention:
CAPT. J. Ayers

24. PFEG — 1
P.O. Box 831
Monterey, CA 93942
Attention:
Mr. J. Norton

25. DMAAC/GGD — 1
15 North Nuroc Drive
Edward's Air Force Base, CA 93524-2070
Attention:
Mr. B. Wideman

26. NOAA — 1
1315 East-West Highway
Silver Spring, MD 20910
Attention:
CAPT K. Schnebele

27. Mathematics Department — 1
Code MA/DD
Naval Postgraduate School
1411 Cunningham Road, Room 341
Monterey, CA 93943-5216
Attention:
Dr. D. Danielson

28. Chairman — 1
Oceanography Department
United States Naval Academy
Annapolis, MD 21402